

Thomas R. Krogstad

Attitude synchronization in spacecraft formations

Theoretical and experimental results

Doctoral thesis
for the degree of philosophiae doctor

Trondheim, November 2009

Norwegian University of Science and Technology
Faculty of Information Technology,
Mathematics and Electrical Engineering
Department of Engineering Cybernetics



NTNU

Norwegian University of Science and Technology

Doctoral thesis
for the degree of philosophiae doctor

Faculty of Information Technology,
Mathematics and Electrical Engineering
Department of Engineering Cybernetics

© 2009 Thomas R. Krogstad.

ISBN 12345666 (printed version)
ISBN 123112355 (electronic version)
ISSN 1503-8181

Doctoral theses at NTNU, 2009:N/A

Printed by NTNU-trykk

Summary

This thesis addresses attitude synchronization in spacecraft formations. In addition to theoretical results the thesis presents the design and implementation of an experimental platform for spacecraft attitude synchronization.

The first part of the thesis gives a general introduction to spacecraft formation flying with possible applications and current proposed and scheduled missions, and background information on relevant related work presented in the literature. We also give some necessary mathematical preliminaries, included for the sake of completeness and to give the reader an introduction to the notation and mathematical models required to grasp the theoretical contents.

The theoretical results are presented in 4 separate chapters based on published and submitted conference papers, journal papers and book chapters.

In the final part of the thesis we present the design and implementation of an experimental platform for spacecraft attitude synchronization. The platform is based on two spherical autonomous underwater vehicles, internally actuated by means of reaction wheels.

In chapter 4 we present an adaptive external synchronization scheme for a spacecraft actuated by means of reaction wheels. The controller use the quaternion parameterization of attitude, and is proven to be globally exponentially stable on $S(3) \times \mathbb{R}^3$ in the known parameter case and globally convergent when using adaptive feedback.

In chapter 5 we present a 6 degrees of freedom (6-DOF) synchronization scheme for a deep space formation of spacecraft. In the design, which is referred to as a mutual synchronization scheme, feedback interconnections are designed in such a way that the spacecraft track a time varying reference trajectory while at the same time keep a prescribed relative attitude and position. The closed-loop system is proven uniformly locally asymptotically stable, with an area of attraction which covers the complete state-space, except when the spacecraft attains an attitude where the inverse kinematics are undefined. The proof is carried out using Matrosov’s Theorem.

The contribution of chapter 6 is a PID+ backstepping controller, as a solution to the problem of coordinated attitude control in spacecraft formations. The control scheme is based on quaternions and modified Rodriguez parameters as attitude representation of

the relative attitude error. Utilizing the invertibility of the modified Rodriguez parameter kinematic differential equation, a globally exponentially stable control law for the relative attitude error dynamics is obtained through the use of integrator augmentation and backstepping.

The contribution of chapter 7 is the design of an observer-controller output feedback scheme for relative spacecraft attitude. The scheme is developed for a leader-follower spacecraft formation, where the leader is assumed to be controlled by an asymptotically stable tracking controller. Furthermore we assume that the follower has knowledge about its own attitude and angular velocity in addition to the relative attitude with respect to the leader. Since we do not know the angular velocity and acceleration of the leader, we design an error observer.

The contribution of chapter 8 is the design of AUVSAT, an experimental platform for relative spacecraft attitude synchronization. We present the mechanical and electrical network design of the vehicles. In addition an overview of the control hardware, including sensors, actuators and computers, and software designed to control the vehicle platforms.

The contribution of chapter 9 is the experimental validation of control algorithms for relative attitude synchronization in a two satellite leader-follower formation. We present experimental results for the PID+ backstepping design of chapter 6 and the output feedback design in chapter 7.

Preface

This thesis presents the research results from my doctoral studies from August 2005 to September 2009 at the Department of Engineering Cybernetics at the Norwegian University of Science and Technology. The project was funded by the Norwegian Research Fundation (NFR) through the strategic university program, Center for Computation Methods in Nonlinear Motion Control (CMinMC).

A lot of people deserve recognition for making it possible for me to conduct the work that culminated in this thesis.

First of all I would like to thank my supervisor Professor Jan Tommy Gravdahl for introducing me to the field of spacecraft control. Without his patience, optimism, encouragement and constructive feedback this work would not have been completed. I am also grateful to Professor Kristin Ytterstad Pettersen who served as my substitute supervisor during the last half of my supervisor’s sabbatical year and to Professor Rodolphe Sepulchre, who let me spend 5 months with his department at the Université de Liège in Belgium. I would also like to thank Dr. Raymond Kristiansen for helpful advise and cooperation during this 4 years.

During the first three years of doctoral studies I was fortunate enough to share office with Even Børhaug. Our daily morning coffees, the time we spent designing, building and programming the Munin autonomous underwater vehicle, and also the time spent outside the office, all served to make the sometimes trying times as a PhD student worthwhile.

I would also like to thank the PhD students at the Department of Engineering Cybernetics for a fun and interesting working environment, Eva Amdahl and Tove Blomset Johnsen in the administration for helping me with every administrative issue, and finally Terje Haugen and the rest of the staff at the department mechanical workshop, without their help and knowledge the experimental part of this thesis would not exist.

Finally, I would like to thank my family for their constant support and encouragement, and especially my partner Ida for her love and support, and for her patience during this final year of late nights and weekends at the office.

Oslo, December 2009

Thomas R. Krogstad

Contents

List of Figures	xiii
List of Tables	xv
List of Abbreviations	xvii
1 Introduction	1
1.1 Motivation	1
1.2 Spacecraft formation flying	2
1.2.1 Introduction	3
1.2.2 Application of formation flying	3
1.2.3 Current projects	5
1.3 Background	6
1.3.1 Synchronization	6
1.3.2 Attitude control	8
1.3.3 Output feedback	8
1.4 Contribution of the thesis	9
1.4.1 Publications	9
1.4.2 Chapter 4	10
1.4.3 Chapter 5	10
1.4.4 Chapter 6	11
1.4.5 Chapter 7	11
1.4.6 Chapter 8	11
1.4.7 Chapter 9	11
2 Mathematical preliminaries	13
2.1 Notation	13
2.2 Stability	14
2.2.1 General Stability	14
2.3 Stability theorems	15

CONTENTS

2.3.1	Practical stability	15
2.3.2	Matrosov’s Theorem	16
2.3.3	Barbalat’s lemma	18
2.3.4	LaSalle’s invariance principle	18
2.3.5	Lyapunov’s direct method	18
3	Mathematical modeling	21
3.1	Coordinate frames	21
3.1.1	Earth-centered inertial frame	22
3.1.2	Orbit frame	22
3.1.3	Body fixed frame	22
3.2	Rotation matrices	22
3.3	Kinematic equations	23
3.4	Attitude parameterizations	23
3.4.1	Angle-axis	24
3.4.2	Euler angles	24
3.4.3	The Euler parameters	26
3.4.4	Modified Rodriguez parameters	28
3.5	The dynamical model	29
3.5.1	Externally actuated rigid body	29
3.5.2	Internally actuated rigid body	29
3.5.3	Inertial coordinate model	32
3.6	External forces and torques	33
3.6.1	Gravitational forces and torques	33
3.6.2	Aerodynamical forces and torques	34
3.6.3	Magnetic torques	34
3.6.4	Solar radiation and solar wind	36
3.6.5	Thruster forces and torques	36
3.6.6	Reaction wheels	37
4	External synchronization of relative attitude	39
4.1	Introduction	39
4.2	Mathematical model	40
4.2.1	Kinematics	40
4.2.2	Dynamic model	40
4.3	External synchronization design	40
4.3.1	Leader controller	41
4.3.2	Adaptive synchronizing controller	46
4.4	Simulations	50
4.5	Conclusions	52

5	6-DOF mutual synchronization of formation flying spacecraft	53
5.1	Introduction	53
5.2	Mathematical model	54
5.2.1	Kinematic model	54
5.2.2	Dynamical model	54
5.3	Control design	55
5.3.1	Synchronization error	56
5.4	Simulations	58
5.5	Conclusion	61
6	PID+ backstepping control of relative spacecraft attitude	63
6.1	Relevant related work	63
6.2	Relative Rotational Motion	64
6.3	Control design	65
6.4	Simulations	68
6.4.1	Results	69
6.5	Conclusion	69
7	Output feedback control of relative spacecraft attitude	71
7.1	Introduction	71
7.1.1	Motivation	72
7.2	Mathematical model	72
7.2.1	Kinematics	72
7.2.2	Dynamic model	73
7.3	Control and observer design	73
7.3.1	Assumptions	73
7.3.2	Control objectives	73
7.3.3	Error dynamics	74
7.3.4	Error observer	75
7.4	Simulation	77
7.4.1	Results	78
7.5	Conclusion	78
7.6	Appendix	78
7.6.1	Bound on Δ_ω	78
8	AUVSAT - an experimental platform for spacecraft formation flying	83
8.1	Introduction	83
8.2	Autonomous underwater vehicle design	84
8.2.1	Specifications	85
8.2.2	Hull and construction	85
8.2.3	Sensors	86

CONTENTS

8.2.4	Actuators	86
8.3	Underwater satellite design	87
8.3.1	Hull design	88
8.3.2	Sensors	88
8.3.3	Actuators	89
8.3.4	Communication	89
8.3.5	Main computer	90
8.3.6	Software design	90
8.3.7	Internal structure	94
9	Experimental results	97
9.1	Mathematical model	98
9.1.1	Model parameters	98
9.2	Measurements	98
9.3	Actuation	99
9.3.1	Moment mapping	99
9.4	Experiment facilities	100
9.5	Measurement filtering	101
9.6	Preliminary experiments	101
9.6.1	Depth control	102
9.6.2	Attitude control	103
9.7	Preliminary synchronization control	104
9.7.1	2 axes stabilized, 1 axis synchronizing	104
9.7.2	PD quaternion feedback synchronization scheme	105
9.8	PID+ backstepping control of relative spacecraft attitude	111
9.8.1	The implemented control algorithm	111
9.8.2	The results	111
9.8.3	Discussion	115
9.9	Output feedback control of relative spacecraft attitude	115
9.9.1	The implemented control algorithm	115
9.9.2	Results	115
9.9.3	Discussion	116
9.10	Discussion	119
10	Concluding remarks	121
10.1	Concluding remarks	121
10.1.1	Theoretical work	121
10.1.2	Experimental work	122
10.2	Future work	122
10.2.1	Theoretical	122
10.2.2	Experimental	122

Bibliography	131
A Mathematical tools and definitions	133
A.1 Mathematical preliminaries	133
A.1.1 Vectors	133
A.1.2 Vector cross product	134
A.1.3 Time derivative of vectors	134
A.2 Quaternion operations	135
A.2.1 Quaternion multiplication	135
A.3 Derivation of the differential kinematics	135
B Mechanical and electrical design	137
B.1 Electrical design	137
B.1.1 Main power network	138
B.1.2 Actuator and sensor signal transmission lines	140
B.2 Mechanical design	140
B.2.1 Main assembly	141
B.2.2 Mechanical drawings	142

CONTENTS

List of Figures

1.1	The infamous starling formations of Rome	1
1.2	Fish school. Image courtesy of http://www.divematrix.com	2
1.3	TanDem-X spacecraft formation. Courtesy of DLR.	3
3.1	Coordinate frame \mathcal{F}_a	21
3.2	Roll-pitch-yaw Euler angles illustration.	25
3.3	Gyrostad illustration	30
3.4	Illustration of the Earth’s magnetic field	35
3.5	4 reaction wheel assemblies in tetrahedron composition	37
4.1	Simulation results	51
5.1	The figure illustrates how the attitudes of the three spacecraft are first mutually synchronized, and then track a desired orientation.	60
5.2	Tracking and synchronization behaviour in position. All units are in <i>km</i> . The triangles indicate the relative position at different time-instants. The initial position is indicated by a *.	60
7.1	Synchronization measure s	78
7.2	Attitude synchronization error \mathbf{q}_e	79
7.3	Synchronization measure s	80
7.4	Attitude synchronization error \mathbf{q}_e	80
7.5	Synchronization angular velocity error $\boldsymbol{\omega}_e$	81
8.1	Computer design of the underwater satellite	84
8.2	Illustration of the Munin AUV performing hovering inspection of an off-shore oil and gas installation.	85
8.3	Overall structure	91
8.4	Communication overview	93
8.5	Hardware parts for the AUVSAT	95

LIST OF FIGURES

9.1	Outdoor facility	97
9.2	Basement facilities	100
9.3	Measurement filtering. Pressure	101
9.4	Measurement filtering. Angular velocity	102
9.5	Results for (9.14). Measured euler angles vs. reference trajectory.	104
9.6	Results for (9.14). Tracking error, $\psi_d - \psi$	104
9.7	Results for (9.14). Torque input.	105
9.8	Results for (9.16). The red line shows the leader yaw angle, ψ_l , the blue line shows the follower yaw angle θ_f	106
9.9	Results for (9.16). The synchronization error $\psi_l - \psi_f$	106
9.10	Results for (9.16). Angular velocity	107
9.11	Results for (9.16). Torque command	107
9.12	Results of (9.17). The plot shows q_l as the dotted lines and q_f as the solid lines.	108
9.13	Results of (9.17). The plot shows ψ_l and ψ_f	108
9.14	Results of (9.17). The plot shows $\psi_l - \psi_f$	109
9.15	Results of (9.17). The plot shows the torque.	109
9.16	Results of (9.17). The plot shows the synchronization error q_e	110
9.17	Results of (9.20). This figure shows the synchronization of the leader and follower yaw angle.	112
9.18	Results of (9.20). Synchronization error in Euler angles	112
9.19	Results of (9.20). Synchronzation error in quaternions	113
9.20	Results of (9.20). Lead vs. follower quaternion. The leader quaternion components are the dotted lines.	113
9.21	Results of (9.20). Torque	114
9.22	Results of (9.20). Leader vs. follower angular velocity. Leader velocities are dotted.	114
9.23	Results of (9.26). Leader vs. follower yaw angle. Leader is black.	116
9.24	Results of (9.26). Synchronization error represented in Euler angles.	116
9.25	Results of (9.26). Synchronization error in quaternion representation.	117
9.26	Results of (9.26). Leader vs. follower quaternion. Leader quaternion components are the dotted lines.	117
9.27	Results of (9.26). \hat{s}	118
9.28	Results of (9.26). Torque.	118
B.1	The vehicle with the top sphere detached to reveal the inner structure and hardware layout.	137

LIST OF FIGURES

B.2 Main power network - This network connects the battery to the three motors and the PC/104 power supply card. The circuit is protected by a 30A main fuse, in addition to 10A fuses on each motor connector, protecting the motors from overloading. A main switch is connected to the battery to enable power during assembly and disassembly. 138

B.3 Auxiliary power network - The auxiliary power network distributes power from the power supply card to hardware without internal voltage regulators. There are two power rails, a +5V and a +12V rail. 139

B.4 This figure gives an overview of the actuator and sensor signal transmission lines. These transmission lines carry analog voltage readings from the pressure senso, a PWM signal controlling the piston tank servo controller and serial communication to and from the IMU and motor controllers. 140

B.5 This figure shows how the different hardware components are attached to the framework. 141

B.6 This figure shows how the different hardware components are attached to the framework. Viewed from below. 141

B.7 Upper mounting disc 142

B.8 Piston tank mounting bracket 143

B.9 Motor mounting bracket 143

B.10 Mounting disc connector 144

B.11 Lower mounting disc 144

B.12 Aluminum part a of reaction wheel 145

B.13 Aluminium part b of reaction wheel 145

B.14 Assembled reaction wheel 146

B.15 Reaction wheel lead core 146

B.16 Reaction wheel shaft. Connecting the reaction wheels to the motor shaft. . 147

B.17 Motor shaft support. Used to limit the load from the reaction wheels on the motor shafts. 147

B.18 Reaction wheel shaft for the yaw axis motor. Connecting the reaction wheels to the motor shaft. 148

B.19 Support framework. Supports the inner assembly inside the glass sphere when the vehicle is rotating. 148

LIST OF FIGURES

List of Tables

4.1	Model parameters	50
4.2	Simulation parameters	50
5.1	Model parameters	59
7.1	Model parameters	77
8.1	Hardware overview for the underwater satellites	87
8.2	Sensor properties	88
9.1	Motor parameters	100

LIST OF TABLES

List of Abbreviations

ADC	Analog to Digital Converter
AS	Asymptotically Stable
AUV	Autonomous Underwater Vehicle
CAD	Computer Aided Design
CNC	Computer Numerical Control
DAC	Digital to Analog Converter
DOF	Degrees of Freedom
ECI	Earth Centered Inertial
ESA	European Space Agency
GES	Uniformly Exponentially Stable
GPS	Global Positioning System
IGRF	International Geomagnetic Reference Field
IMU	Inertial Measurement Unit
LEO	Low Earth Orbit
LFC	Lyapunov Function Candidate
MRP	Modified Rodriguez Parameters
N	Newton (force)
NASA	National Aeronautics and Space Administration
Nm	Newton meter (moment)
PID	Proportional Integral Derivative
RTOS	Real-time Operating System
RTW	Real-time Workshop (Matlab toolbox)
SAR	Syntetic Aperture Radar
SO(3)	Special orthogonal group of dimension 3
UAS	Uniformly Asymptotically Stable
UAV	Unmanned Aerial Vehicle
UGAS	Uniformly Globally Asymptotically Stable
ULAS	Uniformly Locally Asymptotically Stable
ULES	Uniformly Locally Exponentially Stable
UPAS	Uniformly Practically Asymptotically Stable

LIST OF TABLES

Chapter 1

Introduction

In this thesis we consider the problem of attitude synchronization in spacecraft formations. We propose several methods of solving the problem, both based on state feedback and output feedback control schemes. On the most part we focus on what is usually referred to as leader-follower formations, in which we may have two or more vehicles, where one is deemed the formation leader, and the rest of the vehicles followers.

In addition to the theoretical contributions, the thesis also considers the practical implementation of synchronization control laws and the design of an underwater experimental platform for spacecraft attitude control.

1.1 Motivation

The advantages of systems moving in some form of synchronous movement have been observed both in biological and mechanical systems. In biological systems synchronized motion is observed in every level of the food chain, from the swarm intelligence of the zoo plankton, to bird flocking and fish schools, to mammals moving and formation to protect their young or hunting prey (Hainsworth 1987) and (Okubo 1986).

Naturally occurring synchronized motion has inspired several directions of research within the control community. All with the goal of designing coordination control schemes which enable mechanical systems to take advantage of synchronized motion.



Figure 1.1: The infamous starling formations of Rome

INTRODUCTION



Figure 1.2: Fish school. Image courtesy of <http://www.divematrix.com>

The use of autonomous underwater vehicles (AUV) for oceanic sampling and seabed mapping, are areas where motion synchronization have been suggested as a way of improving results or increasing throughput. For oceanic sampling teams of AUVs have been suggested used for gradient estimation of density and temperature fields, and also for searching for sources of chemical spills using chemical sniffers.

In industrial robotics, cooperating robot manipulators have become an everyday thing. Examples include assembly of heavy machinery, where two or more manipulators are coordinated to lift a part too heavy for only one manipulator, and also arc welding of seams and painting.

The focus in this work is on spacecraft formation and in the next section we give an overview of proposed applications and planned missions.

1.2 Spacecraft formation flying

In this chapter the concept of formation flying of satellites will be presented. As the main contribution of this thesis is attitude control, the focus will be on the coordinated control of attitude. We present possible applications and relevant work presented in the literature.



Figure 1.3: TanDem-X spacecraft formation. Courtesy of DLR.

1.2.1 Introduction

Formation flying missions and missions involving the coordinated control of several autonomous vehicles have been areas of increased interest in later years. This is due to the many inherent advantages the distributed design adds to the mission. By distributing payload on several spacecraft, redundancy is added to the system, minimizing the risk of total mission failure, several cooperating spacecraft can solve assignments which are more difficult and expensive, or even impossible to do with a single spacecraft, and the launch costs may be reduced since the spacecrafts may be distributed on more inexpensive launch vehicles. The disadvantage is the requirement for a fully autonomous vehicle, as controlling the spacecraft in close formation is only possible using control. This results in stringent requirements on the control algorithms and measurement systems.

1.2.2 Application of formation flying

The formation flying concept enables several applications that would not have been possible or that are enhanced when compared to using a single large spacecraft. Two such applications are presented in the following; Earth observation and space-based interferometry.

INTRODUCTION

Earth observation

The advantage of formation flight in this application is the ability to use smaller, simpler and cheaper satellites, instead of one large and complex. The formation flying concept is especially useful in synthetic aperture radar, where either several small satellites may operate as one large virtual satellite with a much larger aperture than would be possible on a single satellite, or several satellites with SAR capabilities cooperate in formation, resulting in an enlarged field of view. Other applications include gravitational field mapping, synchronous spatial sampling of atmospheric data and co-observations (i.e. near-simultaneous observations of the same science target by instruments on multiple platforms.) By distributing sensors for science instrumentation, there is an enhanced fault-tolerance. If one small satellite should fail it is easier to replace this by a new satellite, than to use the space shuttle crew to repair or change the instruments on the large single satellite.

Space-based interferometry

In space-based interferometry the advantages in formation flying of spacecraft is not so much in cost and assembly line production, but rather in increased accuracy. Examples of planned missions includes ESA's Darwin mission and NASA's Terrestrial Planet Finder and MAXIM. In these missions interferometry will be applied in the search of earth-like planets. With a large aperture, it would even be possible to look for signs of life, such as ozone. (Beichman, Woolf & Lindensmith 1998).

Interferometry takes advantage of the wave properties of light. The phenomena was first reported in 1803 by Thomas Young, and is popularly known as *Young's two-slit experiment*. In this setup light is impinged upon two slits, the two resulting coherent light sources will interfere and create fringes when the light hits the surface in front of the slits (Tipler 1999).

This is also the basis for space-based interferometry. Here the two slits are replaced by two or more space-based telescopes or collector spacecraft. The observed waves are then transferred to the combiner spacecraft, where the waves interfere to make fringes. To be able to observe a planet, one has to remove the powerful light from the star it is orbiting. The idea is therefor to delay the light from the telescopes by an added phase shift, π , such that the light from the star interferes destructively leaving only the light received from the planet. This is referred to as nulling interferometry (Fridlund 2004). The accuracy is determined by the baseline, i.e. the distance or separation between the spacecraft. Logically with formation flying one is able to increase the separation far more than with a structurally connected craft. The drawback is of course the difficulty of keeping inter-spacecraft position and orientation.

1.2.3 Current projects

There are several current projects which are dealing with the formation flying and coordinated control of satellites.

TanDEM-X

TanDEM-X is a project realized by DLR, EADS Astrium GmbH and GSOC, consisting of two satellites equipped with synthetic aperture radar (SAR). By flying in close and accurate formation the spacecraft form a radar interferometer with a baseline of 1 km. This allows for much higher resolution than any earlier SAR mission, and can deliver digital elevation models with unrivaled accuracy (D’Amico, Ardaens, De Florio & Montenbruck 2008).

PRISMA

PRISMA is a project led by the Swedish Space Corporation (SSC), and will be the first real formation flying space mission launched. This is an experimental mission, and the goal is to validate sensors and actuators for formation flying and to demonstrate formation flying and rendezvous through experiments. (D’Amico et al. 2008)

DARWIN

DARWIN was a project proposed by the European Space Agency (ESA) in 1993 as part of Cosmic Vision 2015-2025 call for proposals, with the goal of launching a space-based telescope aiding in the search for possible life-supporting planets. The telescope would consist of 4 spacecraft flying in autonomous formation around a Lagrange point. The mission was however, much like its American counterpart the Terrestrial Planet Finder, postponed indefinitely in 2007.

XEUS

XEUS is a ESA proposed two-satellite X-Ray observatory, with a detector and mirror satellite. The mirror satellite is the leader of the formation pointing at the area of interest, the detector tracks the focal point of the mirror satellite. However, in 2008 the XEUS mission was merged with Constellation-X mission (NASA) to form the International X-Ray Observatory (IXO), and the formation flying part was canceled in favor of a large single spacecraft bus.

INTRODUCTION

Comments

From the above it is clear that a pure formation flying mission in space using autonomous control has yet to take place. However during the last docking phase of ESA's Automated Transfere Vehicle (ATV) mission to the International Space Station did use autonomous relative positioning in its docking phase. Still as this paragraph was written the PRISMA satellites, are going through their final system integration, and will most probably be the first dedicated formation flying mission launched.

1.3 Background

In this section a review of the problems which have been addressed in the literature is given. The main focus is on the the relative attitude case.

1.3.1 Synchronization

Though most work on formation flying spacecraft, and satellites in particular, have been performed on the relative position problem, there do exist a great deal of literature on the control of relative attitude. The first work in this field, as in the relative position case, stems from the work done on automatic rendezvous and docking control of two spacecraft, as was done on the Apollo missions. Later it was utilized in the Space Shuttle, Skylab and Gemini. (Wang, Hadaegh & Mokuno 2003)

As already mentioned, in the 1990s the focus again shifted to the control of several spacecraft. From the literature one can identify three approach to formation control:

- Leader - follower
- Behavioral
- Virtual structure

Leader-follower

In the leader-follower strategy, one typically divides the spacecraft into subgroups. Within each subgroup one craft is defined as the leader and the rest are defined as followers. While the leader will track a predefined trajectory, the followers are controlled to track the leader. This scheme is easy to understand and implement, it will allow the formation to withstand perturbations in the leader, but may fail if the follower were to be perturbed. Versions of this approach can be found in Wang, Hadaegh & Lau (1999), Pan & Kapila (2001) and Kang & Yeh (2002) and Nijmeijer & Rodriguez-Angeles (2003).

Wang et al. (1999) proposes a control technique to rotate the entire formation about a given axis and synchronize the individual spacecraft with the formation. Both position

and attitude are controlled, and the error is proven to decay to zero exponentially, though under the assumption of no environmental disturbances and implementation difficulties.

In Pan & Kapila (2001) an adaptive nonlinear controller is proposed, which assumes a unknown mass and inertia, and coupled translational and attitude dynamics. Based on a Lyapunov framework they derive a controller which leads to globally asymptotic convergence of the follower spacecraft relative position and attitude.

Kang & Yeh (2002) proposes a more general way to achieve leader/follower synchronization, through the use of reference projections. The control input to each satellite is a function of its own state and the reference projection. Where the reference projection defines a desired state for the closed-loop system, as a function of the measured and desired states of the other satellites.

A general synchronization theory for mechanical systems is developed in the Nijmeijer & Rodriguez-Angeles (2003), for use on robot manipulators. And for general Euler-Lagrange systems and ships output feedback leader-follower synchronization was developed in Kyrkjebø (2007a).

Behavioral

The behavioral strategy, each spacecraft is defined as an agent and the control action for each agent is defined by a weighted average of the controls corresponding to each desired behavior for the agent. This approach eases the implementation of conflicting or competing control objectives, such tracking versus avoidance. It is however difficult to enforce group behavior, and to mathematically guarantee stability and formation convergence. Another problem is that some unforeseen behavior may occur when goals are conflicting.

A lot of results in this area have been reported in field of autonomous mobile robots, and three notable references are Mataric (1992), Balch & Arkin (1998) and Mali (2002). Mali (2002) contains a review of some work done in the field.

Lawton applies the strategy to spacecraft formations in his PhD thesis Lawton (2000). Here he treats both the relative position and the relative attitude case, and includes analytical proofs based on perfect knowledge of the states.

Virtual structure

In the third approach, virtual structure, the spacecraft formation is viewed as a virtual rigid body. The desired states of a single spacecraft, may be specified such that the formation moves as a single structure. In this scheme it is easy to prescribe a coordinated group behavior and the formation may be maintained well during maneuvers, given that the single spacecraft is able to follow its trajectory. The virtual structure may however limit the class of possible maneuvers.

INTRODUCTION

A great deal of work have been done in this area using mobile robots Lewis & Tan (1997), and have recently been applied to spacecraft formations in Ren & Beard (2004), Beard (1998), Beard & Hadaegh (1998) and Beard, Lawton & Hadaegh (2001).

1.3.2 Attitude control

The literature on Attitude control of rigid bodies is vast. It covers orientation control of aerial, space, underwater and surface vehicles, to the handling of objects by a robot manipulators end-effector. In this section we cover the works which inspired and served as background material for this thesis.

Wen & Kreutz-Delgado (1991) presents a general framework for the analysis of the attitude tracking control problem. They analyze several control schemes based on quaternion feedback, and prove stability rigorously using Lyapunov theory. In (Egeland & Godhavn 1994), the authors analyze attitude control laws based on quaternion feedback in a passivity framework. As pointed out in (Bhat & Bernstein 2000), the attitude kinematics in $SO(3)$ cannot be globally stabilized using continuous feedback, (Fragopoulos & Innocenti 2004, Fjellstad & Fossen 1994) therefore proposed quaternion feedback control laws using discontinuous feedback. Attitude control of underactuated satellites was investigated in (Godhavn & Egeland 1995) and (Horri & Hodgart 2003), the former using quaternion feedback, the latter using modified Rodriguez parameters.

1.3.3 Output feedback

Lizarralde & Wen (1996) proposed a control scheme for rigid-body attitude stabilization when the angular velocity is not available, using a velocity filter. A similar approach can be found in (Cotic, Dawson, De Queiroz & Kapila 2000) where an adaptive quaternion based controller is used is used for a single spacecraft and the need for velocity feedback is eliminated using a filter; and the authors conclude global convergence of the system states. Similar to (Cotic et al. 2000), (Singla, Subbarao & Junkins 2006) and (Akella 2001) propose a control scheme without the need for angular velocity measurement, and show convergence of the tracking error using Barbalat’s lemma. A scheme for attitude synchronization in a leader-follower spacecraft formation using attitude feedback only, was presented in (Bondhus, Pettersen & Gravdahl 2005). The controller was designed using backstepping and velocity information is provided by two observers. It was proved that the attitude error rotation matrix converges to the identity matrix. (Bai, Arcak & Wen 2008) derive passivity based controllers for synchronizing orientation of rigid bodies assuming knowledge of relative orientation and angular velocity in body coordinates. In the case of unknown leader reference angular velocity an adaptive design is done in order to keep the convergence properties of the original scheme. In (Kristiansen, Loría, Chaillet & Nicklasson 2009) a synchronizing output feedback controller was also derived for the

case of unknown leader velocity, obtaining similar stability results as our scheme, but without synchronization error observer.

1.4 Contribution of the thesis

1.4.1 Publications

The results of this thesis are published in the following publications:

Journal papers

- Krogstad, T. R. & Gravdahl, J. T. (2009), ‘Output feedback control of relative spacecraft attitude’, *Automatica* . Resubmitted.

Conference papers

- Krogstad, T. R. & Gravdahl, J. T. (2009), Output feedback control of relative spacecraft attitude, *in* ‘Proceedings of the 2009 European Control Conference’.
- Krogstad, T. R. , Gravdahl, J. T. , Pettersen, K. Y. & Børhaug, E. (2008), AU-VSAT - an experimental platform for spacecraft formation flying, *in* ‘Proceedings of the 59th International Astronautical Congress’, Glasgow, Scotland, September 29.-October 3rd, 2008
- Kristiansen, R., T. R. Krogstad, P. J. Nicklasson and J. T. Gravdahl, PID+ tracking in a leader-follower spacecraft formation, *in* ‘Proceedings of the 3rd International Symposium on Formation Flying, Missions and Technologies’ (ISFF), Estec, Holland, 2008
- Krogstad, T. R. , Kristiansen, R., Gravdahl, J. T. & Nicklasson, P. J. (2007), PID+ backstepping control of relative spacecraft attitude, *in* ‘Proceedings of 7th IFAC Symposium on Nonlinear Control Systems’ (NOLCOS), , Pretoria, South Africa, 2007
- Kristiansen, R., T. R. Krogstad, P. J. Nicklasson and J. T. Gravdahl, Spacecraft coordination control using PID backstepping, *in* ‘Proceedings of the 17th IFAC Symposium on Automatic Control in Aerospace’ (ACA), Toulouse, France, 2007
- Krogstad, T. R. & Gravdahl, J. T. (2006b), Mutual synchronization of formation flying spacecraft in 6 DOF, *in* ‘Proceedings of 45th Conference on Decision and Control’.

INTRODUCTION

- Krogstad, T. R. , Gravdahl, J. T. & Kristiansen, R. (2005*b*), Coordinated control of formation flying spacecraft, *in* ‘Proceedings of 56th International Astronautical Congress’.

Book chapters

- Krogstad, T. R. & Gravdahl, J. T. (2006*b*), Coordinated control of formation flying spacecraft, *in* ‘Workshop on Group Coordination and Coordinated Control’, Series: Lecture Notes in Control and Information Sciences, Vol. 336, ISBN: 3-540-33468-8, Springer Verlag, Heidelberg, 2006

Related work

- Paul T., T. R. Krogstad and J. T. Gravdahl, UAV Formation Flight using 3D Potential Field, *in* ‘Proceedings of the 16th Mediterranean Conference on Control and Automation, Corsica, France, June 2008.
- Paul T., T. R. Krogstad and J. T. Gravdahl, Modeling and Simulation of UAV Formation Flight using 3D Potential Field, *in* ‘Simulation Modelling Practice and Theory’, 16(9), pp. 1453-1462, October, 2008

1.4.2 Chapter 4

In chapter 4 we present an adaptive external synchronization scheme for a spacecraft actuated by means of reaction wheels. The controller use the quaternion parameterization of attitude, and is proven to be globally exponentially stable on $S(3) \times \mathbb{R}^3$ in the known parameter case and globally convergent when using adaptive feedback.

1.4.3 Chapter 5

In this chapter we present a 6 degrees of freedom (6-DOF) synchronization scheme for a deep space formation of spacecraft. In the design, which is referred to as a mutual synchronization scheme, feedback interconnections are designed in such a way that the spacecraft track a time varying reference trajectory while at the same time keep a prescribed relative attitude and position. The closed-loop system is proven uniformly locally asymptotically stable, with an area of attraction which covers the complete state-space, except when the spacecraft attains an attitude where the inverse kinematics are undefined. The proof is carried out using Matrosov’s Theorem.

1.4.4 Chapter 6

The contribution of this paper is a PID+ backstepping controller, as a solution to the problem of coordinated attitude control in spacecraft formations. The control scheme is based on quaternions and modified Rodrigues parameters as attitude representation of the relative attitude error. Utilizing the invertibility of the modified Rodrigues parameter kinematic differential equation, a globally exponentially stable control law for the relative attitude error dynamics is obtained through the use of integrator augmentation and backstepping. Finally, simulation results are presented to show controller performance.

1.4.5 Chapter 7

The contribution of this chapter is the design of an observer-controller output feedback scheme for relative spacecraft attitude. The scheme is developed for a leader-follower spacecraft formation, where the leader is assumed to be controlled by an asymptotically stable tracking controller. Furthermore we assume that the follower has knowledge about its own attitude and angular velocity in addition to the relative attitude with respect to the leader. Since we do not know the angular velocity and acceleration of the leader, we design an error observer in spirit of the work presented in (Kyrkjebø 2007a).

1.4.6 Chapter 8

The contribution of this chapter is the design of AUVSAT, an experimental platform for relative spacecraft attitude synchronization. We present the mechanical and electrical network design of the vehicles. In addition an overview of the control hardware, including sensors, actuators and computers, and software designed to control the vehicle platforms.

1.4.7 Chapter 9

The contribution of this chapter is the experimental validation of control algorithms for relative attitude synchronization in a two satellite leader-follower formation. We present experimental results for the PID+ backstepping design of chapter 6 and the output feedback design in chapter 7.

INTRODUCTION

Chapter 2

Mathematical preliminaries

This chapter presents some mathematical preliminaries serving to make the thesis self-contained, and for ease of reference when reviewing the contained proofs and derivations. It also serves as an introduction to the rigid-body kinetic- and kinematic differential equations used throughout the thesis.

2.1 Notation

In the following, \mathbb{N} denotes all nonnegative integers, \mathbb{R} the set of real numbers, \mathbb{R}^n , $n \in \mathbb{N}$ the n -dimensional Euclidean space, $\mathbb{R}_{\geq 0}$ denotes the subset of all non-negative real numbers, $\mathbf{I}_{3 \times 3}$ the identity matrix of dimension 3×3 , $\mathbf{x} \in \mathbb{R}^n$ denotes a column vector of dimension n , i.e. $\mathbf{x} = [x_1, \dots, x_n]^T$, $x_i \in \mathbb{R}$, $\dot{\mathbf{x}} = \frac{d\mathbf{x}}{dt}$ denotes the time derivative of a vector, similarly, $\ddot{\mathbf{x}} = \frac{d^2\mathbf{x}}{dt^2}$, note that we use bold face letters to distinguish column vectors from scalar values, and bold faced capital letters to denote matrices, $SO(3)$ denotes the special orthogonal group of order 3,

A continuous function $\alpha : [0, a) \rightarrow [0, \infty)$ is said to belong to class \mathcal{K} if it is strictly increasing and $\alpha(0) = 0$. Moreover, it is said to belong to class \mathcal{K}_∞ if $a = \infty$ and $\alpha(r) \rightarrow \infty$ as $r \rightarrow \infty$. A continuous function $\beta : [0, a) \times [0, \infty) \rightarrow [0, \infty)$ is said to belong to class \mathcal{KL} if, for each fixed s , the mapping $\beta(r, s)$

\mathcal{B}_r denotes a closed ball in \mathbb{R}^n centered at the origin of radius r , i.e. $\mathcal{B}_r = \{\mathbf{x} \in \mathbb{R}^n \mid \|\mathbf{x}\| \leq r\}$

\mathcal{F}_j denotes coordinate frame j , and a column vector given with coordinates in this frame is denoted \mathbf{x}^j . A rotation matrix corresponding to a rotation from \mathcal{F}_a to \mathcal{F}_b is denoted \mathbb{R}_b^a . A unit-quaternion corresponding to a rotation matrix \mathbb{R}_b^a is denoted \mathbf{q}_{ab} .

$\mathbf{S}(\cdot)$ denotes a skew-symmetric matrix operator, given by

$$\mathbf{S}(\mathbf{z}) \triangleq \begin{bmatrix} 0 & -z_3 & 0 \\ z_3 & 0 & -z_1 \\ -z_2 & z_1 & 0 \end{bmatrix}. \quad (2.1)$$

2.2 Stability

2.2.1 General Stability

In this section we summarize some basic stability definitions for nonlinear systems. It should be noted that we work with stability of points, sets and trajectories in the sense of Lyapunov as first characterized in his work *The General Problem of the Stability of Motion*, published in Russia in 1892 (Lyapunov 1992).

In this context we say that an equilibrium point, \mathbf{x}^* , ($\mathbf{x}^* \in \mathbb{R}^n : f(t, \mathbf{x}^*) = 0$), is *stable* if any solution of the system stays arbitrarily close to it for all future time, *asymptotically stable* if in addition the solution converges asymptotically to the point, *exponentially stable* if the rate of convergence is exponential, and *unstable* if it is not stable. Furthermore, we can define a *region of attraction*, \mathbb{D} in which asymptotic or exponential convergence takes place. If this region covers the whole state-space (i.e. $\mathbb{D} = \mathbb{R}^n$) the equilibrium point is said to be *globally* exponentially stable or *globally* asymptotically stable.

The results presented in this thesis treat time-varying systems, and therefor consider *uniform* stability properties, i.e stability properties which are independent of the initial time t_0 . The following mathematical definition is given in (Khalil 2000)

Definition 2.1. *We consider the non-autonomous, nonlinear system of differential equations*

$$\dot{\mathbf{x}} = \mathbf{f}(t, \mathbf{x}), \quad (2.2)$$

$\mathbf{x} \in \mathbb{R}^n$, $\mathbf{f} : [0, \infty) \times \mathbb{R}^n \rightarrow \mathbb{R}^n$ is piecewise continuous in t and locally Lipschitz in \mathbf{x} on $[0, \infty) \times \mathbb{D}$, $\mathbb{D} \subset \mathbb{R}^n$, and $\mathbf{x} = 0$ is an equilibrium point for (2.2) at $t = 0$, i.e.

$$\mathbf{f}(t, 0) = 0, \quad \forall t \geq 0. \quad (2.3)$$

The equilibrium point is

- *stable* if, for each $\epsilon > 0$, there is $\delta = \delta(\epsilon, t_0) > 0$ such that

$$\|\mathbf{x}(t)\| < \delta \Rightarrow \|\mathbf{x}(t)\| < \epsilon, \quad \forall t \geq t_0 \geq 0. \quad (2.4)$$

- *uniformly locally stable (ULS)* if, for each $\epsilon > 0$, there is $\delta = \delta(\epsilon) > 0$, independent of t_0 such that (2.4) is satisfied.
- *or equivalently, uniformly stable* if and only if there exist a class \mathcal{K} function α and a positive constant c , independent of t_0 , such that

$$\|\mathbf{x}(t)\| \leq \alpha(\|\mathbf{x}(t_0)\|), \quad \forall t \geq t_0 \geq 0, \quad \forall \|\mathbf{x}(t_0)\| < c. \quad (2.5)$$

- *unstable* if it is not stable.

2.3. STABILITY THEOREMS

- *asymptotically stable (AS) if it is stable and there is a positive constant $c = c(t_0)$ such that $\mathbf{x}(t) \rightarrow 0$ as $t \rightarrow \infty$, for all $\|\mathbf{x}(t)\| < c$.*
- *uniformly locally asymptotically stable (ULAS) if it is uniformly stable and there is a positive constant c , independent of t_0 , such that for all $\|\mathbf{x}(t_0)\| < c$, $\mathbf{x} \rightarrow 0$ as $t \rightarrow \infty$, uniformly in t_0 ; that is, for each $\eta > 0$, there is $T = T(\eta) > 0$ such that*

$$\|\mathbf{x}(t)\| < \eta, \quad \forall t \geq t_0 + T(\eta), \quad \forall \|\mathbf{x}(t_0)\| < c. \quad (2.6)$$

- *or equivalently, uniformly locally asymptotically stable if and only if there exist a class \mathcal{KL} function β and a positive constant c , independent of t_0 , such that*

$$\|\mathbf{x}(t)\| \leq \beta(\|\mathbf{x}(t_0)\|, t - t_0), \quad \forall t \geq t_0 \geq 0, \quad \forall \|\mathbf{x}(t_0)\| < c. \quad (2.7)$$

- *uniformly globally asymptotically stable (UGAS) if it is uniformly stable, $\delta(\epsilon)$ can be chosen to satisfy $\lim_{\epsilon \rightarrow \infty} \delta(\epsilon) = \infty$, and, for each pair of positive numbers η and c , there is $T = T(\eta, c) > 0$ such that*

$$\|\mathbf{x}(t)\| < \eta, \quad \forall t \geq t_0 + T(\eta, c), \quad \forall \|\mathbf{x}(t_0)\| < c. \quad (2.8)$$

- *or equivalently, uniformly globally asymptotically stable if and only if inequality (2.7) is satisfied for any initial state $\mathbf{x}(t_0)$.*
- *uniformly locally exponentially stable (ULES) if there exists positive constants c , k , and λ such that for all $t \geq t_0 \geq 0$*

$$\|\mathbf{x}(t)\| \leq k\|\mathbf{x}(t_0)\|e^{-\lambda(t-t_0)}, \quad \forall \|\mathbf{x}(t_0)\| < c. \quad (2.9)$$

- *uniformly globally exponentially stable (UGES) if (2.9) is satisfied for any initial state $\mathbf{x}(t_0)$.*

2.3 Stability theorems

2.3.1 Practical stability

The following definitions and corollaries can be found in (Chaillet 2006, Kristiansen 2008).

For parameterized nonlinear systems of the form

$$\dot{\mathbf{x}} = \mathbf{f}(t, \mathbf{x}, \boldsymbol{\theta}) \quad (2.10)$$

where $\mathbf{f}(t, \mathbf{x}, \boldsymbol{\theta}) : [0, \infty) \times \mathbb{R}^n \times \mathbb{R}^m \rightarrow \mathbb{R}^n$ is locally Lipschitz in \mathbf{x} and piecewise continuous in t for $\boldsymbol{\theta}$ under consideration, the following stability definition is used:

MATHEMATICAL PRELIMINARIES

Definition 2.2. (*Uniform practical asymptotic stability*) Let $\Theta \subset \mathbb{R}^m$ be a set of parameters. The system (2.10) is said to be uniformly practically asymptotically stable (UPAS) on Θ if, given any $\Delta > \delta > 0$ such that $\mathcal{B}_\Delta \subseteq \mathbb{D} \subset \mathbb{R}^n$, there exists $\theta^* \in \Theta$ s.t. for $\dot{\mathbf{x}} = \mathbf{f}(t, \mathbf{x}, \theta^*)$ the ball \mathcal{B}_δ is uniformly asymptotically stable on \mathcal{B}_Δ .

The following corollary was given in (Kristiansen 2008), and applies to the practical stability analysis of systems with a Lyapunov function that can be upper and lower bounded by a polynomial function.

Corollary 2.1. Let $\sigma_i : \mathbb{R}^m \rightarrow \mathbb{R}_{\geq 0}, i \in \{1, \dots, N\}$, be continuous functions, positive over Θ , and let $\underline{a}, \bar{a}, q$ and Δ be positive constants. Assume that, for any $\theta \in \Theta$, there exists a continuously differentiable Lyapunov function $V : \mathbb{R}_{\geq 0} \times \mathbb{D} \rightarrow \mathbb{R}_{\geq 0}$ satisfying, for all $\mathbf{x} \in \mathbb{D}$ and all $t \geq 0$,

$$\underline{a} \min \{\sigma_i(\theta)\} \|\mathbf{x}\|^q \leq V(t, \mathbf{x}) \leq \bar{a} \max \{\sigma_i(\theta)\} \|\mathbf{x}\|^q. \quad (2.11)$$

Assume also that for any $\delta \in (0, \Delta)$, there exists a parameter $\theta^*(\delta) \in \Theta$ and a class \mathcal{K} function α_δ such that, for all $\|\mathbf{x}\| \in [\delta, \Delta]$ and all $t \geq 0$,

$$\frac{\partial V}{\partial t}(t, \mathbf{x}) + \frac{\partial V}{\partial \mathbf{x}}(t, \mathbf{x})\mathbf{f}(t, \mathbf{x}, \theta^*) \leq -\alpha_\delta(\|\mathbf{x}\|). \quad (2.12)$$

Assume also that for all $i \in \{1, \dots, N\}$,

$$\lim_{\delta \rightarrow 0} \sigma_i(\theta^*(\delta))\delta^q = 0 \qquad \lim_{\delta \rightarrow 0} \sigma_i(\theta^*(\delta)) \neq 0. \quad (2.13)$$

Then, the system $\dot{\mathbf{x}} = \mathbf{f}(t, \mathbf{x}, \theta)$ is UPAS on the parameter set Θ . Moreover, when $\delta = 0$ and the parameter θ^* is independent of δ , the conditions in (2.13) are no longer required, and the system $\dot{\mathbf{x}} = \mathbf{f}(t, \mathbf{x}, \theta)$ is UAS.

Note that the domain defined by \mathcal{B}_δ in the above corollary, can be arbitrarily diminished.

2.3.2 Matrosov’s Theorem

This theorem is useful for analyzing nonlinear time-varying (NLTV) closed loop systems where the Lyapunov function candidate derivative is semi-definite. For time invariant systems the solution is to use LaSalle’s invariance principle. For NLTV systems this result can not be invoked. A common solution is to use Barbalat’s convergence result, but this does not allow for asymptotic stability. In this work we instead use stability results due to Matrosov (Matrosov 1962) as they were reported in (Hahn 1967), and a generalization of this result as it was given in (Loria, Panteley, Popovic & Teel 2002).

Theorem 2.3 (Matrosov’s theorem (Hahn 1967)). *Given the system*

$$\dot{x} = f(t, x) \quad (2.14)$$

Let two functions $V(x, t)$ and $W(x, t)$ be given which are continuous on the domain \mathbb{D} and satisfy:

Assumption 2.1. *$V(x, t)$ is positive definite and decreesent.*

Assumption 2.2. *The derivative \dot{V} can be bounded from above by a non-positive continuous t -independent function $U(x)$.*

Assumption 2.3. *The function $W(t, x)$ is bounded.*

Assumption 2.4. *The derivative \dot{W} is definitely non-zero on the set*

$$\mathbb{N} = \{x | U(x) = 0\}. \quad (2.15)$$

Then the equilibrium of (2.14) is uniformly asymptotically stable on \mathbb{D} .

Theorem 2.4 (Generalized Matrosov’s theorem (Loria et al. 2002)). *Under the following assumptions the origin of the system*

$$\dot{x} = f(t, x) \quad (2.16)$$

is UGAS.

Assumption 2.5. *The origin of the system (2.2) is UGS.*

Assumption 2.6. *There exist integers $j, m > 0$ and for each $\Delta > 0$ there exist*

- *a number $\mu > 0$*
- *locally Lipschitz continuous functions $V_i : \mathbb{R} \times \mathbb{R}^n \rightarrow \mathbb{R}, i \in \{1, \dots, m\}$*
- *a (continuous) function $\phi : \mathbb{R} \times \mathbb{R}^n \rightarrow \mathbb{R}^m, i \in \{1, \dots, m\}$*
- *continuous functions $Y_i : \mathbb{R}^n \times \mathbb{R}^m \rightarrow \mathbb{R}, i \in \{1, \dots, j\}$*

such that, for almost all $(t, x) \in \mathbb{R} \times \mathcal{B}(\Delta)^1$,

$$\max\{|V_i(t, x)|, |\phi(t, x)|\} \leq \mu, \quad (2.17)$$

$$\dot{V}_i(t, x) \leq Y_i(x, \phi(t, x)). \quad (2.18)$$

Assumption 2.7. *For each integer $k \in \{1, \dots, j\}$ we have that*

$$\{(z, \psi) \in \mathcal{B}(\Delta) \times \mathcal{B}(\mu), Y_i(z, \psi) = 0 \forall i \in \{1, \dots, k-1\}\} \Rightarrow \{Y_k(z, \psi) \leq 0\}. \quad (2.19)$$

Assumption 2.8. *We have that*

$$\{(z, \psi) \in \mathcal{B}(\Delta) \times \mathcal{B}(\mu), Y_i(z, \psi) = 0 \forall i \in \{1, \dots, j\}\} \Rightarrow \{z = 0\}. \quad (2.20)$$

¹ $\mathcal{B}(\Delta) = \{x \in \mathbb{R}^n | \|x\| \leq \Delta\}$

MATHEMATICAL PRELIMINARIES

2.3.3 Barbalat’s lemma

Lemma 2.1 (Barbalat’s Lemma (Khalil 2000)). *Let $\phi : \mathbb{R} \rightarrow \mathbb{R}$ be a uniformly continuous function on $[0, \infty)$. Suppose that $\lim_{t \rightarrow \infty} \int_0^t \phi(\tau) d\tau$ exists and is finite. Then,*

$$\phi(t) \rightarrow 0 \quad \text{as } t \rightarrow \infty. \quad (2.21)$$

2.3.4 LaSalle’s invariance principle

Theorem 2.5 (LaSalle’s invariance theorem (Khalil 2000)). *Given the autonomous system*

$$\dot{x} = f(x), \quad (2.22)$$

with $x = 0$ as the only equilibrium point. Given that there exists a Lyapunov function V such that:

- $V : \mathbb{R}^n \rightarrow \mathbb{R}, V > 0$, continuously differentiable, radially unbound
- $\dot{V}(x) \leq 0 \quad \forall x \in \mathbb{R}^n$
- *Suppose no other solution than the trivial solution $x(t) \equiv 0$ can stay identically in*
 $S = \left\{ x \in \mathbb{R}^n \mid \dot{V}(x) = 0 \right\}$

Then, the origin is globally asymptotically stable (GAS).

2.3.5 Lyapunov’s direct method

Theorem 2.6 (Uniform stability (Khalil 2000)). *Let $x = 0$ be an equilibrium point for (2.2) and $\mathbb{D} \subset \mathbb{R}^n$ be a domain containing $x = 0$. Let $V : \mathbb{R}_{\geq 0} \times \mathbb{D} \rightarrow \mathbb{R}$ be a continuously differentiable function such that*

$$W_1(x) \leq V(t, x) \leq W_2(x) \quad (2.23)$$

$$\frac{\partial V}{\partial t} + \frac{\partial V}{\partial x} f(t, x) \leq 0 \quad (2.24)$$

$\forall t \geq 0$ and $\forall x \in \mathbb{D}$, where $W_1(x)$ and $W_2(x)$ are continuous positive definite functions on \mathbb{D} . Then, $x = 0$ is uniformly stable. If $\mathbb{D} = \mathbb{R}^n$, then $x = 0$ is uniformly globally stable.

Theorem 2.7 (Uniform global exponential stability (Khalil 2000)). *Let $x = 0$ be an equilibrium point of (2.2) and $\mathbb{D} \subset \mathbb{R}^n$ be a domain containing the origin. Let $V : \mathbb{R}_{\geq 0} \times \mathbb{D} \rightarrow \mathbb{R}$ be a continuously differentiable function such that*

$$k_1 \|s\|^a \leq V(t, x) \leq k_2 \|x\|^a \quad (2.25)$$

2.3. STABILITY THEOREMS

$$\frac{\partial V}{\partial t} + \frac{\partial V}{\partial t} f(t, x) \leq -k_3 \|x\|^a \quad (2.26)$$

$\forall t \geq 0$ and $\forall x \in \mathbb{D}$, where k_1 , k_2 , k_3 , and a are positive constants. Then $x = 0$ is uniformly exponentially stable. If the assumptions hold globally, then $x = 0$ is uniformly globally exponentially stable (UGES).

MATHEMATICAL PRELIMINARIES

Chapter 3

Mathematical modeling

In this chapter differential equations governing the satellite attitude motion are given. The derivations are based on the work presented in (Wertz 1978, Hughes 1986, Egeland & Gravdahl 2002). Specifically, we present coordinate frames and attitude parameterizations used, and the kinematical differential equations describing motion in each parameterization, we also give the dynamical equations of motion relating change of angular velocity to external and internal moments. Finally we give an introduction to the external and internal disturbance and control moments that affect spacecraft.

3.1 Coordinate frames

To represent the attitude of a rotating rigid body we first introduce the concept of coordinate frames. The most convenient coordinate for our use is a dextral orthonormal triad, i.e. coordinate frames given by a set of three orthonormal reference vectors that obey the right hand rule. We use \mathcal{F}_a to denote a coordinate frame constructed from the vectors \vec{a}_1 , \vec{a}_2 and \vec{a}_3 , see fig. 3.1.

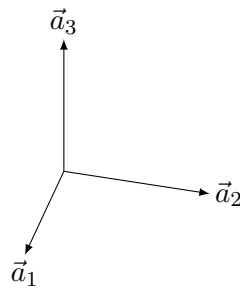


Figure 3.1: Coordinate frame \mathcal{F}_a

3.1.1 Earth-centered inertial frame

This reference frame has its origin in the center of the Earth with the x_i -axis pointing in the vernal equinox direction, Υ . This is in the direction of the vector from the center of the Sun through the center of the Earth during vernal equinox. The y_i -axis points 90° east, spanning the equatorial plane together with the x_i -axis. The z_i -axis points through the North Pole, completing the right-hand system. In the following this frame will be denoted by \mathcal{F}_i .

3.1.2 Orbit frame

This frame, denoted \mathcal{F}_o , has its origin in the satellite’s center of gravity. The z_o -axis points in the nadir direction. The y_o -axis points in the direction of the negative orbit normal. The x_o -axis is chosen as to complete a right-hand coordinate system.

3.1.3 Body fixed frame

The body fixed frame, denoted \mathcal{F}_j , where $j = b$ for single vehicle control schemes, $j \in \{l, f\}$ in leader-follower type schemes and $j \in \{1, \dots, n\}$ in multi-vehicle synchronization schemes. A body fixed frame, has its origin at the center of gravity of the vehicle with the axes pointing along the principal axes of inertia of the satellite.

3.2 Rotation matrices

To represent the attitude of one reference frame relative to another, and to transform a vector between reference frames, we introduce rotation matrices.

Definition 3.1. A rotation matrix is defined as any matrix \mathbf{R} member of the special orthonormal group of order three, $SO(3)$, defined as

$$SO(3) \triangleq \{ \mathbf{R} | \mathbf{R} \in \mathbb{R}^{3 \times 3}, \mathbf{R}^T \mathbf{R} = \mathbf{I}_{3 \times 3}, \det \mathbf{R} = 1 \}. \quad (3.1)$$

To transform a vector $\mathbf{v} \in \mathbb{R}^3$ between \mathcal{F}_a and \mathcal{F}_b we use the notation

$$\mathbf{v}^a = \mathbf{R}_b^a \mathbf{v}^b. \quad (3.2)$$

where \mathbf{R}_b^a is called the rotation matrix from \mathcal{F}_a to \mathcal{F}_b , and is defined as (Egeland & Gravdahl 2002)

$$\mathbf{R}_b^a = \{ \vec{a}_i \cdot \vec{b}_j \}. \quad (3.3)$$

The elements $r_{ij} = \{ \vec{a}_i \cdot \vec{b}_j \}$ are called *directional cosines*, and a rotation matrix is therefore often referred to as a directional cosine matrix.

3.3. KINEMATIC EQUATIONS

For any v^b we have

$$v^b = \mathbf{R}_a^b a = \mathbf{R}_a^b \mathbf{R}_b^a v^b, \quad (3.4)$$

which implies

$$\mathbf{R}_a^b \mathbf{R}_b^a = \mathbf{I}_{3 \times 3} \quad (3.5)$$

and

$$\mathbf{R}_a^b = (\mathbf{R}_b^a)^{-1} = (\mathbf{R}_b^a)^T \quad (3.6)$$

A rotation between frames \mathcal{F}_a and \mathcal{F}_c can be described as a composite rotation by including an intermediate frame \mathcal{F}_b , i.e.

$$\mathbf{R}_c^a = \mathbf{R}_b^a \mathbf{R}_c^b. \quad (3.7)$$

Such a composite rotation may be extended to include two or more intermediate rotations, i.e.

$$\mathbf{R}_d^a = \mathbf{R}_b^a \mathbf{R}_c^b \mathbf{R}_d^c. \quad (3.8)$$

3.3 Kinematic equations

The rotational kinematic of a rigid body, are the differential equations that relate change of orientation to the body’s angular velocity. As shown both in Hughes (1986) and Ege-land & Gravdahl (2002), for SO(3) this relation is given by

$$\dot{\mathbf{R}}_b^a = \mathbf{R}_b^a \mathbf{S}(\omega_{ab}^b) = \mathbf{S}(\omega_{ab}^a) \mathbf{R}_b^a, \quad (3.9)$$

where ω_{ab}^a and ω_{ab}^b denote the angular velocity of the the coordinate frame \mathcal{F}_b relative to \mathcal{F}_a , referenced in \mathcal{F}_b and \mathcal{F}_b respectively.

3.4 Attitude parameterizations

The rotation matrix representation of attitude can be cumbersome both for control and implementation purposes. It can also be hard to interpret physical results and evaluate performance by reviewing the 9 parameters of the rotation matrix. For these reasons one usually introduce an attitude representation of SO(3), which reduces the number of parameters. For a complete survey of available attitude parameterizations the interested reader is referred to (Shuster 1993) and (Hughes 1986).

The rotation matrix has 9 parameters and in addition 6 constraints imposed by the orthonormality of the basis vectors. A minimal representation of SO(3) has 3 parameters and no constraints. However this reduction does introduce a geometric singularity, caused by the fact that these representations are only locally one-to-one and onto mappings of the rotation matrix. Examples of such parameterizations include the Euler angles and

MATHEMATICAL MODELING

the modified Rodriguez parameters. The smallest representations which avoid geometric singularities are 4 parameter representations with 1 constraint (Wen & Kreutz-Delgado 1991), such as the quaternion and the angle-axis parameterization.

3.4.1 Angle-axis

The angle-axis representation of attitude stems directly from Euler’s theorem:

The general displacement of a rigid body with one point fixed is a rotation about some axis.

That is, given a frame \mathcal{F}_b which is rotated with respect to a frame \mathcal{F}_a about their common origin, this rotation can be represented by a rotation ϕ about an axis \vec{k} of unit length, through their common origin. We thus have 4 parameters (ϕ and the elements of \vec{k}), and one constraint $\mathbf{k}^T \mathbf{k} = 1$. The parameters can be obtained from the eigenvalues and eigenvectors of the rotation matrix.

Angle-axis rotation matrix

The rotation matrix corresponding to the angle-axis parameterization is written

$$\mathbf{R}_b^a = \cos \phi \mathbf{I}_{3 \times 3} + \sin \phi \mathbf{S}(\mathbf{k}^a) + (1 - \cos \phi) \mathbf{k}^a (\mathbf{k}^a)^T. \quad (3.10)$$

Though the angle-axis has some attractive properties for control purposes, such as representing and controlling robot manipulator end-effector attitude, angle-axis parameters are here used to define the Euler parameters.

3.4.2 Euler angles

As described in section 3.2 on the rotation matrix, any rotation can be described as a composite rotation, i.e. any rotation matrix can be given as product of other rotation matrices. This is the basis for the Euler angle parameterization, in which a rotation is given by three principal rotations. 24 variations exist, but the most common are the *classical Euler angles* given by

$$\mathbf{R}_b^a = \mathbf{R}_z(\psi) \mathbf{R}_y(\theta) \mathbf{R}_z(\phi), \quad (3.11)$$

and what is commonly known as the *roll-pitch-yaw* angles

$$\mathbf{R}_b^a = \mathbf{R}_z(\psi) \mathbf{R}_y(\theta) \mathbf{R}_x(\phi), \quad (3.12)$$

3.4. ATTITUDE PARAMETERIZATIONS

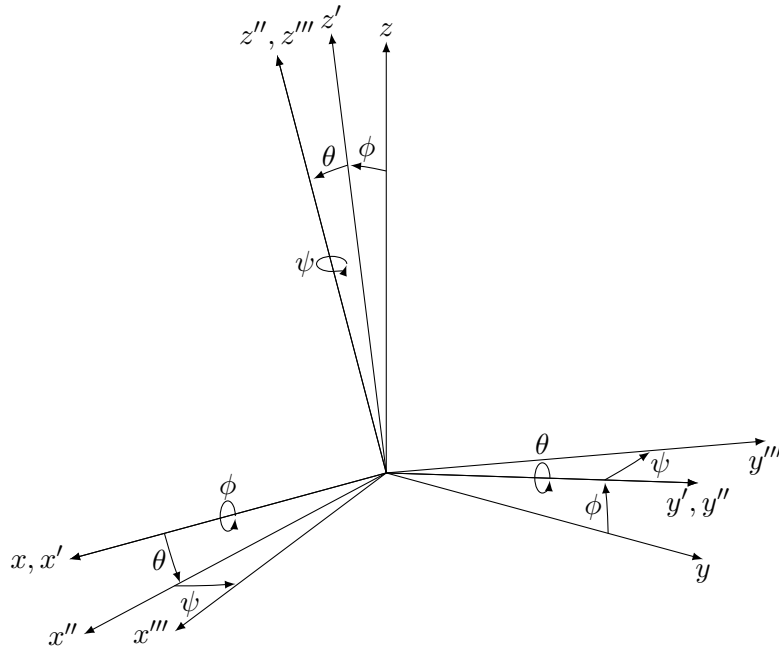


Figure 3.2: Roll-pitch-yaw Euler angles illustration. The figure illustrates a rotation from \mathcal{F}_a to $\mathcal{F}_{a''''}$ via two intermediate frames. We first rotate \mathcal{F}_a an angle ϕ about the x -axis, then the resulting frame is rotated an angle θ about the y' -axis, then finally we obtain the $\mathcal{F}_{a''''}$ by rotating $\mathcal{F}_{a''}$ an angle ψ about the z'' -axis.

where the principal rotation matrices are given by

$$\mathbf{R}_x(\phi) = \begin{bmatrix} 1 & 0 & 0 \\ 0 & \cos \phi & -\sin \phi \\ 0 & \sin \phi & \cos \phi \end{bmatrix} \quad (3.13)$$

$$\mathbf{R}_y(\theta) = \begin{bmatrix} \cos \theta & 0 & \sin \theta \\ 0 & 1 & 0 \\ -\sin \theta & 0 & \cos \theta \end{bmatrix} \quad (3.14)$$

$$\mathbf{R}_z(\psi) = \begin{bmatrix} \cos \psi & -\sin \psi & 0 \\ \sin \psi & \cos \psi & 0 \\ 0 & 0 & 1 \end{bmatrix}. \quad (3.15)$$

The subscripts refer to the axis of the *current frame*, i.e. the rotated body frame, as illustrated in figure 3.2.

MATHEMATICAL MODELING

The complete rotation may be written

$$\mathbf{R}_b^a = \begin{bmatrix} c(\phi)c(\theta) & c(\phi)s(\theta)s(\psi) - s(\phi)c(\psi) & c(\phi)s(\theta)c(\psi) + s(\phi)s(\psi) \\ s(\phi)c(\theta) & s(\phi)s(\theta)s(\psi) + c(\phi)c(\psi) & s(\phi)s(\theta)c(\psi) - c(\phi)s(\psi) \\ -s(\theta) & c(\theta)s(\psi) & c(\theta)c(\psi) \end{bmatrix}, \quad (3.16)$$

where $c(\cdot) = \cos(\cdot)$ and $s(\cdot) = \sin(\cdot)$

This is a three parameter representation (ϕ, θ, ψ) with no constraints, and as such will contain a singularity. For the classical Euler angles this singularity manifests itself at $\theta = 0$. This is an inconvenient position for control purposes, as this places the singularity at the reference condition attitude. For the roll-pitch-yaw angles the singularity is moved to $\theta = \pm\frac{\pi}{2}$, which is convenient for most applications. Since this attitude is avoided in most aerospace and marine applications.

Kinematic differential equation

To describe the rotational kinematic of (3.9) in terms of the Euler angle parameterization, we first note that

$$\boldsymbol{\omega}_{ab}^b = \begin{bmatrix} \dot{\phi} \\ 0 \\ 0 \end{bmatrix} + \mathbf{R}_x^T(\phi) \begin{bmatrix} 0 \\ \dot{\theta} \\ 0 \end{bmatrix} + \mathbf{R}_x^T(\phi)\mathbf{R}_y^T(\theta) \begin{bmatrix} 0 \\ 0 \\ \dot{\psi} \end{bmatrix} \quad (3.17)$$

$$= \begin{bmatrix} 1 & 0 & -\sin\theta \\ 0 & \cos\phi & \sin\phi\cos\theta \\ 0 & -\sin\phi & \cos\phi\cos\theta \end{bmatrix} \dot{\boldsymbol{\Theta}} = \mathbf{T}(\boldsymbol{\Theta})^{-1}\dot{\boldsymbol{\Theta}}, \quad (3.18)$$

where $\boldsymbol{\Theta} = [\phi, \theta, \psi]^T$, and from which it is straightforward to obtain

$$\dot{\boldsymbol{\Theta}} = \mathbf{T}(\boldsymbol{\Theta})\boldsymbol{\omega}_{ab}^b, \quad (3.19)$$

where

$$\mathbf{T}(\boldsymbol{\Theta}) = \frac{1}{\cos\theta} \begin{bmatrix} \cos\theta & \sin\phi\sin\theta & \cos\phi\sin\theta \\ 0 & \cos\phi\cos\theta & \sin\phi\cos\theta \\ 0 & \sin\phi & \cos\phi \end{bmatrix}. \quad (3.20)$$

The singularity is here even clearer, as the matrix $\mathbf{T}(\boldsymbol{\Theta})$ is undefined for $\theta = \pm\frac{\pi}{2}$.

3.4.3 The Euler parameters

A parameterization which is advantageous for control, implementation and simulation purposes, is the Euler parameters or unit quaternion. They follow directly from the angle-axis representation, and as such is a 4 parameter representation with one constraint, and

3.4. ATTITUDE PARAMETERIZATIONS

non-singular for all attitudes. Using the angle axis parameters (\mathbf{k}, θ) the Euler parameters are defined by

$$\eta = \cos \frac{\theta}{2} \quad (3.21)$$

$$\boldsymbol{\epsilon} = \mathbf{k} \sin \frac{\theta}{2}, \quad (3.22)$$

with the constraint $\eta^2 + \boldsymbol{\epsilon}^T \boldsymbol{\epsilon} = 1$.

Quaternion properties

To take advantage of the quaternion properties of the Euler parameters we introduce the vector

$$\mathbf{q}_{ab} = [\eta \quad \boldsymbol{\epsilon}^T]^T, \quad (3.23)$$

corresponding to the rotation matrix \mathbf{R}_b^a .

Given \mathbf{q}_{ab} and \mathbf{q}_{ac} corresponding to \mathbf{R}_b^a and \mathbf{R}_c^a , we have that

$$\mathbf{R}_c^a = \mathbf{R}_b^a \mathbf{R}_c^b \quad (3.24)$$

corresponds to

$$\mathbf{q}_{ac} = \mathbf{q}_{ab} \otimes \mathbf{q}_{bc}, \quad (3.25)$$

where \otimes denotes the quaternion product defined in A.8. This is useful when defining error variables, i.e. given \mathbf{R}_b^a and \mathbf{R}_c^a with corresponding quaternions \mathbf{q}_{ab} and \mathbf{q}_{ac} , the relative orientation between frames \mathcal{F}_b and \mathcal{F}_c , given by

$$\mathbf{R}_c^b = \mathbf{R}_a^b \mathbf{R}_c^a = (\mathbf{R}_b^a)^{-1} \quad (3.26)$$

which in quaternion notation equates to

$$\mathbf{q}_{bc} = \mathbf{q}_{ba} \otimes \mathbf{q}_{ac} = \mathbf{q}_{ab}^{-1} \otimes \mathbf{q}_{ac} \quad (3.27)$$

where we have used that the inverse quaternion, defined

$$\mathbf{q}^{-1} \triangleq \begin{bmatrix} \eta \\ -\boldsymbol{\epsilon} \end{bmatrix} \quad (3.28)$$

corresponds to the reverse rotation \mathbf{R}^{-1} .

Rotation matrix

The rotation matrix \mathbf{R}_b^a corresponding to the quaternion \mathbf{q}_{ab} is given by

$$\mathbf{R}_b^a = \mathbf{R}_e(\eta, \boldsymbol{\epsilon}) = \mathbf{I} + 2\eta \mathbf{S}(\boldsymbol{\epsilon}) + 2\mathbf{S}(\boldsymbol{\epsilon})^2 \quad (3.29)$$

$$= \begin{bmatrix} 1 - 2(\epsilon_2^2 + \epsilon_3^2) & 2(\epsilon_1\epsilon_2 - \eta\epsilon_3) & 2(\epsilon_1\epsilon_3 + \eta\epsilon_2) \\ 2(\epsilon_1\epsilon_2 + \eta\epsilon_3) & 1 - 2(\epsilon_1^2 + \epsilon_3^2) & 2(\epsilon_2\epsilon_3 - \eta\epsilon_1) \\ 2(\epsilon_1\epsilon_2 + \eta\epsilon_3) & 2(\epsilon_2\epsilon_3 + \eta\epsilon_1) & 1 - 2(\epsilon_1^2 + \epsilon_2^2) \end{bmatrix}. \quad (3.30)$$

which in contrast to (3.16) is invertible for all orientations.

Kinematic differential equation

The kinematic differential equations in terms of Euler parameters are given by

$$\dot{\mathbf{q}}_{ab} = \frac{1}{2} \begin{bmatrix} 0 \\ \boldsymbol{\omega}_{ab}^a \end{bmatrix} \otimes \mathbf{q}_{ab} = \frac{1}{2} \mathbf{q}_{ab} \otimes \begin{bmatrix} 0 \\ \boldsymbol{\omega}_{ab}^b \end{bmatrix} \quad (3.31)$$

where $\boldsymbol{\omega}_{ab}^a$ and $\boldsymbol{\omega}_{ab}^b$ are the angular velocity of frame \mathcal{F}_b relative to \mathcal{F}_a , referenced in \mathcal{F}_a and \mathcal{F}_b respectively. The details of this derivation are given in appendix A.3. Using normal vector notation (3.31) may be written

$$\dot{\eta} = -\frac{1}{2} \boldsymbol{\epsilon}^T \boldsymbol{\omega}_{ab}^b = -\frac{1}{2} \boldsymbol{\epsilon}^T \boldsymbol{\omega}_{ab}^a, \quad (3.32)$$

$$\dot{\boldsymbol{\epsilon}} = \frac{1}{2} (\eta \mathbf{I}_{3 \times 3} + \mathbf{S}(\boldsymbol{\epsilon})) \boldsymbol{\omega}_{ab}^b = \frac{1}{2} (\eta \mathbf{I}_{3 \times 3} - \mathbf{S}(\boldsymbol{\epsilon})) \boldsymbol{\omega}_{ab}^a. \quad (3.33)$$

3.4.4 Modified Rodriguez parameters

This is an attitude parameterization which is attractive for control purposes due to its non-singular inverse kinematics. (Shuster 1993, Tsiotras 1996).

The parameterization is defined from the quaternion $\mathbf{q}_{ab} = [\eta, \boldsymbol{\epsilon}^T]^T$ as

$$\boldsymbol{\sigma}_{ab} \triangleq \frac{\boldsymbol{\epsilon}}{1 + \eta}. \quad (3.34)$$

corresponding to the rotation matrix \mathbf{R}_b^a .

The modified Rodriguez parameters representation is a minimal representation, and therefore contains a singularity, which can easily be identified from (3.34) as the point $\eta_{ab} = -1$. The advantage when compared to other minimal representations is that the singularity is moved as far from the equilibrium as possible, that is the singularity is at $\pm 360^\circ$.

Kinematic differential equation

The kinematic differential equation in terms of the modified Rodriguez parameter is given by

$$\dot{\boldsymbol{\sigma}}_{ab} = \mathbf{G}(\boldsymbol{\sigma}_{ab}) \boldsymbol{\omega}_{ab}^b \quad (3.35)$$

where $\boldsymbol{\sigma}_{ab}$ corresponds to \mathbf{R}_b^a , $\boldsymbol{\omega}_{ab}^b$ is the angular velocity of frame \mathcal{F}_b relative to \mathcal{F}_a , and

$$\mathbf{G}(\boldsymbol{\sigma}_{ab}) \triangleq \frac{1}{4} ((1 - \boldsymbol{\sigma}_{ab}^T \boldsymbol{\sigma}_{ab}) \mathbf{I} + 2\mathbf{S}(\boldsymbol{\sigma}_{ab}) - \boldsymbol{\sigma}_{ab} \boldsymbol{\sigma}_{ab}^T). \quad (3.36)$$

Note that $\mathbf{G}^{-1}(\boldsymbol{\sigma}_{ab})$ is well defined for all $\boldsymbol{\sigma}_{ab}$, a property we take advantage of in chapter 6.

3.5 The dynamical model

The dynamical model of a rigid body relates the change of angular velocity to the internal and external moments acting on the body. In this section we give models both for vehicles actuated by means of external actuator (thrusters, magnetic torquers, solar sail) and internal actuators (momentum wheels, reaction wheels).

3.5.1 Externally actuated rigid body

The dynamical model for a rigid body actuated by means of external moments and subject to external disturbance moments is given by Euler’s momentum equation

$$\dot{\omega}_{ib}^b = \mathbf{S} \left(\mathbf{J}_b \omega_{ib}^b \right) \omega_{ib}^b + \tau_a^b + \tau_d^b, \quad (3.37)$$

where ω_{ib}^b is the angular velocity of the body relative to an inertial frame, \mathbf{J}_b is the body inertia matrix, τ_a^b is the control input, and τ_d^b disturbance moments.

3.5.2 Internally actuated rigid body

Using Newton-Euler equations of motion, a mathematical model for an internally actuated vehicle is given. The vehicle consists of an assumed rigid structure, with electronic devices, sensors, etc., and four reaction wheels which are spinning about a fixed axis of inertial symmetry, such that the total moment of inertia may be assumed constant in the body frame. Such a mechanical device, consisting of a rigid body combined with several spinning rotors or wheels, is commonly referred to as a gyrostat (Hughes 1986).

Looking at figure 3.3, one can see the placement of the mass centra of the body, the i ’th wheel and the total mass marked \oplus_b , \oplus_w and \oplus respectively. To derive a general model, it will be developed in the O coordinate system displaced from the center of mass. The total mass m is equal to the sum of the mass of the wheels and the rigid body:

$$m = m_b + \sum_{i=1}^4 m_{w,i}, \quad (3.38)$$

where m_b is the mass of the rigid structure and $m_{w,i}$ is the mass of the i ’th wheel. We define the first and second moment of inertia about the point O as

$$\vec{c} = \vec{c}_b + \sum_{i=1}^4 m_{w,i} \vec{b}_i \quad (3.39)$$

$$\vec{J} = \vec{J}_b + \sum_{i=1}^4 \vec{I}_{w,i} + m_{w,i} (b_i^2 \vec{1} - \vec{b}_i \vec{b}_i), \quad (3.40)$$

MATHEMATICAL MODELING

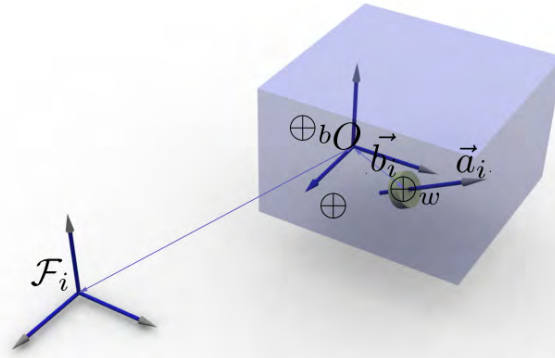


Figure 3.3: Gyrostat illustration

where \vec{c}_b is the first moment of inertia of the rigid body, \vec{b}_i is the vector from O to the i 'th wheel's center of mass, \vec{J}_b is the (second) moment of inertia of the body about O .

We may now define the linear and angular momenta of the rigid body and wheel i as

$$\vec{p}_b = m_b \vec{v} + \vec{\omega}_{ib} \times \vec{c}_b \quad (3.41)$$

$$\vec{p}_{w,i} = m_w \vec{v} + m_{w,i} \vec{\omega}_{ib} \times \vec{b}_i \quad (3.42)$$

$$\vec{h}_{b/o} = \vec{c}_b \times \vec{v} + \vec{J}_b \cdot \vec{\omega}_{ib} \quad (3.43)$$

$$\vec{h}_{w,i/c} = \vec{I}_{w,i} \cdot \vec{\omega}_{w,i}, \quad (3.44)$$

where \vec{p}_b is the linear momentum of the rigid body, $\vec{p}_{w,i}$ is the linear momentum of the i 'th wheel, $\vec{h}_{b/o}$ is the angular momentum about O , $\vec{h}_{w,i/c}$ is the angular momentum about the i 'th wheel's center of gravity, \vec{v} is the linear velocity, $\vec{\omega}_{ib}$ is the angular velocity of the body with respect to \mathcal{F}_i and $\vec{\omega}_{w,i}$ is the angular velocity of the wheel frame with respect to \mathcal{F}_i .

The total angular momentum about O , $\vec{h}_{/o}$, can now be written as

$$\vec{h}_{/o} = \vec{h}_{b/o} + \sum_{i=1}^m (\vec{h}_{w,i/c} + \vec{b}_i \times \vec{p}_{w,i}), \quad (3.45)$$

3.5. THE DYNAMICAL MODEL

where m is the number of wheels, and we have used that the the angular momentum about a point O is equal to the angular momentum about the center of gravity plus the vector between O and $\oplus_{w,i}$ crossed with the linear momentum. Using the assumption of axial symmetry of the wheels and some algebraic manipulations, the expression may be written as

$$\vec{h}_{/o} = \vec{c} \times \vec{v} + \vec{J} \cdot \vec{\omega}_{ib} + \sum_{i=1}^m \vec{a}_i I_{s,i} \omega_{s,i}, \quad (3.46)$$

where \vec{a}_i is the axial vector of the i 'th wheel, $I_{s,i}$ is the axial moment of inertia and $\omega_{s,i}$ is the angular velocity about the axis.

If we now apply that the change of total angular momentum is due to an external force on the gyrostat, and the time derivative of a vector in a rotating frame (A.6) we obtain the expression for the change of angular momentum as

$$\frac{{}^i d}{dt} \vec{h}_{/o} = \frac{{}^b d}{dt} \vec{h}_{/o} + \vec{\omega}_{ib} \times \vec{h}_{/o} \triangleq \vec{\tau}_e \quad (3.47)$$

$$= \vec{c} \times \frac{{}^b d}{dt} \vec{v} + \underbrace{\vec{J} \cdot \frac{{}^b d}{dt} \vec{\omega}_{ib} + \sum_{i=1}^m \vec{a}_i I_{s,i} \frac{d}{dt} \omega_{s,i}}_{\frac{{}^b d}{dt} \vec{h}} + \vec{\omega}_{ib} \times \vec{h}_{/o} \quad (3.48)$$

Next we derive the components of $\vec{h}_{w,i}$ along the axial direction

$$h_{a,i} = \vec{a}_i \cdot \vec{h}_{w,i} = \vec{a}_i \cdot \vec{I}_{w,i} \cdot \vec{\omega}_{w,i} \quad (3.49)$$

$$= \vec{a}_i \cdot (I_{t,i} \vec{1} + (I_{s,i} - I_{t,i}) \vec{a}_i \vec{a}_i) \cdot (\vec{\omega}_{ib} + \vec{a}_i \omega_{s,i}) \quad (3.50)$$

$$= I_{s,i} \vec{a}_i \cdot \vec{\omega}_{ib} + I_{s,i} \omega_{s,i}, \quad (3.51)$$

where it has been used that the wheel inertia may be written as

$$\vec{I}_{w,i} = I_{t,i} \vec{1} + (I_{s,i} - I_{t,i}) \vec{a}_i \vec{a}_i, \quad (3.52)$$

where $I_{t,i}$ is the total wheel inertia, $\vec{1}$ is the identity dyadic, and $I_{s,i}$ is the inertia about the axial direction.

We now write the expressions for the total angular momentum $\vec{h}_{/o}$ and axial angular momentum of the wheels in \mathcal{F}_b as

$$\mathbf{h}^b = \mathbf{J} \boldsymbol{\omega}_{ib}^b + \mathbf{A} \mathbf{I}_s \boldsymbol{\omega}_s \quad (3.53a)$$

$$\mathbf{h}_a = \mathbf{I}_s \mathbf{A}^T \boldsymbol{\omega}_{ib}^b + \mathbf{I}_s \boldsymbol{\omega}_s, \quad (3.53b)$$

where $\mathbf{A} \in \mathbb{R}^{3 \times m}$ is a matrix of wheel axis in body coordinates, $\mathbf{I}_s \in \mathbb{R}^{m \times m}$ a diagonal matrix of wheel axial inertias, $\boldsymbol{\omega}_s \in \mathbb{R}^m$ a vector of wheel velocities.

MATHEMATICAL MODELING

Writing (3.48) in coordinate form in \mathcal{F}_b , we obtain

$$\dot{\mathbf{h}}^b + \mathbf{S}(\boldsymbol{\omega}_{ib}^b)\mathbf{h}^b + \mathbf{S}(\mathbf{c}^b)\dot{v}^b = \boldsymbol{\tau}_e. \quad (3.54)$$

Through some manipulation using (3.53a), (3.53b) and (3.54) and assuming that the O coincides with the center of mass such that $\mathbf{c}^b \equiv 0$, we obtain the differential equation describing the rotational motion of the gyrostat as

$$\dot{\mathbf{h}}^b = \mathbf{S}(\mathbf{h}^b)\bar{\mathbf{J}}^{-1}(\mathbf{h}^b - \mathbf{A}\mathbf{h}_a) + \boldsymbol{\tau}_e^b \quad (3.55a)$$

$$\dot{\mathbf{h}}_a = \boldsymbol{\tau}_a, \quad (3.55b)$$

where $\bar{\mathbf{J}} \in \mathbb{R}^{3 \times 3}$ is an inertia-like matrix defined as

$$\bar{\mathbf{J}} \triangleq \mathbf{J} - \mathbf{A}\mathbf{I}_s\mathbf{A}^T. \quad (3.56)$$

(3.55b) may also be written in terms of the angular velocities as

$$\mathbf{J}\dot{\boldsymbol{\omega}}_{ib}^b = \mathbf{S}(\mathbf{J}\boldsymbol{\omega}_{ib}^b)\boldsymbol{\omega}_{ib}^b + \mathbf{S}(\mathbf{A}\mathbf{I}_s\boldsymbol{\omega}_s)\boldsymbol{\omega}_{ib}^b - \mathbf{A}\boldsymbol{\tau}_a + \boldsymbol{\tau}_e \quad (3.57a)$$

$$\mathbf{I}_s\dot{\boldsymbol{\omega}}_s = \boldsymbol{\tau}_a - \mathbf{I}_s\mathbf{A}\dot{\boldsymbol{\omega}}_{ib}^b \quad (3.57b)$$

3.5.3 Inertial coordinate model

The model derived in the previous section, may also be given in inertial coordinates using the kinematic equation which relates angular velocity to the derivative of the attitude parameter.

Using the kinematic equation (5.1), the inverse kinematics relating the angular velocity and acceleration to the first and second derivative of the Euler angles is

$$\boldsymbol{\omega}_{ib}^b = \mathbf{T}^{-1}(\boldsymbol{\Theta})\dot{\boldsymbol{\Theta}}, \quad (3.58)$$

$$\dot{\boldsymbol{\omega}}_{ib}^b = \dot{\mathbf{T}}^{-1}(\boldsymbol{\Theta})\dot{\boldsymbol{\Theta}} + \mathbf{T}^{-1}(\boldsymbol{\Theta})\ddot{\boldsymbol{\Theta}}. \quad (3.59)$$

Inserting for $\boldsymbol{\omega}_{ib}^b$ and $\dot{\boldsymbol{\omega}}_{ib}^b$, and multiplying each side with the transpose inverse kinematic matrix we obtain

$$\mathbf{M}^*(\boldsymbol{\Theta})\ddot{\boldsymbol{\Theta}} + \mathbf{C}(\boldsymbol{\Theta}, \dot{\boldsymbol{\Theta}})\dot{\boldsymbol{\Theta}} = -\mathbf{A}^*(\boldsymbol{\Theta})\boldsymbol{\tau}_a + \mathbf{T}^{-T}(\boldsymbol{\Theta})\boldsymbol{\tau}_e \quad (3.60)$$

where

$$\mathbf{M}^*(\boldsymbol{\Theta}) = \mathbf{T}^{-T}(\boldsymbol{\Theta})\mathbf{J}\mathbf{T}^{-1}(\boldsymbol{\Theta}) \quad (3.61)$$

$$\begin{aligned} \mathbf{C}(\boldsymbol{\Theta}, \dot{\boldsymbol{\Theta}}) &= -\mathbf{T}^{-T}(\boldsymbol{\Theta})\mathbf{S}(\mathbf{J}\mathbf{T}^{-1}(\boldsymbol{\Theta})\dot{\boldsymbol{\Theta}} + \mathbf{A}\mathbf{I}_s\boldsymbol{\omega}_s)\mathbf{T}^{-1}(\boldsymbol{\Theta}) \\ &\quad + \mathbf{T}^{-T}(\boldsymbol{\Theta})\mathbf{J}\dot{\mathbf{T}}^{-T}(\boldsymbol{\Theta}). \end{aligned} \quad (3.62)$$

$$\mathbf{A}^*(\boldsymbol{\Theta}) = \mathbf{T}^{-T}(\boldsymbol{\Theta})\mathbf{A} \quad (3.63)$$

3.6. EXTERNAL FORCES AND TORQUES

It can also be shown the the matrices have the following important properties

$$\mathbf{M}^* = \mathbf{M}^{*T} > 0 \quad (3.64)$$

$$\mathbf{x}^T (\dot{\mathbf{M}}^* - 2\mathbf{C}^*) \mathbf{x} \equiv 0, \forall \mathbf{x} \in \mathbb{R}^3 \quad (3.65)$$

Remark 3.1. *The derivation is done using Euler angles, but it is straightforward to extend this to Euler parameters. A drawback is that $\mathbf{M}(\mathbf{q})^*$ becomes singular for $\eta = \pm 1$.*

3.6 External forces and torques

In this section we derive expressions for the external forces and torques that affect the satellite while orbiting Earth, both environmental and the actuator generated.

3.6.1 Gravitational forces and torques

The gravitational force field in space, is the result of gravitational forces acting between every body in the Universe. The forces are dependent on the bodies’ mass and the square of the distance between them. The field is thus non-uniform, with the result that any non-symmetrical object in space will experience a torque about its center of mass. In the most general form, the forces and torques on the body due to n celestial bodies are expressed:

$$\vec{f} = \int_B d\vec{f} = -G \sum_{n=1}^N \int_{B_n} \int_B \frac{\vec{\rho}_n dm_n dm}{\rho_n^3} \quad (3.66)$$

$$\vec{g}_o = \int_B \vec{r} \times d\vec{f} = -G \sum_{n=1}^N \int_{B_n} \int_B \frac{\vec{r} \times \vec{\rho}_n dm_n dm}{\rho_n^3} \quad (3.67)$$

These forms are too general to be of practical use, as their multiple integrations make analytical progress virtually impossible (Hughes 1986). Instead, Hughes makes four assumptions that simplifies the gravitational torque expressions.

- (1) Only one celestial primary need be considered
- (2) This primary possesses a spherical symmetrical mass distribution
- (3) The spacecraft is small compared to its distance from the mass center of the primary
- (4) The spacecraft consists of a single body

MATHEMATICAL MODELING

Assumption 1 means that the sums in (3.66) and (3.67) can be replaced by a single term. Assumption 2 leads to the removal of the integration over B_n , replacing it with a point mass in the mass center of B_n . Assumption 3 is equal to the statement $\frac{r}{R_c} \ll 1$ and finally assumption 4 allows us to choose the mass center as the reference point without loss of generality. Using these assumptions one may derive the following expression for the gravitational torque:

$$\vec{\tau}_g \triangleq 3 \left(\frac{\mu}{R_c^3} \right) \vec{z}_{o3} \times \vec{I} \cdot \vec{z}_{o3}, \quad (3.68)$$

where μ is the gravitational constant of the primary celestial body, R_c is the distance between the mass centers of the two bodies, \vec{z}_{o3} is the nadir pointing vector and \vec{I} is the inertia dyadic. We note that the nadir pointing vector in body coordinates is equal to the third column in the rotation matrix between \mathcal{F}_b and \mathcal{F}_o , using that the nadir pointing vector in orbit coordinates is equal to the z_o - axis

$$\mathbf{z}_{o3}^b = \mathbf{R}_o^b \mathbf{z}_o^o = \mathbf{R}_o^b \begin{bmatrix} 0 \\ 0 \\ 1 \end{bmatrix}. \quad (3.69)$$

We may now give the gravity gradient torque in coordinate vectors in the body system as:

$$\boldsymbol{\tau}_g = 3\omega_o^2 (\mathbf{z}_{o3}^b)^\times \mathbf{I} \mathbf{z}_{o3}^b, \quad (3.70)$$

where we have also used that $\frac{\mu}{R_c^3} = \omega_o^2$.

3.6.2 Aerodynamical forces and torques

The aerodynamical torque on the satellite results from particles in the atmosphere colliding with a non-symmetric cross section. This effect is most severe for LEO. In the worst-case this torque is given by:

$$\boldsymbol{\tau}_d = F(c_{pa} - c_g), \quad (3.71)$$

where $F = 0.5\rho C_d A V^2$ and ρ is the atmospheric density, C_d is the drag coefficient, A is the surface area and V is the spacecraft velocity.

3.6.3 Magnetic torques

Due to electric currents in liquid portions of the Earth’s iron core, there is a magnetic field surrounding the planet as can be seen in figure 3.4 (Freedman & Kaufmann III 2002). Since the field is not generated by a permanent magnet, but instead by a liquid, the field is constantly changing and changes sign about once every 1 million years. Due to this, one needs an up to date model of the field to be able to evaluate its effect on the

3.6. EXTERNAL FORCES AND TORQUES

spacecraft. Such a model is published every five years by the International Association of Geomagnetism and Astronomy (IAGA), and is called the International Geomagnetic Reference Field (IGRF). This model give the magnetic field values for a given longitude and latitude at a given decimal date between 1900-2010 (International Association of Geomagnetism and Aeronomy 2005).

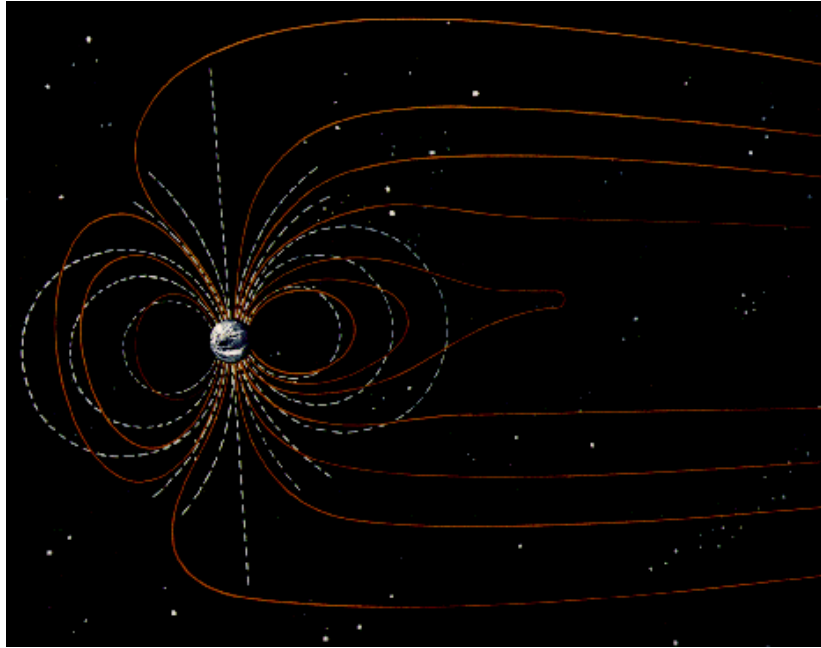


Figure 3.4: Illustration of the Earth’s magnetic field

As basic physics tells us, a magnet exposed to a magnetic field, will experience a torque which tries to align the magnetic field generated by the magnet with the surrounding field. The same effect is experienced by a spacecraft orbiting Earth, due to permanent magnets and current loops. This may generate unwanted disturbance torques if not balanced properly. But it may also be used as an advantage by including a controlled magnetic moment (Hughes 1986), generating a torque given by

$$\vec{\tau}_m = \vec{m} \times \vec{B}(t), \quad (3.72)$$

where \vec{m} is the generated magnetic moment and $\vec{B}(t)$ is the local geomagnetic field.

The magnetic moment is generated by electromagnetic actuators, often referred to as magnetic torquers, and consist of two basic configurations. One is the coil based, where current is sent through a current loop which generates the magnetic moment proportional to the area of the coil and the number of windings. The other type is the magnetic rod, where a wire is wound around a rod made of high permeability material.

MATHEMATICAL MODELING

3.6.4 Solar radiation and solar wind

Solar radiation is due to the constant bombardment of photons, and will generate a solar pressure force on the surface of the satellite, acting through a point referred to as the center of solar pressure, c_{sp} . The force is very small, dependent on the satellite’s surface material, geometry and location, it will give only 5N to a surface of 1 km^2 , it may be given by (Vallado 2001)

$$F = \frac{F_s}{c} A_s (1 + q) \cos i, \quad (3.73)$$

where F_s is the solar constant 1.367 W/m^2 , c is the speed of light, A_s is the surface area, q is the reflectance factor and i is the angle of incidence of the Sun. Solar wind on the other hand consists of ionized nuclei and electrons, and is typically 100-1000 times smaller than the solar radiation forces. Dependent on the position of c_{sp} relative to the center of gravity, c_g , the force will generate a torque about c_g given by

$$\tau_{sp} = F(c_{sp} - c_g), \quad (3.74)$$

where F is given by (3.73).

These environmental forces, are usually considered disturbances, but has also been considered both for propulsion and attitude control for long term missions. On Mariner IV, launched 1969, solar vanes were used to align the probe with the sun and thereby maximize power. Experiments have also been conducted by ESA on OST-2, a geostationary communication satellite, where attitude was controlled by manipulating the solar panels. Recently control algorithms using feedback linearization and adaptive feedback have been researched in Singh & Yim (1995), Singh & Yim (2002) and Singh & Yim (1996). A review of previous literature on attitude control by means of solar pressure, is given in Venkatachalam (1993).

For propulsion, it has been proposed to use vast solar sails to generate force for interstellar exploration. And in Wallace, Ayon & Sprague (2000) it is proposed as the key enabling technology for such missions. To date no missions using solar sail technology have been successful. The solar sail spacecraft Cosmos 1 was launched in June 2005, and would have been the first solar sail propelled spacecraft in orbit. However, a failure in the Russian launch vehicle prevented the vehicle from reaching orbit. Currently no other missions are scheduled.

3.6.5 Thruster forces and torques

Thrusters produce torque by expelling mass through a valve. The simplest and most common valve is strictly on-off and single level, but variable and dual-level thrusters are available. We divide the thrusters into cold- and hot-gas systems. In hot-gas systems the energy is produced in a chemical reaction, while in cold-gas systems it comes from the latent heat of a phase change or from the work of compression without a phase change.

3.6. EXTERNAL FORCES AND TORQUES

Typical force capabilities of thrusters are between 0.5 to 9000 N for hot-gas systems and less than 5 N for cold-gas systems, depending on size. The torque amount from a given thruster is dependent on its distance from the center of mass (Vallado 2001).

The advantage of thrusters are that they can supply a reliable torque in any direction, anywhere in the orbit, and the possibility of large torques resulting in high slew rates. The disadvantage is of course fuel requirements, which dictates spacecraft life.

3.6.6 Reaction wheels

A reaction wheel is essentially a torque providing motor with a relatively high rotor inertia. It is able to load and unload angular momentum internally, and is thus often referred to as momentum exchange devices as they do not change the overall angular momentum of the satellite, but redistributes the angular momentum due to rotational motion to rotation of the wheels. The amount of torque that is provided is dependent on the size of the rotor and motor, and is in the range from $0.01Nm$ to $1Nm$.

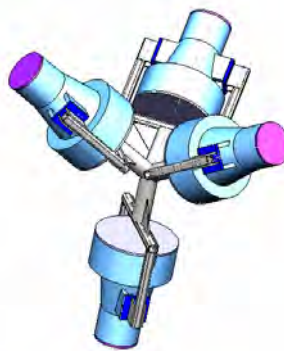


Figure 3.5: 4 reaction wheel assemblies in tetrahedron composition

A wheel complete with motor and drive electronics, is usually referred to as a reaction wheel assembly (RWA). Three wheels, one along each axis, is needed for full three-axis control. For redundancy and performance a composition of RWAs usually consists of more than three wheels. One such composition is the tetrahedron composition (Figure 3.5). A regular tetrahedron is a pyramid composed of four equilateral triangular faces, three of which meets at each vertex. Each wheel-axis is orthogonal on a face, and crosses through the center of the pyramid.

The torque from a wheel to the body equals the torque applied to the wheel from a motor attached to the body, but with opposite sign. The torque in body coordinated is equal to

$$\boldsymbol{\tau}_{a,i}^b = \mathbf{a}_i^b \tau_{a,i}, \quad (3.75)$$

MATHEMATICAL MODELING

where \mathbf{a}_i^b is the unit wheel axis in body coordinates. The total torque may then be written as

$$\boldsymbol{\tau}_a^b = \mathbf{A}\boldsymbol{\tau}_a \quad (3.76)$$

where $\boldsymbol{\tau}_a$ is a vector of wheel torques and \mathbf{A} is given by

$$\mathbf{A} = \begin{bmatrix} \sqrt{\frac{1}{3}} & \sqrt{\frac{1}{3}} & -\sqrt{\frac{1}{3}} & -\sqrt{\frac{1}{3}} \\ \sqrt{\frac{2}{3}} & -\sqrt{\frac{2}{3}} & 0 & 0 \\ 0 & 0 & -\sqrt{\frac{2}{3}} & \sqrt{\frac{2}{3}} \end{bmatrix}. \quad (3.77)$$

Chapter 4

External synchronization of relative attitude

In this chapter we derive a coordinated control scheme to control relative attitude of a formation of satellites using methods from nonlinear control theory. We first give control laws for the leader satellite, and then propose an adaptive synchronizing control law for the follower. Global convergence of the synchronization errors are proven mathematically and the resulting controllers are simulated in presence of environmental disturbances and measurement noise.

This chapter is based on (Krogstad & Gravdahl 2006*b*).

4.1 Introduction

In this chapter we design a coordinated control scheme, referred to as external synchronization, based on theory derived by (Rodriguez-Angeles 2002). This may be viewed as a version of the leader-follower approach, where one designs interconnections, virtual or physical, between designated leaders and followers.

We visualize and evaluate the performance of the controllers by applying them to a satellite formation consisting of two micro-satellites. The satellites are actuated by means of reaction wheels for 3-axis attitude control and use thrusters for position control. Attitude is assumed measured at all times, with an accuracy of 0.001 degrees in all axis. The measurement signal is assumed to be noise contaminated. The angular velocity is assumed to be either estimated or measured.

4.2 Mathematical model

4.2.1 Kinematics

In this chapter we use the kinematical differential equations parameterized using the Euler parameters

$$\dot{\eta}_{ib} = -\frac{1}{2}\boldsymbol{\epsilon}_{ib}^T \boldsymbol{\omega}_{ib}^b \quad (4.1a)$$

$$\dot{\boldsymbol{\epsilon}}_{ib} = \frac{1}{2}[\eta_{ib}\mathbf{I}_{3\times 3} + \mathbf{S}(\boldsymbol{\epsilon}_{ib})]\boldsymbol{\omega}_{ib}^b, \quad (4.1b)$$

where $\boldsymbol{\omega}_{ib}^b$ is the angular velocity of the body relative to an inertial frame. Given the quaternion vector

$$\mathbf{q}_{ib} \triangleq \begin{bmatrix} \eta_{ib} \\ \boldsymbol{\epsilon}_{ib} \end{bmatrix}, \quad (4.2)$$

we may write the (4.1) in compact form

$$\dot{\mathbf{q}}_{ib} = \frac{1}{2}\mathbf{Q}(\mathbf{q}_{ib})\boldsymbol{\omega}_{ib}^b, \quad \text{where} \quad \mathbf{Q}(\mathbf{q}_{ib}) \triangleq \begin{bmatrix} -\boldsymbol{\epsilon}_{ib}^T \\ \eta_{ib}\mathbf{I}_{3\times 3} + \mathbf{S}(\boldsymbol{\epsilon}_{ib}) \end{bmatrix} \quad (4.3)$$

Euler angles, or roll-pitch-yaw angles, have been applied in the visualization of results, since these are easier to relate to physical motion.

4.2.2 Dynamic model

In this chapter we use the dynamic model of a gyrostat, which was derived in section 3.5.2 as

$$\mathbf{J}_b \dot{\boldsymbol{\omega}}_{ib}^b = \mathbf{S}(\mathbf{J}_b \boldsymbol{\omega}_{ib}^b) \boldsymbol{\omega}_{ib}^b + \mathbf{S}(\mathbf{A}\mathbf{I}_s \boldsymbol{\omega}_s) \boldsymbol{\omega}_{ib}^b - \mathbf{A}\boldsymbol{\tau}_a + \boldsymbol{\tau}_e \quad (4.4a)$$

$$\mathbf{I}_s \dot{\boldsymbol{\omega}}_s = \boldsymbol{\tau}_a - \mathbf{I}_s \mathbf{A} \dot{\boldsymbol{\omega}}_{ib}^b \quad (4.4b)$$

4.3 External synchronization design

In this synchronization scheme the leader satellite is controlled separately, either by a tracking or a stabilizing controller. The goal is to design feedback interconnections from the leader to the follower, in such a way that the follower synchronizes its orientation with that of the leader. The design is done by first designing controllers for the leader, then designing a synchronizing controller for the follower.

4.3.1 Leader controller

Three different controllers are proposed for the control of the leader; set-point control in \mathcal{F}_i , set-point control in \mathcal{F}_o and finally trajectory tracking in \mathcal{F}_i . The controllers are based the quaternion feedback schemes presented in (Wen & Kreutz-Delgado 1991) and (Fjellstad 1994), but with some differences in the mathematical proofs.

Set-point in \mathcal{F}_i

If the leader is to point in a specific constant direction in inertial space, as in the case of space-based interferometry missions as DARWIN and XEUS, a set-point stabilizing controller is sufficient. We define the desired satellite orientation in the inertial frame, as the quaternion \mathbf{q}_{id} and the desired angular velocity as zero, resulting in the error variables

$$\mathbf{q}_e \triangleq \mathbf{q}_{dl} = \mathbf{q}_{id}^{-1} \otimes \mathbf{q}_{il} \quad (4.5)$$

$$\boldsymbol{\omega}_e \triangleq \boldsymbol{\omega}_{dl}^l = \boldsymbol{\omega}_{il}^l - \boldsymbol{\omega}_{id}^l = \boldsymbol{\omega}_{il}^l - 0 = \boldsymbol{\omega}_{il}^l. \quad (4.6)$$

By writing the dynamics as

$$\dot{\mathbf{q}}_{il} = \frac{1}{2} \mathbf{Q}(\mathbf{q}_{il}) \boldsymbol{\omega}_{il}^l, \quad (4.7a)$$

$$\mathbf{J}_l \dot{\boldsymbol{\omega}}_{il}^l = \mathbf{S} \left(\mathbf{J}_l \boldsymbol{\omega}_{il}^l + \mathbf{A} \mathbf{I}_{s,l} \boldsymbol{\omega}_{s,l} \right) \boldsymbol{\omega}_{il}^l - \mathbf{A} \boldsymbol{\tau}_{a,l} + \boldsymbol{\tau}_{g,l}, \quad (4.7b)$$

the error-dynamics may be written

$$\dot{\mathbf{q}}_e = \frac{1}{2} \mathbf{Q}(\mathbf{q}_e) \boldsymbol{\omega}_e \quad (4.8a)$$

$$\mathbf{J}_b \dot{\boldsymbol{\omega}}_e = \mathbf{S} \left(\mathbf{J}_b \boldsymbol{\omega}_e + \mathbf{A} \mathbf{I}_{s,l} \boldsymbol{\omega}_{s,l} \right) \boldsymbol{\omega}_e - \mathbf{A} \boldsymbol{\tau}_{a,l} + \boldsymbol{\tau}_{g,l} \quad (4.8b)$$

Proposition 4.1. *The leader satellite, with dynamics (4.7b)-(4.7a), and error-dynamics (4.8a)-(4.8b), with control law given by*

$$\boldsymbol{\tau}_{a,l} = -\mathbf{A}^\dagger \left(-\boldsymbol{\tau}_{g,l} - k_d \boldsymbol{\omega}_e + k_p \frac{dH(\eta_e)}{d\eta_e} \boldsymbol{\epsilon}_e \right), \quad (4.9)$$

where \mathbf{A}^\dagger is the pseudo inverse and $H(\cdot)$ is a scalar function satisfying

- $H(\cdot) : [-1; 1] \rightarrow \mathbb{R}_+$ (non-negative)
- $H(-1) = 0$ or/and $H(1) = 0$
- $H(\cdot)$ is assumed C^1 , with bounded derivatives

EXTERNAL SYNCHRONIZATION OF RELATIVE ATTITUDE

which in the following this function is chosen as

$$H(\eta_e) = 1 - |\eta_e|, \quad (4.10)$$

with derivative

$$-\frac{dH}{d\eta_e}(\eta_e) = \text{sgn}(\eta_e) = \begin{cases} 1, & \text{if } x \geq 0 \\ -1, & \text{if } x < 0 \end{cases}, \quad (4.11)$$

has a globally asymptotically stable (GAS) origin $(\omega_e, \mathbf{y}) = (\mathbf{0}, \mathbf{0})$, where $\mathbf{y} = \text{col}(1 - |\eta_e|, \boldsymbol{\epsilon}_e)$.

Proof. To prove the proposition we choose the Lyapunov function candidate

$$V = \frac{1}{2}\boldsymbol{\omega}_e^T \mathbf{J}_l \boldsymbol{\omega}_e + 2k_p H(\eta_e), \quad (4.12)$$

which is positive definite, zero at the origin and radially unbounded. The time-derivative along the trajectories is given by

$$\dot{V} = \boldsymbol{\omega}_e^T \mathbf{J}_l \dot{\boldsymbol{\omega}}_e + 2k_p \frac{dH(\eta_e)}{d\eta_e} \dot{\eta}_e \quad (4.13)$$

$$= \boldsymbol{\omega}_e^T \left[\mathbf{S} \left(\mathbf{J}_l \boldsymbol{\omega}_{il}^l + \mathbf{A} \mathbf{I}_{s,l} \boldsymbol{\omega}_{s,l} \right) \boldsymbol{\omega}_{il}^l - \mathbf{A} \boldsymbol{\tau}_{a,l} + \boldsymbol{\tau}_{g,l} \right] - k_p \frac{dH(\eta_e)}{d\eta_e} \boldsymbol{\epsilon}_e^T \boldsymbol{\omega}_e \quad (4.14)$$

$$= \boldsymbol{\omega}_e^T \left[-\mathbf{A} \boldsymbol{\tau}_{a,l} + \boldsymbol{\tau}_{g,l} - k_p \frac{dH(\eta_e)}{d\eta_e} \boldsymbol{\epsilon}_e \right] \quad (4.15)$$

If we now select the control input (4.9), we get

$$\dot{V} = -k_d \boldsymbol{\omega}_e^T \boldsymbol{\omega}_e \leq -k_d \|\boldsymbol{\omega}_e\|_2^2 \leq 0. \quad (4.16)$$

Since this is a time-invariant system we have fulfilled the criteria of LaSalle’s invariance principle (Khalil 2000), and have convergence to the region

$$E = \left\{ x \in \Omega_c \mid \dot{V} = 0 \right\}, \quad (4.17)$$

where $\Omega_c = \{x \in \mathbb{R}^7 \mid V \leq c\}$ and $x = \text{col}(\boldsymbol{\omega}_e, 1 - |\eta_e|, \boldsymbol{\epsilon}_e)$. We can show that the largest invariant set M in E is the origin, and hence we have global asymptotic stability. \square

Set-point in \mathcal{F}_o

If the leader satellite is supposed to be stabilized to a fixed attitude in \mathcal{F}_o rather than \mathcal{F}_i , as is the case in some Earth observation missions, we have to solve the problem as a

4.3. EXTERNAL SYNCHRONIZATION DESIGN

tracking problem in the inertial frame. We now define the desired attitude and angular velocities as

$$\mathbf{q}_{id} \triangleq \mathbf{q}_{io}(t) \otimes \mathbf{q}_{od} \quad (4.18)$$

$$\boldsymbol{\omega}_{id}^l \triangleq \mathbf{R}_o^l \boldsymbol{\omega}_{io}^o, \quad (4.19)$$

where \mathbf{q}_{od} is the desired offset from nadir, $\boldsymbol{\omega}_{io}^o$ is the orbit angular velocity and $\mathbf{q}_{io}(t)$ is the quaternion describing the orientation of \mathcal{F}_o in \mathcal{F}_i . Assuming a circular orbit this quaternion is periodic in time, with period equal to the orbit-period. This results in the error-variables

$$\mathbf{q}_e = \mathbf{q}_{od}^{-1} \otimes \mathbf{q}_{io}^{-1}(t) \otimes \mathbf{q}_{il} \quad (4.20)$$

$$\boldsymbol{\omega}_e = \boldsymbol{\omega}_{il}^l - \mathbf{R}_o^l \boldsymbol{\omega}_{io}^o, \quad (4.21)$$

and error-dynamics

$$\mathbf{J}_l \dot{\boldsymbol{\omega}}_e = \mathbf{S} \left(\mathbf{J}_l \boldsymbol{\omega}_{il}^l + \mathbf{A} \mathbf{I}_{s,l} \boldsymbol{\omega}_{s,l} \right) \boldsymbol{\omega}_{il}^l - \mathbf{A} \boldsymbol{\tau}_{a,l} + \boldsymbol{\tau}_{g,l} + \mathbf{J}_l \mathbf{S} \left(\boldsymbol{\omega}_{ol}^l \right) \mathbf{R}_o^l \boldsymbol{\omega}_{io}^o \quad (4.22a)$$

$$\dot{\mathbf{q}}_e = \frac{1}{2} \mathbf{Q}(\mathbf{q}_e) \boldsymbol{\omega}_e \quad (4.22b)$$

Proposition 4.2. *The satellite leader, with dynamics (4.7b)-(4.7b) and error-dynamics (4.22a)-(4.22b), where the control is given by*

$$\begin{aligned} \boldsymbol{\tau}_{a,l} = -\mathbf{A}^\dagger \left(-\boldsymbol{\tau}_{g,l} - \mathbf{S} \left(\mathbf{J}_l \boldsymbol{\omega}_{il}^l + \mathbf{A} \mathbf{I}_{s,l} \boldsymbol{\omega}_{s,l} \right) \mathbf{R}_o^l \boldsymbol{\omega}_{io}^o - \mathbf{J}_l \mathbf{S} \left(\boldsymbol{\omega}_{ol}^l \right) \mathbf{R}_o^l \boldsymbol{\omega}_{io}^o \right. \\ \left. + k_p \frac{dH(\boldsymbol{\eta}_e)}{d\boldsymbol{\eta}_e} \boldsymbol{\epsilon}_e - k_d \boldsymbol{\omega}_e \right) \end{aligned} \quad (4.23)$$

has a uniformly globally asymptotically stable (UGAS) origin $(\boldsymbol{\omega}_e, \mathbf{y}) = (\mathbf{0}, \mathbf{0})$, where $\mathbf{y} = \text{col}(1 - |\boldsymbol{\eta}_e|, \boldsymbol{\epsilon}_e)$, under the assumption of a fixed desired attitude in the orbit frame.

Proof. We prove the proposition by choosing the Lyapunov function candidate (4.12). Taking the time-derivative along the trajectories of the solution to (4.22) and selecting the control as (4.23), we obtain

$$\dot{V} = \boldsymbol{\omega}_e^T \left[\mathbf{S} \left(\mathbf{J}_l \boldsymbol{\omega}_{il}^l + \mathbf{A} \mathbf{I}_{s,l} \boldsymbol{\omega}_{s,l} \right) \boldsymbol{\omega}_e - k_d \boldsymbol{\omega}_e \right] = k_d \boldsymbol{\omega}_e^T \boldsymbol{\omega}_e \leq 0, \quad (4.24)$$

where we have used property $\mathbf{a}^T \mathbf{S}(\mathbf{b}) \mathbf{a} = 0$. Since the error-dynamics (4.22a)-(4.22b) and the V is periodic with equal period, and V is positive definite and radially unbounded; Krasovskii-LaSalle’s theorem (Vidyasagar 1993) is applicable and the origin of the error-dynamics is proven to be UGAS. \square

Trajectory tracking in \mathcal{F}_i

We now show stability of a nonlinear state feedback controller for tracking in the inertial frame. That is, given a smooth trajectory $\mathbf{q}_{id}(t) \in C^2$, such that $\dot{\mathbf{q}}_{id}(t)$, $\ddot{\mathbf{q}}_{id}(t)$ are well defined for $t \geq 0$, we obtain uniform global asymptotic stability of the tracking error.

Let the desired angular velocity and acceleration be given by

$$\boldsymbol{\omega}_{id}^d = 2\mathbf{Q}(\mathbf{q}_{id})^T \dot{\mathbf{q}}_{id} \quad \text{and} \quad \dot{\boldsymbol{\omega}}_{id}^d = 2\mathbf{Q}^T(\mathbf{q}_{id}) \ddot{\mathbf{q}}_{id}. \quad (4.25)$$

Further, we define the tracking errors as

$$\boldsymbol{\omega}_e \triangleq \boldsymbol{\omega}_{dl}^l = \boldsymbol{\omega}_{il}^l - \mathbf{R}_d^l \boldsymbol{\omega}_{id}^d \quad (4.26)$$

$$\mathbf{q}_e \triangleq \mathbf{q}_{dl} = \mathbf{q}_{id}^{-1}(t) \otimes \mathbf{q}_{il}, \quad (4.27)$$

such that the error-dynamics can be written

$$\dot{\mathbf{q}}_e = \frac{1}{2}\mathbf{Q}(\mathbf{q}_e)\boldsymbol{\omega}_e. \quad (4.28a)$$

$$\mathbf{J}_l \dot{\boldsymbol{\omega}}_e = \mathbf{S} \left(\mathbf{J}_l \boldsymbol{\omega}_{il}^l + \mathbf{A} \mathbf{J}_{s,l} \boldsymbol{\omega}_{s,l} \right) \boldsymbol{\omega}_{il}^l - \mathbf{A} \boldsymbol{\tau}_{a,l} + \boldsymbol{\tau}_{g,l} + \mathbf{J}_l \mathbf{S}(\boldsymbol{\omega}_e) \mathbf{R}_d^l \boldsymbol{\omega}_{id}^d - \mathbf{J}_l \mathbf{R}_d^l \dot{\boldsymbol{\omega}}_{id}^d \quad (4.28b)$$

Proposition 4.3. *Given the smooth continuous trajectory $\mathbf{q}_{id}(t) \in C^2$, error-dynamics (4.28), and control input*

$$\boldsymbol{\tau}_{a,l} = -\mathbf{A}^\dagger \left\{ -\boldsymbol{\tau}_{g,l} - \mathbf{S} \left(\mathbf{J}_l \boldsymbol{\omega}_{il}^l + \mathbf{A} \mathbf{I}_{s,l} \boldsymbol{\omega}_{s,l} \right) \mathbf{R}_d^l \boldsymbol{\omega}_{id}^d - \mathbf{J}_l \mathbf{S}(\boldsymbol{\omega}_e) \mathbf{R}_d^l \boldsymbol{\omega}_{id}^d + \mathbf{J}_l \mathbf{R}_d^l \dot{\boldsymbol{\omega}}_{id}^d - k_p \text{sgn}(\eta_e) \boldsymbol{\epsilon}_e - k_d \boldsymbol{\omega}_e \right\}, \quad (4.29)$$

the origin $(\boldsymbol{\omega}_e, \mathbf{y}) = (\mathbf{0}, \mathbf{0})$, where $\mathbf{y} = \text{col}(1 - |\eta_e|, \boldsymbol{\epsilon}_e)$, is uniformly globally asymptotically stable, UGAS.

Proof. Since the trajectory is an explicit function of time, we now have to deal with a nonlinear time-varying system (NLTV). This adds some difficulties to the analysis of the error-dynamics, as the invariance principle due to LaSalle (Khalil 2000) is no longer applicable in the case of a semi-definite Lyapunov derivative. A common solution to this is to use the convergence theorem due to Barbalat, but one cannot conclude asymptotic stability. We instead prove the proposition using the generalized Matrosov theorem (Matrosov 1962), given in (Loria et al. 2002), where four assumptions have to be satisfied in order to conclude uniform global asymptotic stability. The result is summarized in Theorem 2.4

Satisfying Assumption 2.5

Choosing the Lyapunov function

$$V = \frac{1}{2} \boldsymbol{\omega}_e^T \mathbf{J}_l \boldsymbol{\omega}_e + k_p \mathbf{y}^T \mathbf{y}, \quad (4.30)$$

4.3. EXTERNAL SYNCHRONIZATION DESIGN

with time derivative

$$\dot{V} = \boldsymbol{\omega}_e^T \mathbf{J}_l \dot{\boldsymbol{\omega}}_e + k_p \text{sgn}(\eta_e) \boldsymbol{\epsilon}_e^T \boldsymbol{\omega}_e \quad (4.31)$$

$$= \boldsymbol{\omega}_e^T [k_p \text{sgn}(\eta_e) \boldsymbol{\epsilon}_e - \mathbf{S} (\mathbf{J}_l \boldsymbol{\omega}_{il}^l + \mathbf{A} \mathbf{I}_{s,l} \boldsymbol{\omega}_{s,l})] \boldsymbol{\omega}_{il}^l + \mathbf{A} \boldsymbol{\tau}_a - \boldsymbol{\tau}_{g,l} \quad (4.32)$$

$$- \mathbf{J}_l \mathbf{S}(\boldsymbol{\omega}_e) \mathbf{R}_d^l \boldsymbol{\omega}_{id}^d + \mathbf{J}_l \mathbf{R}_d^l \dot{\boldsymbol{\omega}}_{id}^d], \quad (4.33)$$

and inserting for (4.29), results in

$$\dot{V} = -k_d \boldsymbol{\omega}_e^T \boldsymbol{\omega}_e \leq 0, \quad (4.34)$$

which guarantees uniform global stability (UGS) for the error-dynamics, satisfying Assumption 2.5 in (Loria et al. 2002).

Remark 4.1. *From this result it is possible to show asymptotic convergence as in (Fjellstad 1994), by using Barbalat’s Lemma and showing that convergence of $\boldsymbol{\omega}_e$ leads to convergence of $\boldsymbol{\epsilon}_e$.*

Satisfying Assumption 2.6

Since the origin is UGS, $\dot{\boldsymbol{\omega}}_e$, $\boldsymbol{\omega}_e$, \mathbf{y} are bounded functions of time. For $i = 1$ we choose

$$V_1 \triangleq V \quad (4.35)$$

$$\phi_1 \triangleq 0 \quad (4.36)$$

$$Y_1 \triangleq -\beta \|\boldsymbol{\omega}_e\| \leq 0 \quad (4.37)$$

V_1 is continuously differentiable and bounded, ϕ_1 is continuous and bounded, and finally Y_1 is continuous and hence Assumption 2.6 in (Loria et al. 2002) is satisfied for $i = 1$.

For $i = 2$, we choose

$$V_2 \triangleq \boldsymbol{\omega}_e^T \mathbf{I}_b \boldsymbol{\epsilon}_e \eta_e \quad (4.38)$$

$$\phi_2 \triangleq \dot{\boldsymbol{\omega}}_e \quad (4.39)$$

$$Y_2 \triangleq \eta_e \phi_2^T \mathbf{I}_b \boldsymbol{\epsilon}_e + \eta_e \boldsymbol{\omega}_e^T \mathbf{I}_b \dot{\boldsymbol{\epsilon}}_e + \dot{\eta}_e \boldsymbol{\omega}_e^T \mathbf{I}_b \boldsymbol{\epsilon}_e \quad (4.40)$$

Since $\dot{\boldsymbol{\omega}}_e$, $\boldsymbol{\omega}_e$, \mathbf{y} , η_e are bounded functions of time, V_2 , ϕ_2 and Y_2 are bounded. Moreover, V_2 is continuously differentiable, and ϕ_2 and Y_2 are continuous in their arguments. Hence, Assumption 2.6 in (Loria et al. 2002) is satisfied for $i = 2$.

Satisfying Assumption 2.7

$Y_1 \leq 0$ for all $\boldsymbol{\omega}_e \in \mathbb{R}^3$, satisfying Assumption 3 in (Loria et al. 2002) for $i = 1$. Moreover,

$$Y_1 = 0 \Rightarrow \|\boldsymbol{\omega}_e\| = 0 \Rightarrow Y_2 = \eta_e \phi_2^T \mathbf{I}_b \boldsymbol{\epsilon}_e \quad (4.41)$$

EXTERNAL SYNCHRONIZATION OF RELATIVE ATTITUDE

Inserting for ϕ_2 and $\omega_e = 0$, gives

$$Y_2 = -k_p \eta_e \text{sgn}(\eta_e) \epsilon_e^T \epsilon_e = -k_p |\eta_e| \epsilon_e^T \epsilon_e \leq 0. \quad (4.42)$$

Thus, Assumption 2.7 has been satisfied for both $i \in \{1, 2\}$.

Satisfying Assumption 2.8

It can now be seen that

$$\{Y_1 = 0, Y_2 = 0\} \Rightarrow \omega_e = 0, \epsilon_e = 0 \Rightarrow 1 - |\eta_e| = 0, \quad (4.43)$$

satisfying Assumption 2.8 in (Loria et al. 2002) for $i \in \{1, 2\}$.

Remark 4.2. *This hold as long as η_e is different from zero. Using UGS property of Assumption 2.5 and that $\eta_e = 0$ is an unstable equilibrium point when using the given definition of signum, as shown in (Fjellstad 1994), the condition is met by requiring η_e to initially be different from 0.*

The Assumptions of Matrosov’s Theorem are satisfied, and we may conclude *uniform global asymptotic stability*. \square

4.3.2 Adaptive synchronizing controller

In this section we derive a synchronizing controller, to synchronize the attitude of the satellites in the formation. We have considered the two-satellite formation problem, as it appears in applications such as SAR missions and XEUS. We assume that the absolute angular velocity is measured relative to \mathcal{F}_i and that the relative attitude is measured with the required accuracy for mission specifications. For XEUS the specifications requires relative attitude knowledge with such accuracy that normal methods using star-trackers and inertial navigation is insufficient, instead some form of laser-metrology is required.

In some cases the inertia matrix may be unknown or poorly known, and it may also change over time due to mass expulsion when firing thrusters. Assuming the parameters are constant or slowly varying, we may remedy the lack of information using an adaptive controller. We first assume perfect model knowledge and design a controller for this scenario. This controller is extended with a parameter update law in the following step. The design method is based on vectorial integrator backstepping as was done in (Fossen 2002) for ships and in (Bondhus et al. 2005) for a satellite actuated by means of thrusters. A similar approach was also designed in (Egeland & Godhavn 1994) using passivity arguments.

We first define the synchronization measure s as a linear parametrization of the angular velocity synchronization error and the quaternion synchronization error,

$$s \triangleq \omega_{se} + \lambda e, \quad (4.44)$$

4.3. EXTERNAL SYNCHRONIZATION DESIGN

where $\omega_{se} = \omega_{lf}^f$ and $e = \epsilon_{lf}$ are defined by

$$\mathbf{q}_{lf} = \begin{bmatrix} \eta_{lf} \\ \epsilon_{lf} \end{bmatrix} \triangleq \mathbf{q}_{il}^{-1} \otimes \mathbf{q}_{if} \quad \text{and} \quad \omega_{lf}^f = \omega_{if}^f - \omega_{il}^f. \quad (4.45)$$

Further, we define ω_r as

$$\omega_r \triangleq \omega_{il}^f - \lambda e, \quad (4.46)$$

such that we may write

$$\mathbf{s} = \omega_{if}^f - \omega_r. \quad (4.47)$$

ω_r may be viewed as a virtual reference trajectory. Defining the parametrization

$$\mathbf{Y}(\dot{\omega}_r, \omega_r, \omega_{if}^f) \boldsymbol{\theta} = \mathbf{J}_f \dot{\omega}_r - \mathbf{S}(\mathbf{J}_f \omega_{if}^f) \omega_r, \quad (4.48)$$

where, if \mathbf{J}_f is diagonal,

$$\mathbf{Y}(\dot{\omega}_r, \omega_r, \omega_{if}^f) = \begin{bmatrix} \dot{\omega}_{r1} & -\omega_2 \omega_{r3} & \omega_3 \omega_{r2} \\ \omega_1 \omega_{r3} & \dot{\omega}_{r2} & -\omega_3 \omega_{r1} \\ \omega_1 \omega_{r2} & -\omega_2 \omega_{r1} & \dot{\omega}_{r3} \end{bmatrix}, \quad (4.49)$$

is the so called regressor matrix, with $\dot{\omega}_{ri}$, ω_{ri} and ω_i being the components of $\dot{\omega}_r$, ω_r and ω_{if}^f and

$$\boldsymbol{\theta} = [i_{xx}, i_{yy}, i_{zz}]^T \quad (4.50)$$

the parameter vector containing the diagonal elements of the inertia matrix. A differential equation in terms of \mathbf{s} and \mathbf{q}_e may be defined as

$$\dot{\mathbf{q}}_e = \frac{1}{2} \mathbf{Q}(\mathbf{q}_e) (\mathbf{s} - \lambda \epsilon_e) \quad (4.51a)$$

$$\mathbf{J}_f \dot{\mathbf{s}} - \mathbf{S}(\mathbf{J}_f \omega_{if}^f + \mathbf{A} \mathbf{I}_{s,f} \omega_{s,f}) \mathbf{s} = -\mathbf{A} \boldsymbol{\tau}_{a,f} + \boldsymbol{\tau}_{g,f} + \mathbf{S}(\mathbf{A} \mathbf{I}_{s,f} \omega_{s,f}) \omega_r - \mathbf{Y} \boldsymbol{\theta}. \quad (4.51b)$$

Proposition 4.4. *Given the dynamics (4.51a)-(4.51b), and the control $\boldsymbol{\tau}_{a,f}$ selected as*

$$\boldsymbol{\tau}_{a,f} = \mathbf{A}^\dagger \left(-\mathbf{Y}(\dot{\omega}_r, \omega_r, \omega_{if}^f) \boldsymbol{\theta} - \mathbf{S}(\mathbf{A} \mathbf{I}_{s,f} \omega_{s,f}) \omega_r - \boldsymbol{\tau}_{g,f} - \mathbf{K}_d \mathbf{s} - \epsilon_e \right), \quad (4.52)$$

the origin $(\mathbf{s}, \epsilon_e) = (\mathbf{0}, \mathbf{0})$ is uniformly globally exponentially stable (UGES). This implies exponential convergence of ω_e to $\mathbf{0}$, and to the convergence of η_e to 1.

Proof. To prove UGES of the origin we start with the subsystem (4.51a). The control Lyapunov function for the first subsystem is chosen as

$$V_1 = \epsilon_e^T \epsilon_e + (1 - \eta_e)^2. \quad (4.53)$$

EXTERNAL SYNCHRONIZATION OF RELATIVE ATTITUDE

Calculating the time-derivative of (4.53) along the solution trajectories of (4.51a) results in

$$\dot{V}_1 = 2\epsilon_e^T \dot{\epsilon}_e - 2\dot{\eta}_e + 2\eta_e \dot{\eta}_e \quad (4.54)$$

$$= \epsilon_e^T (\eta_e \mathbf{I}_{3 \times 3} - \mathbf{S}(\epsilon_e)) (\mathbf{s} - \lambda \epsilon_e) - \epsilon_e^T (\mathbf{s} - \lambda \epsilon_e) - \eta_e \epsilon_e^T (\mathbf{s} - \lambda \epsilon_e) \quad (4.55)$$

$$= -\lambda \epsilon_e^T \epsilon_e + \mathbf{s}^T \epsilon_e. \quad (4.56)$$

In the next step a Control Lyapunov function is selected as

$$V_2 = \frac{1}{2} \mathbf{s}^T \mathbf{J}_l \mathbf{s} + V_1, \quad (4.57)$$

with time-derivative along the solution trajectories of (4.51b) given by

$$\dot{V}_2 = \mathbf{s}^T \mathbf{J}_f \dot{\mathbf{s}} + \dot{V}_1 \quad (4.58)$$

$$= \mathbf{s}^T \left[\mathbf{S} \left(\mathbf{J}_f \boldsymbol{\omega}_{i_f}^f - \mathbf{A} \mathbf{I}_{s,f} \boldsymbol{\omega}_{s,f} \right) \mathbf{s} + \mathbf{S} \left(\mathbf{A} \mathbf{I}_{s,f} \boldsymbol{\omega}_{s,f} \right) \boldsymbol{\omega}_r - \mathbf{A} \boldsymbol{\tau}_{a,f} + \boldsymbol{\tau}_{g,f} \right. \quad (4.59)$$

$$\left. - \mathbf{Y}(\dot{\boldsymbol{\omega}}_r, \boldsymbol{\omega}_r, \boldsymbol{\omega}_{i_f}^f, \boldsymbol{\omega}_{s,f}) \boldsymbol{\theta} \right] - \lambda \epsilon_e^T \epsilon_e + \mathbf{s}^T \epsilon_e. \quad (4.60)$$

Selecting the control as

$$\boldsymbol{\tau}_{a,f} = \mathbf{A}^\dagger \left(-\mathbf{Y}(\dot{\boldsymbol{\omega}}_r, \boldsymbol{\omega}_r, \boldsymbol{\omega}_{i_f}^f) \boldsymbol{\theta} - \mathbf{S} \left(\mathbf{A} \mathbf{I}_{s,f} \boldsymbol{\omega}_{s,f} \right) \boldsymbol{\omega}_r - \boldsymbol{\tau}_{g,f} - \mathbf{K}_d \mathbf{s} - \epsilon_e \right), \quad (4.61)$$

equation (4.60) may be written as

$$\dot{V}_2 = -\mathbf{s}^T \mathbf{K}_d \mathbf{s} - \lambda \epsilon_e^T \epsilon_e \quad (4.62)$$

$$= -\mathbf{s}^T \mathbf{K}_d \mathbf{s} - \lambda(1 - \alpha) \epsilon_e^T \epsilon_e - \alpha \lambda (1 - \eta_e^2) \quad (4.63)$$

$$\leq -\mathbf{s}^T \mathbf{K}_d \mathbf{s} - \lambda(1 - \alpha) \epsilon_e^T \epsilon_e - \alpha \lambda (1 - |\eta_e|)^2 < 0, \quad (4.64)$$

for any $0 < \alpha < 1$. Since V_2 fulfills the requirements of uniform global exponential stability as given in (Khalil 2000), with the squared two norm, $\mathbb{D} = \mathbb{R}^n$ and the constants defined as

$$k_1 = \lambda_{\min}(\mathbf{P}) \quad (4.65)$$

$$k_2 = \lambda_{\max}(\mathbf{P}) \quad (4.66)$$

$$k_3 = \lambda_{\min}(\mathbf{Q}), \quad (4.67)$$

where $\mathbf{P} = \text{diag}(\mathbf{J}_f, \mathbf{I}_{3 \times 3}, 1)$, $\mathbf{Q} = \text{diag}(\mathbf{K}_d, \mathbf{I}_{3 \times 3}, 1)$, and $\lambda_{\min}(\cdot)$ and $\lambda_{\max}(\cdot)$ is the minimum and maximum eigenvalue respectively.

This shows that both \mathbf{s} and ϵ_e converges to zero exponentially, which implies exponential convergence of $\boldsymbol{\omega}_e$ to zero and of η_e to 1. \square

4.3. EXTERNAL SYNCHRONIZATION DESIGN

Remark 4.3. *Though the synchronizing controller was proven UGES to the origin $(\omega_e, \epsilon_e) = (0, 0)$, indicating ULES of the scalar quaternion error to either 1 or -1, inspection of the equilibrium points show that $\eta_e = -1$ is actually an unstable equilibrium point. This is a known fact for controllers using the quaternion error feedback, and was pointed out both in (Fjellstad 1994), (Egeland & Godhavn 1994) and (Wen & Kreutz-Delgado 1991). This translates to global stability in the state space $S(3) \times \mathbb{R}^3$, and local stability in the space $SO(3) \times \mathbb{R}^3$, where $S(3)$ is the unit sphere in \mathbb{R}^3 (Wen & Kreutz-Delgado 1991). In (Fjellstad 1994), feedback $e = \text{sgn}(\eta_e)\epsilon_e$ was used, which resulted in two stable equilibrium points.*

Since the error-dynamics (4.51a)-(4.51b), satisfies the *matching condition* (Krstic, Kanellakopoulos & Kokotovic 1995): The terms containing the unknown parameters are in the span of the control, that is, they can be directly cancelled by $\tau_{a,f}$ when the parameters are known, an adaptive control law may be defined by exchanging the real parameter vector with estimated parameters, and defining a parameter estimate update law.

Proposition 4.5. *Given the dynamics (4.51a)-(4.51b), choosing the control τ_a as*

$$\tau_{a,f} = \mathbf{A}^\dagger \left(-\mathbf{Y}(\dot{\omega}_r, \omega_r, \omega_{i,f}^f, \omega_{s,f})\hat{\boldsymbol{\theta}} - \tau_{g,f} - \mathbf{K}_d \mathbf{s} - \epsilon_e \right), \quad (4.68)$$

with the parameter estimate update law given by

$$\dot{\hat{\boldsymbol{\theta}}} = -\Gamma^{-1} \mathbf{Y}^T \mathbf{s} \quad (4.69)$$

renders the origin $(\mathbf{s}, \epsilon_e) = (\mathbf{0}, \mathbf{0})$ globally convergent. This implies convergence of ω_e to 0 and to the convergence of η_e to 1.

Proof. The first part of the proof follows directly from the proof of Proposition 4.4, and is not repeated. We now select

$$V_2 = \frac{1}{2} \mathbf{s}^T \mathbf{J}_f \mathbf{s} + \frac{1}{2} \tilde{\boldsymbol{\theta}}^T \Gamma \tilde{\boldsymbol{\theta}} + V_1. \quad (4.70)$$

If the control law and parameter update law is given by (4.68) and (4.69) respectively, the time-derivative \dot{V}_2 .

$$\dot{V}_2 = -\mathbf{s}^T \mathbf{K}_d \mathbf{s} - \lambda \epsilon_e^T \epsilon_e \leq 0 \quad (4.71)$$

Since V_2 can be lower bounded, \dot{V}_2 is negative semi-definite and uniformly continuous in time, the conditions of Barbalat’s Lemma (Khalil 2000) are satisfied and we have convergence of (\mathbf{s}, ϵ_e) to $(\mathbf{0}, \mathbf{0})$ globally, which as in the proof of Proposition 4.4, leads to

$$\omega_e \rightarrow 0, \eta_e \rightarrow 1, \text{ as } t \rightarrow \infty. \quad (4.72)$$

□

EXTERNAL SYNCHRONIZATION OF RELATIVE ATTITUDE

Remark 4.4. *Though we can not guarantee convergence of the parameter estimation error, we know that the error will stay bounded. To obtain true parameter estimation it is necessary for the input to the adaptive update law to be persistently exciting (PE). In this case the input is the synchronization error, thus the PE property will only be possible during transients. This is observed during simulations, as the convergence of the parameter estimate stops when the synchronization error has reached zero.*

4.4 Simulations

In this section we present simulations of the synchronizing controller. The model used is based on realistic values for a cubic small-size satellite, and a summary of model parameters is given in Table 7.1 and the simulation initial conditions and parameters are summarized in Table 4.2.

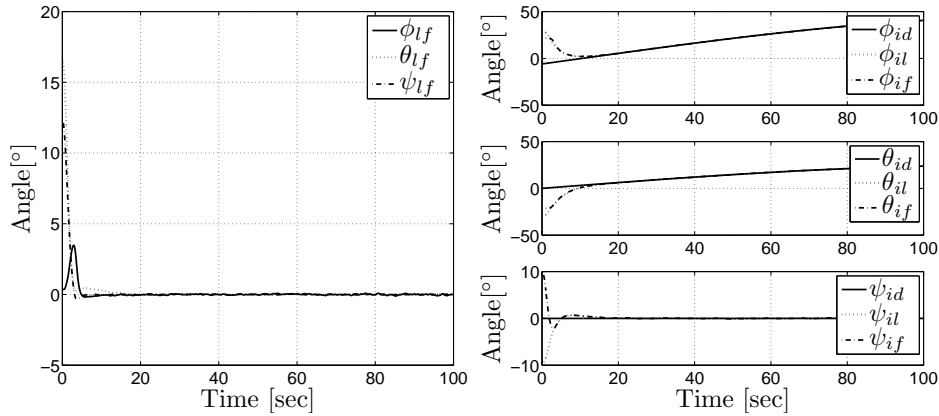
Table 4.1: Model parameters

Parameter	Value
Inertia matrix	$\text{diag}\{4, 4, 3\} [kgm^2]$
Wheel inertia	$8 \cdot 10^{-3} [kgm^2]$
Max magnetic moment	$40 [Am^2]$
Max wheel torque	$0.2 [Nm]$
Max wheel speed	$400 [rad/s]$

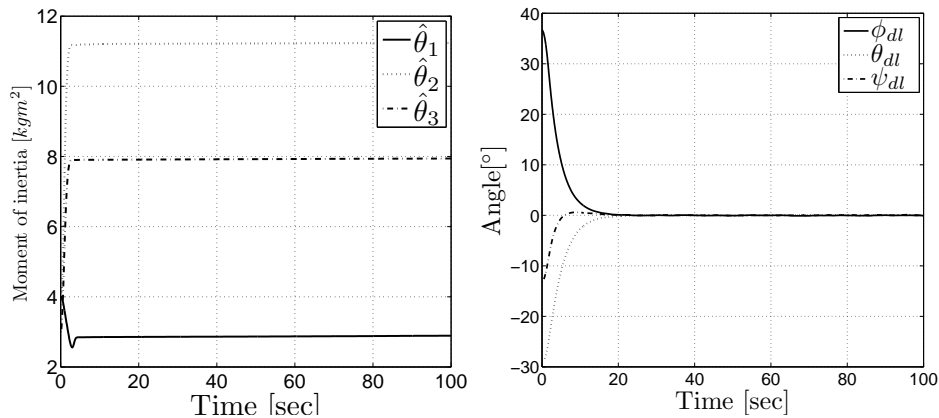
Table 4.2: Simulation parameters

Parameter	Value
Controller gains	$k_p = 1, k_d = 5$
Orbit angular velocity	$1.083 \cdot 10^{-3} [rad/s]$
Initial leader attitude	$[30, -30, -10]^T [^\circ]$
Initial follower attitude	$[20, -20, 10]^T [^\circ]$
Initial leader angular velocity	$10^{-3} \cdot [1, 3, 1]^T [rad/s]$
Initial follower angular velocity	$10^{-3} \cdot [1, 3, 1]^T [rad/s]$
Desired attitude	$\begin{bmatrix} 45 \sin \frac{2\pi}{500} t \\ 25 \sin \frac{2\pi}{500} t \\ 0 \end{bmatrix} [^\circ]$

4.4. SIMULATIONS



(a) Synchronization error transient, q_{lf} , visualized using Euler angles (b) Simulation results showing the attitude of the leader and follower versus the desired



(c) Plot of the convergence of the estimated inertia estimates (d) Tracking error of the leader

Figure 4.1: Simulation results

In Fig. 4.1(a) the transient synchronization error is presented, clearly indicating convergence of the errors. The final synchronization error is dependent on factors such as actuator bandwidth, measurement accuracy, actuator saturation, and so on. In the simulations actuator saturation and noise contaminated measurements were employed to model the uncertainties. An estimate of the achievable control accuracy was found to be about 0.1° . The tracking error of the leader satellite is displayed in Fig. 4.1(d), and the previous statement is also valid for this result.

In Fig. 4.1(c) we see that we have convergence of the estimates, but as commented in Remark 4.4, the convergence is dependent on the excitation level of the synchronization

EXTERNAL SYNCHRONIZATION OF RELATIVE ATTITUDE

error, and as the plot show we do not have convergence to the actual inertia parameters.

Finally, Fig. 4.1(b) shows the how the attitude of follower satellite tracks that of the leader.

4.5 Conclusions

We have in this chapter presented the design of an adaptive synchronizing controller, for a satellite actuated by means of redundant wheels in a tetrahedron composition. The proposed controller was proved to be uniformly globally exponentially stable for the case of parameter knowledge, and globally convergent when the parameters where estimated using a parameter update law. Simulations have been utilized to support the propositions, showing that the control system performs to specifications also when no knowledge of the parameters are available.

Chapter 5

6-DOF mutual synchronization of formation flying spacecraft

In this chapter we present a 6 degrees of freedom (6-DOF) synchronization scheme for a deep space formation of spacecraft. In the design, which is referred to as a mutual synchronization scheme, feedback interconnections are designed in such a way that the spacecraft track a time varying reference trajectory while at the same time keep a prescribed relative attitude and position. The closed-loop system is proven uniformly locally asymptotically stable, with an area of attraction which covers the complete state-space, except when the spacecraft attains an attitude where the inverse kinematics are undefined. The proof is carried out using Matrosov’s Theorem.

The contents of this chapter is based on (Krogstad & Gravdahl 2006a).

5.1 Introduction

In this work we apply theory derived in (Nijmeijer & Rodriguez-Angeles 2003), on mutual synchronization of robot manipulators, to design a synchronization scheme for a formation of autonomous spacecraft. The formation is assumed to be located such that influences from celestial objects can be ignored, a location often referred to as *deep space* in the literature. The goal is to have the attitude and position of each spacecraft track a desired trajectory, while simultaneously making sure that the spacecraft is synchronized with respect to the other formation members. The approach may be viewed as a combination of the leader-follower approach with a virtual leader and the behavioral approach, in that the spacecraft must attempt to achieve two possibly conflicting goals. Please refer to chapter 1 for details on these approaches and relevant references.

5.2 Mathematical model

5.2.1 Kinematic model

The kinematic differential equation in terms of Euler angles as derived in section 3.4.2 is given by

$$\dot{\Theta} = T(\Theta)\omega, \quad (5.1)$$

where

$$T(\Theta) = \frac{1}{\cos \theta} \begin{bmatrix} \cos \theta & \sin \phi \sin \theta & \cos \phi \sin \theta \\ 0 & \cos \phi \cos \theta & \sin \phi \cos \theta \\ 0 & \sin \phi & \cos \phi \end{bmatrix}. \quad (5.2)$$

5.2.2 Dynamical model

We use the dynamical model derived in section 3.5.3

$$\mathbf{J}\dot{\omega}_{ib}^b = (\mathbf{J}_b\omega_{ib}^b)^\times \omega_{ib}^b + (\mathbf{A}\mathbf{I}_s\omega_s)^\times \omega_{ib}^b - \mathbf{A}\tau_a + \tau_d \quad (5.3a)$$

$$\mathbf{I}_s\dot{\omega}_s = \tau_a - \mathbf{I}_s\mathbf{A}\dot{\omega}_{ib}^b \quad (5.3b)$$

For the purpose of control design we rewrite the model in terms of Euler angles and their first and second derivatives. Using the inverse kinematics

$$\omega_{ib}^b = T^{-1}(\Theta)\dot{\Theta}, \quad (5.4)$$

$$\dot{\omega}_{ib}^b = \dot{T}^{-1}(\Theta)\dot{\Theta} + T^{-1}(\Theta)\ddot{\Theta}, \quad (5.5)$$

we obtain the model

$$M(\Theta)\ddot{\Theta} = -C(\Theta, \dot{\Theta})\dot{\Theta} - A^*(\Theta)\tau_a + T^{-T}(\Theta)\tau_d \quad (5.6a)$$

$$\mathbf{I}_s\dot{\omega}_s = \tau_a - \mathbf{I}_s\mathbf{A}[\dot{T}^{-1}(\Theta)\dot{\Theta} + T^{-1}(\Theta)\ddot{\Theta}], \quad (5.6b)$$

where

$$M(\Theta) = T^{-T}(\Theta)JT^{-1}(\Theta) \quad (5.7)$$

$$C(\Theta, \dot{\Theta}) = -T^{-T}(\Theta)S(JT^{-1}(\Theta)\dot{\Theta}) + \mathbf{A}\mathbf{I}_s\omega_s T^{-1}(\Theta) + T^{-T}(\Theta)J\dot{T}^{-1}(\Theta) \quad (5.8)$$

$$A^*(\Theta) = T^{-T}(\Theta)\mathbf{A}. \quad (5.9)$$

It can also be shown the the matrices have the following properties

$$M = M^T > 0 \quad (5.10)$$

$$x^T(\dot{M} - 2C)x \equiv 0, \forall x \in \mathbb{R}^3 \quad (5.11)$$

Translational dynamics

The translational dynamics is derived for the case of formation flying in deep space, where the influence of other celestial objects is negligible. Under this assumption we model the translational dynamics as

$$m_b \mathbf{I}_{3 \times 3} \ddot{\mathbf{p}}^i = \mathbf{R}_b^i \mathbf{f}_d^b + \mathbf{R}_b^i \mathbf{f}_c^b, \quad (5.12)$$

where m_b is the mass of the spacecraft, \mathbf{p}^i is the inertial position of the center of gravity, \mathbf{f}_d^b and \mathbf{f}_c^b the disturbance and control forces respectively and \mathbf{R}_b^i the rotation matrix between \mathcal{F}_i and \mathcal{F}_b .

Complete 6 degrees of freedom model

A complete 6 DOF model may now be written as:

$$\mathbf{M}^*(\mathbf{x}) \ddot{\mathbf{x}} = -\mathbf{C}^*(\mathbf{x}, \dot{\mathbf{x}}) \dot{\mathbf{x}} - \mathbf{B}_1(\mathbf{x}) \mathbf{u} + \mathbf{B}_2(\mathbf{x}) \mathbf{w}, \quad (5.13a)$$

where

$$\mathbf{x} \triangleq [\mathbf{p}^i, \boldsymbol{\Theta}]^T \quad (5.14)$$

$$\mathbf{u} \triangleq [\mathbf{f}_c, \boldsymbol{\tau}_a^b]^T \quad (5.15)$$

$$\mathbf{w} \triangleq [\mathbf{f}_d, \boldsymbol{\tau}_d^b]^T \quad (5.16)$$

$$\mathbf{M}^*(\mathbf{x}) = \begin{bmatrix} m_b \mathbf{I}_{3 \times 3} & 0 \\ 0 & \mathbf{M}_{22}(\boldsymbol{\Theta}) \end{bmatrix} \quad (5.17)$$

$$\mathbf{C}^*(\mathbf{x}, \dot{\mathbf{x}}) = \begin{bmatrix} 0 & 0 \\ 0 & \mathbf{C}(\boldsymbol{\Theta}, \dot{\boldsymbol{\Theta}}) \end{bmatrix} \quad (5.18)$$

$$\mathbf{B}_1(\mathbf{x}) = \begin{bmatrix} \mathbf{R}_b^i & 0 \\ 0 & \mathbf{A}^*(\boldsymbol{\Theta}) \end{bmatrix} \quad (5.19)$$

$$\mathbf{B}_2(\mathbf{x}) = \begin{bmatrix} \mathbf{R}_b^i & 0 \\ 0 & \mathbf{T}^{-T}(\boldsymbol{\Theta}) \end{bmatrix} \quad (5.20)$$

Which retains the properties

$$\mathbf{M}^* = \mathbf{M}^{*T} > 0 \quad (5.21)$$

$$\mathbf{x}^T (\dot{\mathbf{M}}^* - 2\mathbf{C}^*) \mathbf{x} \equiv 0, \forall \mathbf{x} \in \mathbb{R}^3 \quad (5.22)$$

5.3 Control design

In this chapter we design a synchronization controller for attitude and position control of a spacecraft formation. The intuition behind the design is to develop a synchronization

6-DOF MUTUAL SYNCHRONIZATION OF FORMATION FLYING SPACECRAFT

scheme such that the spacecraft are synchronized both with respect to a desired attitude and position trajectory and at the same time maintaining the formation by keeping the relative attitude and distance. This may be necessary during formation reconfiguration to keep the spacecraft moving in a synchronized manner.

5.3.1 Synchronization error

Before we propose the controller we define the *mutual synchronization error* of the k 'th spacecraft as

$$\mathbf{s}_k \triangleq \mathbf{x}_k - \mathbf{x}_{rk}, \quad (5.23)$$

where \mathbf{x}_{rk} is defined by

$$\mathbf{x}_{rk} \triangleq \begin{bmatrix} \mathbf{K}_k \mathbf{p}_{dk}^i - \sum_{j=1, j \neq k}^n \mathbf{K}_{k,j} (\mathbf{p}_j^i - \mathbf{p}_k^i - \mathbf{p}_{dkj}^i) \\ \Theta_d - \sum_{j=1, j \neq k}^n \mathbf{K}_{k,j} (\Theta_j - \Theta_k) \end{bmatrix}, \quad (5.24)$$

which may be viewed as a virtual reference trajectory, combining the goals of tracking a desired reference attitude and position trajectory and synchronizing with the other spacecraft in the formation.

Assuming negligible disturbances, the error dynamic can be written as

$$\mathbf{M}_k^*(\mathbf{x}_k) \ddot{\mathbf{s}}_k = -\mathbf{C}^*(\mathbf{x}_k, \dot{\mathbf{x}}_k) \dot{\mathbf{x}}_k - \mathbf{B}_1(\mathbf{x}_k) \mathbf{u}_k - \mathbf{M}_k^*(\mathbf{x}_k) \ddot{\mathbf{x}}_{rk}. \quad (5.25)$$

Proposition 5.1. *The error dynamics (5.25), with control input*

$$\begin{aligned} \mathbf{B}_1(\mathbf{x}_k) \mathbf{u}_k &\triangleq \mathbf{C}^*(\mathbf{x}_k, \dot{\mathbf{x}}_k) \dot{\mathbf{x}}_{rk} + \mathbf{M}_k^*(\mathbf{x}_k) \ddot{\mathbf{x}}_{rk} \\ &\quad - \mathbf{K}_{p,k} \mathbf{s}_k - \mathbf{K}_{d,k} \dot{\mathbf{s}}_k, \forall k \in \{1, \dots, n\}, \end{aligned} \quad (5.26)$$

where $\mathbf{K}_{p,k}$ and $\mathbf{K}_{d,k}$ are positive definite gain matrices, has a uniformly asymptotically stable (UAS) origin $(\mathbf{s}_k, \dot{\mathbf{s}}_k) = (\mathbf{0}, \mathbf{0}) \forall k \in \{1, \dots, n\}$, for all initial conditions $(\mathbf{s}_{k0}, \dot{\mathbf{s}}_{k0})$ in any ball about the origin not containing $\theta_k = \pm \frac{\pi}{2}$. This implies UAS for the tracking error and the synchronization error.

Proof. By combining (5.25) and (5.26) the closed-loop error-dynamics can be written

$$\mathbf{M}_k^*(\mathbf{x}_k) \ddot{\mathbf{s}}_k + \mathbf{K}_{d,k} \dot{\mathbf{s}}_k + \mathbf{K}_{p,k} \mathbf{s}_k = -\mathbf{C}^*(\mathbf{x}_k, \dot{\mathbf{x}}_k) \dot{\mathbf{s}}_k. \quad (5.27)$$

As the error-variable is actually a function of the system state and a time-varying reference signal, the system is non-autonomous. This implies that the often invoked Lasalle's invariance principle (Khalil 2000), is no longer applicable in the case of a semi-definite Lyapunov derivative. We remedy this by invoking Matrosov's theorem (Matrosov 1962),

as it was given in (Hahn 1967). For ease of reference the theorem is summarized in section 2.3.2. We now proceed to satisfy the four assumptions of the theorem.

Satisfying Assumption 2.1: Taking $V(\mathbf{s}, \dot{\mathbf{s}}, t)$ as the quadratic lyapunov function candidate

$$V = \sum_{k=1}^n \left[\frac{1}{2} \dot{\mathbf{s}}_k^T \mathbf{M}_k^*(\mathbf{x}_k) \dot{\mathbf{s}}_k + \frac{1}{2} \mathbf{s}_k^T \mathbf{K}_{p,k} \mathbf{s}_k \right], \quad (5.28)$$

which is clearly continuous and positive definite and decrescent, we have satisfied the first assumption.

Satisfying Assumption 2.2: Taking the time derivative along solution trajectories and using (5.22), we obtain

$$\dot{V} = \sum_{k=1}^n \left[\dot{\mathbf{s}}_k^T \mathbf{M}_k^*(\mathbf{x}_k) \ddot{\mathbf{s}}_k + \frac{1}{2} \dot{\mathbf{s}}_k^T \dot{\mathbf{M}}_k^*(\mathbf{x}_k) \mathbf{s}_k + \dot{\mathbf{s}}_k^T \mathbf{K}_{p,k} \dot{\mathbf{s}}_k \right] \quad (5.29)$$

$$= \sum_{k=1}^n \dot{\mathbf{s}}_k^T \left[-\mathbf{K}_{d,k} \dot{\mathbf{s}}_k + \frac{1}{2} \dot{\mathbf{M}}_k^*(\mathbf{x}_k) \dot{\mathbf{s}}_k - \mathbf{C}^*(\mathbf{x}_k, \dot{\mathbf{x}}_k) \dot{\mathbf{s}}_k \right] \quad (5.30)$$

$$= \sum_{k=1}^n -\dot{\mathbf{s}}_k^T \mathbf{K}_{d,k} \dot{\mathbf{s}}_k = U(x) \leq 0. \quad (5.31)$$

Since the time derivative is negative semi-definite on any ball such that $\theta_k \neq \frac{\pi}{2} \forall k \in \{1, \dots, n\}$, \dot{V} can be bounded by a non-positive and continuous function, which is independent of time. Hence the second assumption is satisfied.

Satisfying Assumption 2.3: We take $W(\mathbf{x}, t)$ ¹ as

$$W \triangleq \sum_{k=1}^n \dot{\mathbf{s}}_k^T \mathbf{K}_{p,k} \mathbf{s}_k. \quad (5.32)$$

As Assumption 2 implies a uniformly stable closed-loop system, the states \mathbf{s} and $\dot{\mathbf{s}}$ are bounded, which in turn leads to the boundedness of $W(\mathbf{x}, t)$ satisfying the third assumption.

Satisfying Assumption 2.4: The final step is to show that when $\dot{V} = 0$, \dot{W} is definitely non-zero. Taking the time-derivative of W along the solution trajectories of (5.27) we obtain

$$\dot{W} = \sum_{k=1}^n \left[\dot{\mathbf{s}}_k^T \mathbf{K}_{p,k} \dot{\mathbf{s}}_k + \dot{\mathbf{s}}_k^T \mathbf{K}_{p,k} \ddot{\mathbf{s}}_k \right], \quad (5.33)$$

which on the set \mathbb{N} , as defined in (2.15), can be written

$$\dot{W} = \sum_{k=1}^n -\mathbf{s}_k^T \mathbf{K}_{p,k}^T \mathbf{M}_k^{*T}(\mathbf{x}_k) \mathbf{K}_{p,k} \mathbf{s}_k < 0, \quad \forall \mathbf{s}_k \neq 0 \quad (5.34)$$

¹Notice that there is no requirement for $W(\mathbf{x}, t)$ to be positive definite

6-DOF MUTUAL SYNCHRONIZATION OF FORMATION FLYING SPACECRAFT

Since it is non-zero for any $s_k \neq 0$ the last assumption is satisfied, and the system is *uniformly asymptotically stable* for any (s_{0k}, \dot{s}_{k0}) in any ball not containing $\theta_k = \pm \frac{\pi}{2}$.

Remark 5.1. *The limitation in the area of attraction comes from an inherent singularity in the Euler angle representation of attitude. Possible methods of avoiding this problem do exist. One way, similar to what was done in (Fjellstad & Fossen 1994), is to express the kinematics using a singularity free attitude representation like the unit quaternion, another possibility is to let the control system operate with two body frames and two sets of desired angles, such that the singularity can be avoided as in (Singla, Mortari & Junkins 2005). As the error would be the same, no discontinuities would appear in the control input, and an area of attraction covering the full state-space is achieved.*

The next step is to show that UAS of the origin $(s, \dot{s}) = (\mathbf{0}, \mathbf{0})$ implies UAS of the tracking and synchronization errors. We first rewrite the synchronization error s_k in terms of the position and attitude errors as

$$s_k = \begin{bmatrix} (\mathbf{K}_k - \sum_{j=1, j \neq k}^n \mathbf{K}_{k,j}) \tilde{p}_k^i - \sum_{j=1, j \neq k}^n \mathbf{K}_{kj} \tilde{p}_j^i \\ \tilde{\Theta}_{k,k} - \sum_{j=1, j \neq k}^p \mathbf{K}_{1,j} \tilde{\Theta}_{k,j} \end{bmatrix} \quad (5.35)$$

where we have defined

$$\tilde{p}_k^i \triangleq p_{dk}^i - p_k^i \quad (5.36)$$

$$\tilde{\Theta}_{k,k} \triangleq \Theta_d - \Theta_k \quad (5.37)$$

$$\tilde{\Theta}_{k,j} \triangleq \Theta_j - \Theta_k, \quad (5.38)$$

provided that the desired trajectory p_{dk}^i , have been defined such that the relative distances are feasible. The synchronization errors can be written in terms of the tracking position errors and the attitude tracking and synchronization errors as (5.40) and (5.39). With proper selection of the gain matrices \mathbf{K}_k and $\mathbf{K}_{k,j}$, such that the matrices \mathbf{G}_1 and \mathbf{G}_2 , result in unique solutions to (5.40) and (5.39), we have that convergence of the synchronization errors s_k imply $\Theta_k \rightarrow \Theta_d$ and $\tilde{p}_k \rightarrow 0, \forall k \in \{1, \dots, n\}$.

Similarly, one can show the convergence $\dot{x}_i \rightarrow \dot{x}_d$. This concludes the proof. \square

5.4 Simulations

We here present a simulation of the proposed synchronization scheme. We simulate a formation of 3 spacecraft, which have desired attitude and position trajectories, as well as desired relative distances.

5.4. SIMULATIONS

$$\underbrace{\begin{bmatrix} (\mathbf{I}_{3 \times 3} + \sum_{j=1, j \neq 1}^n \mathbf{K}_{1,j}) & -\mathbf{K}_{1,2} & \cdots & -\mathbf{K}_{1,n} \\ -\mathbf{K}_{2,1} & (\mathbf{I}_{3 \times 3} + \sum_{j=1, j \neq 2}^n \mathbf{K}_{2,j}) & \cdots & -\mathbf{K}_{2,n} \\ \vdots & \vdots & \ddots & \vdots \\ -\mathbf{K}_{n,1} & -\mathbf{K}_{n,2} & \cdots & (\mathbf{I}_{3 \times 3} + \sum_{j=1, j \neq n}^n \mathbf{K}_{n,j}) \end{bmatrix}}_{\mathbf{G}_1} \begin{bmatrix} \Theta_1 \\ \Theta_2 \\ \vdots \\ \Theta_n \end{bmatrix} = \begin{bmatrix} \Theta_d \\ \Theta_d \\ \vdots \\ \Theta_d \end{bmatrix} \quad (5.39)$$

$$\underbrace{\begin{bmatrix} (\mathbf{K}_1 - \sum_{j=1, j \neq 1}^n \mathbf{K}_{1,j}) & -\mathbf{K}_{1,2} & \cdots & -\mathbf{K}_{1,n} \\ -\mathbf{K}_{2,1} & (\mathbf{K}_1 - \sum_{j=1, j \neq 2}^n \mathbf{K}_{2,j}) & \cdots & -\mathbf{K}_{2,n} \\ \vdots & \vdots & \ddots & \vdots \\ -\mathbf{K}_{n,1} & -\mathbf{K}_{n,2} & \cdots & (\mathbf{K}_n - \sum_{j=1, j \neq n}^n \mathbf{K}_{n,j}) \end{bmatrix}}_{\mathbf{G}_2} \begin{bmatrix} \tilde{\mathbf{p}}_1^i \\ \tilde{\mathbf{p}}_2^i \\ \vdots \\ \tilde{\mathbf{p}}_n^i \end{bmatrix} = \begin{bmatrix} 0 \\ 0 \\ \vdots \\ 0 \end{bmatrix} \quad (5.40)$$

Table 5.1: Model parameters

Parameter	Value
Inertia matrix	$\text{diag}\{4, 4, 3\} [kgm^2]$
Wheel inertia	$8 \cdot 10^{-3} [kgm^2]$
Max wheel torque	$0.2 [Nm]$
Max wheel speed	$400 [rad/s]$
Max position thrust	$10 [N]$

$$\mathbf{p}_{1d}(t) = [t, 0, -t + 5]^T [km] \quad (5.41)$$

$$\mathbf{p}_{1d}(t) = [t + 1, 0, -t]^T [km] \quad (5.42)$$

$$\mathbf{p}_{1d}(t) = [t + 1, 1, -t]^T [km] \quad (5.43)$$

$$\Theta_d = 20^\circ \sin t \quad (5.44)$$

$$(5.45)$$

Initial conditions are given by

$$\mathbf{x}_1 = [5 \text{ km}, 0 \text{ km}, 0 \text{ km}, 10^\circ, 0^\circ, 21^\circ]^T \quad (5.46)$$

$$\mathbf{x}_2 = [0 \text{ km}, 10 \text{ km}, 0 \text{ km}, -20^\circ, 10^\circ, 35^\circ]^T \quad (5.47)$$

$$\mathbf{x}_3 = [0 \text{ km}, -10 \text{ km}, 0 \text{ km}, 20^\circ, 20^\circ, -35^\circ]^T \quad (5.48)$$

$$(5.49)$$

6-DOF MUTUAL SYNCHRONIZATION OF FORMATION FLYING SPACECRAFT

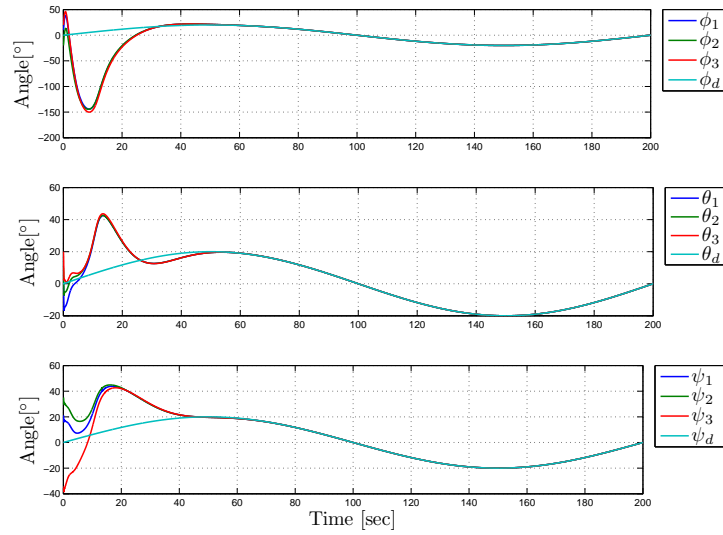


Figure 5.1: The figure illustrates how the attitudes of the three spacecraft are first mutually synchronized, and then track a desired orientation.

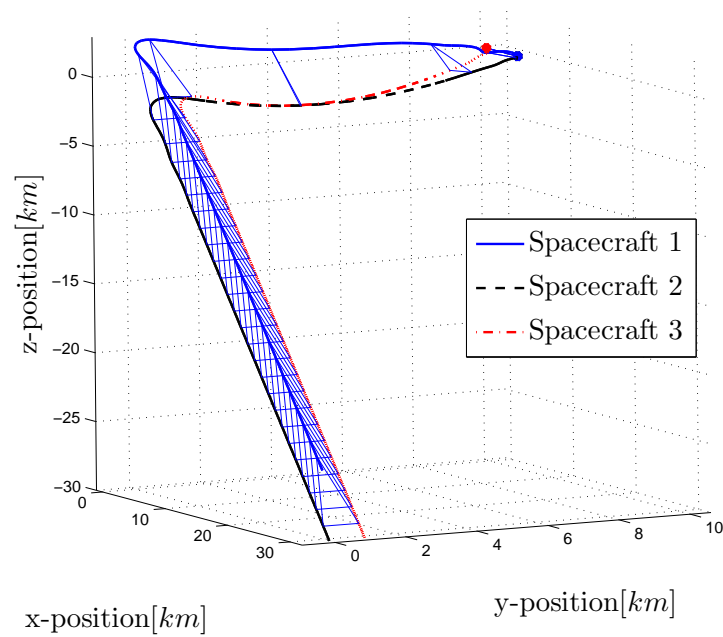


Figure 5.2: Tracking and synchronization behaviour in position. All units are in *km*. The triangles indicate the relative position at different time-instants. The initial position is indicated by a *.

In this simulation the satellites are controlled to follow a straight line movement through space, while retaining a triangular formation. The common desired attitude is selected as a sinusoidal function of time.

Simulations show that the trajectories, for both position and attitude, are tracked and that the synchronization errors converge. This behaviour is decided by selecting the gains of the controller such that synchronization errors are more penalized than tracking error. By decreasing the gains on the synchronization error, we obtain a behaviour where the spacecraft move towards the desired trajectory individually rather than in a synchronized manner.

Remark 5.2. *In the present design, collision avoidance is not implemented. One possibility is to implement a collision avoidance scheme on top of this low-level design.*

5.5 Conclusion

In this chapter we have given the design of 6 DOF mutual synchronization controller for a formation of spacecraft, similar to what has earlier been proposed for robotic manipulators. We have proved that the controller yields uniformly asymptotically stable error dynamics, such that all states converge to the desired states, in a synchronized manner. The proposition has been proved mathematically and its validity is demonstrated by numerical simulations.

6-DOF MUTUAL SYNCHRONIZATION OF FORMATION FLYING SPACECRAFT

Chapter 6

PID+ backstepping control of relative spacecraft attitude

In this chapter we present a PID+ backstepping controller, as a solution to the problem of coordinated attitude control in spacecraft formations. The control scheme is based on quaternions and modified Rodrigues parameters as attitude representation of the relative attitude error. Utilizing the invertibility of the modified Rodrigues parameter kinematic differential equation, a globally exponentially stable control law for the relative attitude error dynamics is obtained through the use of integrator augmentation and backstepping. Finally, simulation results are presented to show controller performance.

This chapter is based on (Krogstad, Kristiansen, Gravdahl & Nicklasson 2007, Kristiansen, Krogstad, Nicklasson & Gravdahl 2008, Kristiansen, Krogstad, Nicklasson & Gravdahl 2007).

6.1 Relevant related work

The controller is called PID+ to account for the fact that we have a PID controller, with the addition of some nonlinear terms (Paden & Panja 1988). In the design, we utilize the advantages of the modified Rodrigues parameter kinematic to obtain a globally exponentially stable relative attitude error dynamics. The use of the MRP for control of attitude has previously been reported in Tsiotras (1996), and this work extends this approach to case of spacecraft formation coordination and by including integral action to counter constant perturbations, along the lines of what was reported in Fossen (2002).

6.2 Relative Rotational Motion

In this chapter we use Euler parameters and modified Rodriguez parameters to represent attitude kinematics. From section 3.4.4 we have that the kinematic differential equation is given by

$$\dot{\mathbf{q}}_{ij} = \mathbf{T}(\mathbf{q}_{ij}) \boldsymbol{\omega}_{ij}^j, \mathbf{T}(\mathbf{q}_{ij}) = \frac{1}{2} \begin{bmatrix} -\boldsymbol{\epsilon}^T \\ \eta \mathbf{I} + \mathbf{S}(\boldsymbol{\epsilon}) \end{bmatrix} \quad (6.1)$$

where \mathbf{q}_{ij} corresponds to \mathbf{R}_j^i , $\boldsymbol{\omega}_{ij}^j$ is the angular velocity of the spacecraft body frame relative to the inertial frame, referenced in the body frame. Similarly the differential kinematics in terms of modified Rodriguez parameters is given by

$$\dot{\boldsymbol{\sigma}}_{ij} = \mathbf{G}(\boldsymbol{\sigma}_{ij}) \boldsymbol{\omega}_{ij}^j \quad (6.2)$$

where

$$\mathbf{G}(\boldsymbol{\sigma}_{ij}) \triangleq \frac{1}{4} ((1 - \boldsymbol{\sigma}_{ij}^T \boldsymbol{\sigma}_{ij}) \mathbf{I} + 2\mathbf{S}(\boldsymbol{\sigma}_{ij}) - \boldsymbol{\sigma}_{ij} \boldsymbol{\sigma}_{ij}^T) \quad (6.3)$$

With the assumptions of rigid body movement, the dynamical model of a spacecraft is given by Euler’s momentum equation as

$$\mathbf{J}_j \dot{\boldsymbol{\omega}}_{ij}^j = -\mathbf{S}(\boldsymbol{\omega}_{ij}^j) \mathbf{J}_j \boldsymbol{\omega}_{ij}^j + \boldsymbol{\tau}_{dj}^j + \boldsymbol{\tau}_{aj}^j \quad (6.4)$$

where $j \in \{l, b\}$, \mathbf{J}_j is the spacecraft inertia matrix and $\boldsymbol{\omega}_{ij}^j$ is the angular velocity of the spacecraft body frame relative to the inertial frame, expressed in the body frame, $\boldsymbol{\tau}_{dj}^j$ is the disturbance torque, $\boldsymbol{\tau}_{aj}^j$ is the actuator torque.

Further, by expressing the relations in (6.1) and (6.4)-(??) for both the leader and the follower spacecraft, and defining the quaternion describing the relative rotation as

$$\mathbf{q} \triangleq \bar{\mathbf{q}}_l \otimes \mathbf{q}_{l,f} \otimes \mathbf{q}_f, \quad (6.5)$$

where $\mathbf{q}_{l,f}$ describes the rotation between the leader and follower orbit frames, the relative attitude kinematics can be expressed as (Fjellstad & Fossen 1994)

$$\dot{\mathbf{q}} = \begin{bmatrix} \dot{\eta} \\ \dot{\boldsymbol{\epsilon}} \end{bmatrix} = \mathbf{T}(\mathbf{q}) \boldsymbol{\omega} \quad (6.6)$$

where

$$\boldsymbol{\omega} = \boldsymbol{\omega}_{if}^f - \mathbf{R}_l^f \boldsymbol{\omega}_{il}^l \quad (6.7)$$

is the relative angular velocity between the leader body reference frame and the follower body reference frame. Moreover, from (6.7) the relative attitude dynamics can be expressed as

$$\begin{aligned} \mathbf{J}_f \dot{\boldsymbol{\omega}} &= \mathbf{J}_f \dot{\boldsymbol{\omega}}_{if}^f - \mathbf{J}_f \dot{\mathbf{R}}_l^f \boldsymbol{\omega}_{il}^l - \mathbf{J}_f \mathbf{R}_l^f \dot{\boldsymbol{\omega}}_{il}^l \\ &= \mathbf{J}_f \dot{\boldsymbol{\omega}}_{if}^f - \mathbf{J}_f \mathbf{S} \left(\boldsymbol{\omega}_{il}^l \right) \boldsymbol{\omega} - \mathbf{J}_f \mathbf{R}_l^f \dot{\boldsymbol{\omega}}_{il}^l \end{aligned} \quad (6.8)$$

where (3.9) and the facts that $\boldsymbol{\omega}_{if}^f = \boldsymbol{\omega}$ and $\mathbf{S}(\mathbf{a})\mathbf{b} = -\mathbf{S}(\mathbf{b})\mathbf{a}$, $\forall \mathbf{a}, \mathbf{b} \in \mathcal{R}^3$ have been used. Insertion of (6.4), evaluated for both the leader and follower, into (6.8) results in (Kristiansen, Grøtli, Nicklasson & Gravdahl 2007)

$$\mathbf{J}_f \dot{\boldsymbol{\omega}} + \mathbf{C}_r(\boldsymbol{\omega}) \boldsymbol{\omega} + \mathbf{n}_r(\boldsymbol{\omega}) = \boldsymbol{\Upsilon}_d + \boldsymbol{\Upsilon}_a \quad (6.9)$$

where

$$\mathbf{C}_r(\boldsymbol{\omega}) = \mathbf{J}_f \mathbf{S} \left(\mathbf{R}_l^f \boldsymbol{\omega}_{il}^l \right) + \mathbf{S} \left(\mathbf{R}_l^f \boldsymbol{\omega}_{il}^l \right) \mathbf{J}_f - \mathbf{S} \left(\mathbf{J}_f \left(\boldsymbol{\omega} + \mathbf{R}_l^f \boldsymbol{\omega}_{il}^l \right) \right) \quad (6.10)$$

is a skew-symmetric matrix, $\mathbf{C}_r(\boldsymbol{\omega}) \in SS(3)$,

$$\mathbf{n}_r(\boldsymbol{\omega}) = \mathbf{S} \left(\mathbf{R}_l^f \boldsymbol{\omega}_{il}^l \right) \mathbf{J}_f \mathbf{R}_l^f \boldsymbol{\omega}_{il}^l - \mathbf{J}_f \mathbf{R}_l^f \mathbf{J}_l^{-1} \mathbf{S} \left(\boldsymbol{\omega}_{il}^l \right) \mathbf{J}_l \boldsymbol{\omega}_{il}^l \quad (6.11)$$

is a nonlinear term, and

$$\boldsymbol{\Upsilon}_d = \boldsymbol{\tau}_{df}^f - \mathbf{J}_f \mathbf{R}_l^f \mathbf{J}_l^{-1} \boldsymbol{\tau}_{dl}^l, \quad (6.12)$$

$$\boldsymbol{\Upsilon}_a = \boldsymbol{\tau}_{af}^f - \mathbf{J}_f \mathbf{R}_l^f \mathbf{J}_l^{-1} \boldsymbol{\tau}_{al}^l \quad (6.13)$$

are the relative disturbance torques and relative actuator torques, respectively.

6.3 Control design

In this paper we consider coordinated control of a two-satellite formation, where the control objective is to have the relative attitude track a desired time-varying smooth trajectory.

We define the error between the relative attitude and the desired relative attitude in quaternion notation as

$$\mathbf{q}_e = \bar{\mathbf{q}}_d \otimes \mathbf{q}, \quad (6.14)$$

which has a corresponding modified Rodrigues parameter

$$\boldsymbol{\sigma}_e \triangleq \frac{\boldsymbol{\epsilon}_e}{1 + \eta_e}, \quad (6.15)$$

PID+ BACKSTEPPING CONTROL OF RELATIVE SPACECRAFT ATTITUDE

with kinematic differential equation

$$\dot{\boldsymbol{\sigma}}_e = \mathbf{G}(\boldsymbol{\sigma}_e)\boldsymbol{\omega}_e, \quad (6.16)$$

where $\boldsymbol{\omega}_e \triangleq \boldsymbol{\omega} - \mathbf{R}(\mathbf{q}_e)\boldsymbol{\omega}_d$ and $\mathbf{G}(\boldsymbol{\sigma}_e)$ is given by (6.3).

For controller design we use the backstepping procedure. The first step is to augment our system with a state equal to the integral of our selected error variable, to implement integral action and resistance to unknown constant perturbations. We select this state as the first backstepping variable,

$$\mathbf{z}_0 \triangleq \int_{t_0}^t \boldsymbol{\sigma}_e d\tau, \quad (6.17)$$

with the trivial dynamics

$$\dot{\mathbf{z}}_0 = \boldsymbol{\sigma}_e. \quad (6.18)$$

We select $\boldsymbol{\sigma}_e$ as the virtual input, defined as

$$\boldsymbol{\sigma}_e \triangleq \boldsymbol{\alpha}_0 + \mathbf{z}_1, \quad (6.19)$$

where $\boldsymbol{\alpha}_0$ is a stabilizing control for the \mathbf{z}_0 -dynamics to be defined, and \mathbf{z}_1 is the next backstepping variable. Moreover, we define the first Lyapunov function candidate

$$V_0 = \frac{1}{2} \mathbf{z}_0^T \mathbf{z}_0, \quad (6.20)$$

with derivative along the system trajectories

$$\dot{V}_0 = \mathbf{z}_0^T \dot{\mathbf{z}}_0 = \mathbf{z}_0^T (\boldsymbol{\alpha}_0 + \mathbf{z}_1). \quad (6.21)$$

Taking the stabilizing function as

$$\boldsymbol{\alpha}_0 = -\mathbf{K}_0 \mathbf{z}_0, \quad (6.22)$$

where $\mathbf{K}_0 = \mathbf{K}_0^T > 0$, we obtain

$$\dot{V}_0 = -\mathbf{z}_0^T \mathbf{K}_0 \mathbf{z}_0 + \mathbf{z}_1^T \mathbf{z}_0. \quad (6.23)$$

We proceed to define the \mathbf{z}_1 -dynamics, using (6.19), as

$$\dot{\mathbf{z}}_1 = \dot{\boldsymbol{\sigma}}_e - \dot{\boldsymbol{\alpha}}_0 = \mathbf{G}\boldsymbol{\omega}_e - \dot{\boldsymbol{\alpha}}_0, \quad (6.24)$$

and select $\boldsymbol{\omega}_e$ as the virtual input. The virtual input is defined

$$\boldsymbol{\omega}_e = \boldsymbol{\alpha}_1 + \mathbf{z}_2. \quad (6.25)$$

As in the preceding step we define a Lyapunov function candidate

$$V_1 = V_0 + \frac{1}{2} \mathbf{z}_1^T \mathbf{z}_1, \quad (6.26)$$

with derivative along the system trajectories

$$\dot{V}_1 = -z_0^T \mathbf{K}_0 z_0 + z_1^T (z_0 - \dot{\alpha}_0 + \mathbf{G} \omega_e). \quad (6.27)$$

The stabilizing function for the second backstepping subsystem is selected as

$$\alpha_1 \triangleq \mathbf{G}^{-1}(-\mathbf{K}_1 z_1 + \dot{\alpha}_0 - z_0), \quad (6.28)$$

where $\mathbf{K}_1 = \mathbf{K}_1^T > 0$, and obtain

$$\dot{V}_1 = -z_0^T \mathbf{K}_0 z_0 - z_1^T \mathbf{K}_1 z_1 + z_1^T \mathbf{G} z_2 \quad (6.29)$$

Remark 6.1. *In this step we take advantage of the crucial property that $\mathbf{G}^{-1}(\sigma_e)$ is well defined for all σ_e .*

The dynamics governing the z_2 -dynamics is obtained through differentiation of (6.25) and insertion of (6.8)

$$\begin{aligned} \mathbf{J}_f \dot{z}_2 &= \mathbf{J}_f \dot{\omega}_e - \mathbf{J}_f \dot{\alpha}_1 \\ &= \mathbf{J}_f \dot{\omega} - \mathbf{J}_f \frac{d}{dt}(\mathbf{R}(\mathbf{q}_e) \omega_d) - \mathbf{J}_f \dot{\alpha}_1 \\ &= -\mathbf{C}_r(\omega) \omega - \mathbf{n}_r(\omega) + \Upsilon_a - \mathbf{J}_f \frac{d}{dt}(\mathbf{R}(\mathbf{q}_e) \omega_d) - \mathbf{J}_f \dot{\alpha}_1. \end{aligned} \quad (6.30)$$

We continue to define a Lyapunov function candidate

$$V_2 = V_1 + \frac{1}{2} z_2^T \mathbf{J} z_2, \quad (6.31)$$

with derivative along the system trajectories

$$\begin{aligned} \dot{V}_2 &= -z_0^T \mathbf{K}_0 z_0 - z_1^T \mathbf{K}_1 z_1 + z_2^T \left\{ \mathbf{G}^T z_1 \right. \\ &\quad \left. - \mathbf{C}_r(\omega) \omega - \mathbf{n}_r(\omega) + \Upsilon_a - \mathbf{J}_f \frac{d}{dt}(\mathbf{R}(\mathbf{q}_e) \omega_d) - \mathbf{J}_f \dot{\alpha}_1 \right\} \end{aligned} \quad (6.32)$$

Assuming that the leader is controlled by an asymptotically stable controller, such that we only need to control the follower, we design the control input to the follower as

$$\tau_f \triangleq \Upsilon_a \triangleq -\mathbf{G}^T z_1 + \mathbf{C}_r(\omega) \omega + \mathbf{n}_r(\omega) + \mathbf{J}_f \frac{d}{dt}(\mathbf{R}(\mathbf{q}_e) \omega_d - \mathbf{K}_2 z_2) \quad (6.33)$$

which results in

$$\dot{V}_2 = -z_0^T \mathbf{K}_0 z_0 - z_1^T \mathbf{K}_1 z_1 - z_2^T \mathbf{K} z_2. \quad (6.34)$$

Proposition 6.1. *The closed-loop error dynamics*

$$\dot{z}_0 = -\mathbf{K}_0 z_0 + z_1 \quad (6.35)$$

$$\dot{z}_1 = -\mathbf{K}_1 z_1 - z_0 + z_2 \quad (6.36)$$

$$\dot{z}_2 = -\mathbf{K}_2 z_2 - z_1 \quad (6.37)$$

obtained through the backstepping procedure, is globally exponentially stable (GES), resulting in exponential convergence of the relative attitude tracking error $(\sigma_e, \omega_e) \rightarrow (0, 0)$.

Proof. The GES property of the closed loop dynamics (6.35)-(6.37), follows from the the Lyapunov function candidate (6.31) and its derivative (6.34). V_2 is positive definite and decrescent, and $V_2 = z^T \mathbf{P} z$ with $z = [z_0^T, z_1^T, z_2^T]^T$ and $\mathbf{P} = \text{diag}(\mathbf{I}, \mathbf{I}, \mathbf{J}_f)$. From (6.34) it is clear that \dot{V}_2 is negative definite, and $\dot{V}_2 = -z^T \mathbf{Q} z$ with $\mathbf{Q} = \text{diag}(\mathbf{K}_0, \mathbf{K}_1, \mathbf{K}_2)$. It is now straightforward to invoke standard Lyapunov theorems (Khalil 2000), concluding global exponential stability of the obtained error dynamics. That is $[z_0^T, z_1^T, z_2^T]^T$ approaches zero exponentially. Moreover we have that $z_0 \equiv 0$ and $z_1 \equiv 0 \Rightarrow \sigma_e \equiv \alpha_0 \equiv -\mathbf{K}_0 z_0 \equiv 0$, and $z_2 \equiv 0 \Rightarrow \omega_e \equiv \alpha_1 \equiv 0$. □

Remark 6.2. *Our result is global in the sense that for any initial condition, $(\sigma_e, \omega_e) \rightarrow (0, 0)$ exponentially. However since we are using a minimal attitude representation, a singularity will be introduced at some level. In this case, the singularity is moved to the translation from quaternion error to modified Rodrigues parameters, since the quaternion $[-1, \mathbf{0}^T]^T$ does not have a well defined MRP vector.*

6.4 Simulations

We here present the simulation of a two-satellite formation. The leader satellite is controlled by a exponentially stable tracking controller, while the follower is controlled by the proposed controller to track a desired relative orientation.

The moment of inertia of both spacecraft are $\mathbf{J} = \text{diag}(4, 3.9, 0.3)[kg \cdot m^2]$ and the initial orientation are $\mathbf{q}_f = [0.213, 0.674, 0.674, -0.213]$ for follower. The spacecraft

For simplicity the desired relative orientation is given as a sinusoidal signal in Euler angles, given by

$$\Psi_d = \begin{bmatrix} \frac{25\pi}{180} \sin\left(\frac{2\pi}{500}\right) \\ \frac{60\pi}{180} \sin\left(\frac{2\pi}{400}\right) \\ -\frac{60\pi}{180} \sin\left(\frac{2\pi}{400}\right) \end{bmatrix}. \quad (6.38)$$

6.4.1 Results

The simulation results for relative orientation tracking are presented in figure 6.2, with the corresponding transient error plot in figure 6.1.

As determined by the theoretical results, the relative orientation converge exponentially to the desired reference trajectory.

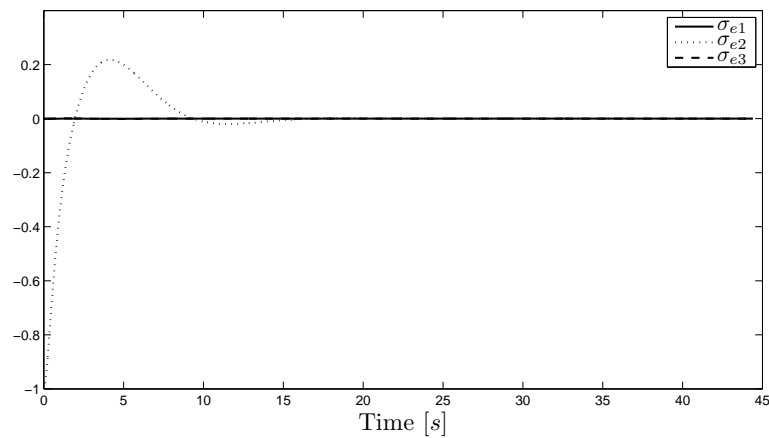


Figure 6.1: Transient error expressed in modified Rodrigues parameters.

6.5 Conclusion

In this chapter we presented a control algorithm for relative spacecraft attitude. The controller was derived using the relative attitude model of (Kristiansen, Grøtli, Nicklasson & Gravdahl 2007) and modified Rodrigues parameters to describe the kinematic model. Using the method of integrator augmentation and backstepping a controller which rendered the closed loop dynamic uniformly exponentially stable was derived. The theoretical result was supported by simulations performed in Matlab Simulink.

PID+ BACKSTEPPING CONTROL OF RELATIVE SPACECRAFT ATTITUDE

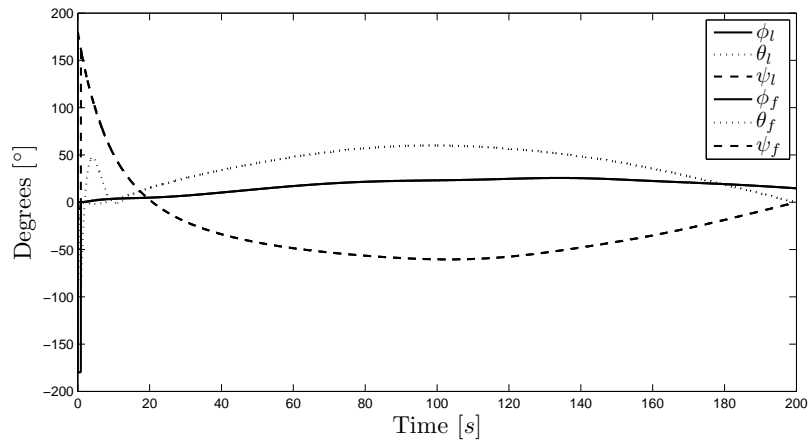


Figure 6.2: Tracking of desired relative attitude, expressed in Euler angles.

Chapter 7

Output feedback control of relative spacecraft attitude

In this chapter we present a controller-observer scheme for relative spacecraft attitude control. The system of interest is a leader-follower formation, where we assume that the leader is controlled by some stable controller and we want the follower to track the attitude of the leader. Furthermore we assume that only the relative attitude is available for control purposes, and to estimate the relative angular velocity we introduce an error observer. The resulting closed-loop system is proved to be uniformly practically asymptotically stable to a ball centered at the origin.

The content of this chapter is based on (Krogstad & Gravdahl 2009*a*, Krogstad & Gravdahl 2009*b*)

7.1 Introduction

The contribution of this chapter is the design of an observer-controller output feedback scheme for relative spacecraft attitude. The scheme is developed for a leader-follower spacecraft formation, where the leader is assumed to be controlled by a tracking controller. Furthermore we assume that the follower has knowledge about its own attitude and angular velocity in addition to the relative attitude with respect to the leader. Since we do not know the angular velocity and acceleration of the leader, we design an error observer in spirit of the work presented in (Kyrkjebø 2007*a*), where an error observer design is presented for Euler-Lagrange systems. In this work we apply a similar observer to a model described using quaternion kinematics.

Lizarralde & Wen (1996) proposed a control scheme for rigid-body attitude stabilization when the angular velocity is not available, using a velocity filter. A similar approach can be found in (Cotic et al. 2000) where an adaptive quaternion based controller is used

OUTPUT FEEDBACK CONTROL OF RELATIVE SPACECRAFT ATTITUDE

is used for a single spacecraft and the need for velocity feedback is eliminated using a filter; and the authors conclude global convergence of the system states. Similar to (Cotic et al. 2000), (Singla et al. 2006) and (Akella 2001) propose a control scheme without the need for angular velocity measurement, and show convergence of the tracking error using Barbalat’s lemma. A scheme for attitude synchronization in a leader-follower spacecraft formation using attitude feedback only, was presented in (Bondhus et al. 2005). The controller was designed using backstepping and velocity information is provided by two observers. It was proved that the attitude error rotation matrix converges to the identity matrix. (Bai et al. 2008) derive passivity based controllers for synchronizing orientation of rigid bodies assuming knowledge of relative orientation and angular velocity in body coordinates. In the case of unknown leader reference angular velocity an adaptive design is done in order to keep the convergence properties of the original scheme. In (Kristiansen et al. 2009) a synchronizing output feedback controller was also derived for the case of unknown leader velocity, obtaining similar stability results as our scheme, but without synchronization error observer.

In our approach the inclusion of the observer allows us to conclude uniform practical asymptotic stability of the error dynamics, as defined in section 2.3.1. The UPAS property ensures convergence and stability of a ball around the origin, which can be arbitrarily diminished.

7.1.1 Motivation

The problem of controlling relative attitude without using measurements of relative angular velocity follows naturally from the fact that this measurement often is not directly available. Take as an example the DARWIN spacecraft formation. In this setup the relative attitude is measured very accurately using optical instruments, but no such measurement exists for the relative angular velocity. This motivates for control schemes which are independent of angular velocity measurements.

7.2 Mathematical model

7.2.1 Kinematics

In this chapter we use the kinematical differential equations parameterized using the Euler parameters

$$\dot{\eta}_{ib} = -\frac{1}{2}\epsilon_{ib}^T \omega_{ib}^b \quad (7.1a)$$

$$\dot{\epsilon}_{ib} = \frac{1}{2}[\eta_{ib} \mathbf{I}_{3 \times 3} + \mathbf{S}(\epsilon_{ib})] \omega_{ib}^b, \quad (7.1b)$$

where ω_{ib}^b is the angular velocity of the body relative to an inertial frame. Given the quaternion vector

$$\mathbf{q}_{ib} \triangleq \begin{bmatrix} \eta_{ib} \\ \boldsymbol{\epsilon}_{ib} \end{bmatrix}, \quad (7.2)$$

we may write the (7.1) in compact form

$$\dot{\mathbf{q}}_{ib} = \frac{1}{2} \mathbf{Q}(\mathbf{q}_{ib}) \omega_{ib}^b, \quad \text{where} \quad \mathbf{Q}(\mathbf{q}_{ib}) \triangleq \begin{bmatrix} -\boldsymbol{\epsilon}_{ib}^T \\ \eta_{ib} \mathbf{I}_{3 \times 3} + \mathbf{S}(\boldsymbol{\epsilon}_{ib}) \end{bmatrix} \quad (7.3)$$

Euler angles, or roll-pitch-yaw angles, have been applied in the visualization of results, since these are easier to relate to physical motion.

7.2.2 Dynamic model

In this chapter a dynamical model for a rigid body actuated by means of external moments, given by Euler’s momentum equation

$$\dot{\omega}_{ib}^b = \mathbf{S}(\mathbf{J}_b \omega_{ib}^b) \omega_{ib}^b + \boldsymbol{\tau}_a^b + \boldsymbol{\tau}_d^b, \quad (7.4)$$

where ω_{ib}^b is the angular velocity of the body relative to an inertial frame, \mathbf{J}_b is the body inertia matrix, $\boldsymbol{\tau}_a^b$ is the control input, and $\boldsymbol{\tau}_d^b$ disturbance moments.

7.3 Control and observer design

7.3.1 Assumptions

We have assumed that the available measurements are the orientation and angular velocity of the follower and the relative orientation with respect to the leader. Furthermore we assume that the angular acceleration and angular velocity of the leader vehicle are bounded. These assumptions are reasonable since the leader is assumed to be controlled by an asymptotically stable tracking controller.

7.3.2 Control objectives

The control objective is for the follower to track the attitude motion of the leader, expressed as

$$\lim_{t \rightarrow \infty} \omega_e = \mathbf{0} \quad (7.5)$$

$$\lim_{t \rightarrow \infty} \mathbf{q}_e = [1, 0, 0, 0]^T, \quad (7.6)$$

OUTPUT FEEDBACK CONTROL OF RELATIVE SPACECRAFT ATTITUDE

where ω_e and q_e are relative angular velocity and orientation respectively, defined by

$$\omega_e \triangleq \omega_{if}^f - (\mathbf{R}_f^l)^T \omega_{il}^l, \quad (7.7)$$

$$q_e \triangleq q_{il}^{-1} \otimes q_{if}. \quad (7.8)$$

where ω_{il}^l and ω_{if}^f are leader and follower angular velocities respectively, and \mathbf{R}_f^l is the rotation matrix corresponding to the relative attitude error q_e as defined in (3.29).

7.3.3 Error dynamics

We define a synchronization measure

$$s \triangleq \omega_e + \lambda \epsilon_e. \quad (7.9)$$

Moreover, we define a virtual reference trajectory for the follower spacecraft as

$$\omega_r = (\mathbf{R}_f^l)^T \omega_{il}^l - \lambda \epsilon_e, \quad (7.10)$$

enabling us to rewrite the synchronization measure as

$$s = \omega_{if}^f - \omega_r. \quad (7.11)$$

We can now write the system dynamics as

$$\mathbf{J}_f \dot{s} = \mathbf{S} \left(\mathbf{J}_f \omega_{if}^f \right) \omega_{if}^f + \tau - \mathbf{J}_f \dot{\omega}_r \quad (7.12a)$$

$$\dot{q}_e = \frac{1}{2} \mathbf{Q}(q_e)(s - \lambda \epsilon_e) \quad (7.12b)$$

Proposition 7.1. *The system (7.22a)-(7.12b), with the control input defined as*

$$\tau_f = -k_d s - k_p \epsilon_e + \mathbf{J}_f \dot{\omega}_r - \mathbf{S} \left(\mathbf{J}_f \omega_{if}^f \right) \omega_{if}^f, \quad (7.13)$$

where $k_d \in \mathbb{R}_{>0}$ and $k_p \in \mathbb{R}_{>0}$ are constants, has a locally uniformly exponentially stable (ULES) origin $(s, \epsilon_e) = (0, 0)$. From (7.9) which we can conclude exponential convergence of the relative attitude and orientation errors as defined in (7.5) and (7.6).

Proof. The proof can be carried out as in (Wen & Kreutz-Delgado 1991), using the radially unbounded, positive definite Lyapunov function

$$V = \frac{1}{2} s^T \mathbf{J}_f s + 2k_p(1 - \eta_e), \quad (7.14)$$

which has time-derivative along the trajectories

$$\dot{V} = -k_d s^T s - k_p \lambda \epsilon_e^T \epsilon_e < 0, \quad (7.15)$$

which is negative definite. Hence we can conclude uniform local asymptotic stability, definition 2.7, of the system origin. \square

7.3.4 Error observer

As the relative angular velocity is not available, the controller in Proposition 7.1 cannot be implemented. Inspired by (Kyrkjebø 2007a, Kyrkjebø 2007b), we therefore design an error-observer to estimate the synchronization measure using the measured relative attitude.

We define the error-variables

$$\tilde{s} \triangleq s - \hat{s} \quad (7.16)$$

$$\tilde{q}_e \triangleq q_e^{-1} \otimes \hat{q}_e, \quad (7.17)$$

where \hat{s} is the estimate of the synchronization measure and \hat{q}_e is the estimate of the relative attitude. The observer is implemented as

$$\mathbf{J}_f \dot{\hat{s}} = \mathbf{S} \left(\mathbf{J}_f \omega_{if}^f \right) \omega_{if}^f + \tau_f - l_2 \tilde{\epsilon}_e \quad (7.18)$$

$$\dot{\hat{q}}_e = \frac{1}{2} \mathbf{Q}(\hat{q}_e) (\tilde{\mathbf{R}}_e^T (\hat{s} - \lambda \epsilon) - l_1 \tilde{\epsilon}_e), \quad (7.19)$$

which imply that the observer error dynamics can be written as

$$\mathbf{J} \dot{\tilde{s}} = -\mathbf{J} \dot{\omega}_r + l_2 \tilde{\epsilon}_e \quad (7.20a)$$

$$\dot{\tilde{q}} = \frac{1}{2} \mathbf{Q}(\tilde{q}_e) (-\tilde{\mathbf{R}}_e^T \tilde{s} - l_1 \tilde{\epsilon}_e). \quad (7.20b)$$

We first introduce the state vector,

$$\chi \triangleq \begin{bmatrix} s \\ \epsilon_e \\ \tilde{s} \\ \tilde{\epsilon}_e \end{bmatrix} \quad (7.21)$$

with the differential equation

$$\mathbf{J}_f \dot{s} = \mathbf{S} \left(\mathbf{J}_f \omega_{if}^f \right) \omega_{if}^f + \tau_f - \mathbf{J}_f \dot{\omega}_r \quad (7.22a)$$

$$\dot{\epsilon}_e = \frac{1}{2} (\eta_e \mathbf{I}_{3 \times 3} + \mathbf{S}(\epsilon_e)) (s - \lambda \epsilon_e) \quad (7.22b)$$

$$\mathbf{J} \dot{\tilde{s}} = -\mathbf{J} \dot{\omega}_r + l_2 \tilde{\epsilon}_e \quad (7.22c)$$

$$\dot{\tilde{\epsilon}} = \frac{1}{2} (\eta_e \mathbf{I}_{3 \times 3} + \mathbf{S}(\epsilon_e)) \left(-\tilde{\mathbf{R}}_e^T \tilde{s} - l_1 \tilde{\epsilon}_e \right). \quad (7.22d)$$

We are now ready to state the main result of the paper.

Proposition 7.2. *The system dynamics (7.22), with the control input of the follower as*

$$\tau = -\mathbf{S} \left(\mathbf{J}_f \omega_{if}^f \right) \omega_{if}^f - k_p \epsilon_e - k_d \hat{s}, \quad (7.23)$$

OUTPUT FEEDBACK CONTROL OF RELATIVE SPACECRAFT ATTITUDE

is uniformly practically asymptotically stable (UPAS) as defined in section 2.3.1. In addition since $s = 0$ and $\epsilon_e = 0$ corresponds to $\omega_e = 0$, we can conclude UPAS of the relative attitude and angular velocity.

Proof. The stability proof is conducted using the Lyapunov function

$$V = \frac{1}{2} \mathbf{s}^T \mathbf{J}_f \mathbf{s} + \frac{1}{2} \tilde{\mathbf{s}}^T \mathbf{J}_f \tilde{\mathbf{s}} - c \mathbf{s}^T \mathbf{J}_f \tilde{\mathbf{s}} + 2k_p(1 - \eta_e) + 2l_1(1 - \tilde{\eta}_e), \quad (7.24)$$

which is positive definite and radially unbounded for $0 < c < 1$. Taking the time derivative along the system trajectories we obtain

$$\dot{V} = -\boldsymbol{\chi}^T \mathbf{Q} \boldsymbol{\chi} + \Delta_\omega, \quad (7.25)$$

where

$$\mathbf{Q} = \begin{bmatrix} k_d \mathbf{I} & \mathbf{0} & -\frac{1}{2} k_d c \mathbf{I} & \frac{1}{2} c l_2 \mathbf{I} \\ \mathbf{0} & k_p \lambda \mathbf{I} & \frac{1}{2} c k_p \mathbf{I} & \mathbf{0} \\ -\frac{1}{2} k_d c \mathbf{I} & \frac{1}{2} c k_p \mathbf{I} & c k_d \mathbf{I} & \frac{1}{2} (l_1 \tilde{\mathbf{R}}_e - l_2 \mathbf{I}) \\ \frac{1}{2} c l_2 \mathbf{I} & \mathbf{0} & \frac{1}{2} (l_1 \tilde{\mathbf{R}}_e^T - l_2 \mathbf{I}) & l_1^2 \mathbf{I} \end{bmatrix} \quad (7.26)$$

and

$$\Delta_\omega = \boldsymbol{\chi}^T \begin{bmatrix} -\mathbf{J} \dot{\boldsymbol{\omega}}_r \\ 0 \\ -\mathbf{J} \dot{\boldsymbol{\omega}}_r \\ 0 \end{bmatrix}. \quad (7.27)$$

We reorganize the terms in \dot{V} to be able to see which gains result in a positive definite \mathbf{Q}

$$\begin{aligned} \dot{V} = & -\frac{1}{2} \begin{bmatrix} \mathbf{s} \\ \tilde{\mathbf{s}} \end{bmatrix}^T \underbrace{\begin{bmatrix} k_d \mathbf{I} & -k_d c \mathbf{I} \\ -k_d c \mathbf{I} & \frac{2}{3} k_d c \mathbf{I} \end{bmatrix}}_{\mathbf{Q}_1} \begin{bmatrix} \mathbf{s} \\ \tilde{\mathbf{s}} \end{bmatrix} - \frac{1}{2} \begin{bmatrix} \boldsymbol{\epsilon}_e \\ \tilde{\boldsymbol{\epsilon}}_e \end{bmatrix}^T \underbrace{\begin{bmatrix} k_p \lambda \mathbf{I} & \mathbf{0} \\ \mathbf{0} & \frac{2}{3} l_1^2 \mathbf{I} \end{bmatrix}}_{\mathbf{Q}_2} \begin{bmatrix} \boldsymbol{\epsilon}_e \\ \tilde{\boldsymbol{\epsilon}}_e \end{bmatrix} \\ & - \frac{1}{2} \begin{bmatrix} \mathbf{s} \\ \tilde{\boldsymbol{\epsilon}}_e \end{bmatrix}^T \underbrace{\begin{bmatrix} k_d \mathbf{I} & c l_2 \mathbf{I} \\ c l_2 \mathbf{I} & \frac{2}{3} l_1^2 \mathbf{I} \end{bmatrix}}_{\mathbf{Q}_3} \begin{bmatrix} \mathbf{s} \\ \tilde{\boldsymbol{\epsilon}}_e \end{bmatrix} - \frac{1}{2} \begin{bmatrix} \tilde{\mathbf{s}} \\ \boldsymbol{\epsilon}_e \end{bmatrix}^T \underbrace{\begin{bmatrix} \frac{2}{3} c k_d \mathbf{I} & c k_p \mathbf{I} \\ c k_p \mathbf{I} & k_p \lambda \mathbf{I} \end{bmatrix}}_{\mathbf{Q}_4} \begin{bmatrix} \tilde{\mathbf{s}} \\ \boldsymbol{\epsilon}_e \end{bmatrix} \\ & - \frac{1}{2} \begin{bmatrix} \tilde{\mathbf{s}} \\ \tilde{\boldsymbol{\epsilon}}_e \end{bmatrix}^T \underbrace{\begin{bmatrix} \frac{2}{6} c k_d \mathbf{I} & -l_2 \mathbf{I} \\ -l_2 \mathbf{I} & \frac{2}{6} l_1^2 \mathbf{I} \end{bmatrix}}_{\mathbf{Q}_5} \begin{bmatrix} \tilde{\mathbf{s}} \\ \tilde{\boldsymbol{\epsilon}}_e \end{bmatrix} - \frac{1}{2} \begin{bmatrix} \tilde{\mathbf{s}} \\ \tilde{\boldsymbol{\epsilon}}_e \end{bmatrix}^T \underbrace{\begin{bmatrix} \frac{2}{6} c k_d \mathbf{I} & l_1 \tilde{\mathbf{R}}_e \\ l_1 \tilde{\mathbf{R}}_e^T & \frac{2}{6} l_1^2 \mathbf{I} \end{bmatrix}}_{\mathbf{Q}_5} \begin{bmatrix} \tilde{\mathbf{s}} \\ \tilde{\boldsymbol{\epsilon}}_e \end{bmatrix} + \Delta_\omega. \quad (7.28) \end{aligned}$$

By examining the determinant of the matrices \mathbf{Q}_i we find the following conditions on the controller and observer gains, and the Lyapunov function parameters

$$0 < c < \frac{2}{3} \quad (7.29)$$

$$k_d > \max \left\{ \frac{9l_2^2}{cl_1^2}, 9c, \frac{3ck_p}{2\lambda} \right\} \quad (7.30)$$

for which V is positive definite and radially unbounded, and \mathbf{Q} is a positive definite matrix.

Furthermore, using bounds on Δ_ω , derived in (7.36) in the chapter appendix in section 7.6, we rewrite the Lyapunov function derivative as

$$\dot{V} \leq -q_m \|\boldsymbol{\chi}\|^2 + c_1 \|\boldsymbol{\chi}\|^2 + c_2 \|\boldsymbol{\chi}\|, \quad (7.31)$$

where q_m is the smallest eigenvalue of \mathbf{Q} . Note that q_m can be adjusted by appropriately selecting the controller and observer gains. By restricting the norm of the system state to $\|\boldsymbol{\chi}\| \geq \delta$, we obtain

$$\dot{V} \leq -\frac{1}{2}q_m \|\boldsymbol{\chi}\|^2 - \left(\frac{1}{2}q_m - \frac{c_1}{\delta} - c_2\right) \|\boldsymbol{\chi}\|^2. \quad (7.32)$$

Which, when constricting the controller observer gains such that

$$\frac{1}{2}q_m \geq \frac{c_1}{\delta} + c_2 \quad (7.33)$$

we obtain

$$\dot{V} \leq -\frac{1}{2}q_m \|\boldsymbol{\chi}\|^2, \quad (7.34)$$

for all $\|\boldsymbol{\chi}\| \in \mathbb{D}$ such that $\|\boldsymbol{\chi}\| \geq \delta$. And we can conclude UPAS of the closed loop system as defined in definition 2.2, according to Corollary 2.1. \square

7.4 Simulation

In this section a leader-follower spacecraft formation is simulated using the proposed observer-controller structure. The model properties, along with controller and observer gains can be found in table 7.1.

Table 7.1: Model parameters

Parameter	Value
Inertia matrix leader, \mathbf{J}_l	diag{1, 3, 4} [kgm ²]
Inertia matrix follower, \mathbf{J}_f	diag{10, 3, 4} [kgm ²]
Initial angular velocity leader, $\boldsymbol{\omega}_{il,0}^l$	[0.1, 0, 0] ^T [rad/s]
Initial angular velocity follower, $\boldsymbol{\omega}_{if,0}^f$	[0, 0, 0] ^T [rad/s]
Initial orientation leader, \mathbf{q}_l	[-1, 0, 0, 0] ^T
Initial orientation follower, \mathbf{q}_f	[0.5, 0.5, 0.5, 0.5] ^T
$[k_p, k_d, l_1, l_2, \lambda]$	[700, 4000, 120, 1000, 0.5]

The leader is controlled by an exponentially stable tracking controller, and commanded to do a slew maneuver. After the initialization of the simulation, the leader is perturbed by torque inputs of 10[mN] every 35 seconds.

7.4.1 Results

As one can see from fig. 1 and 2, both the synchronization measure and the observer error approach a ball about the origin, which corresponds well with the theoretical findings. Moreover, fig. 3 and 4 suggest that we also have UPAS for the observer error dynamics. While fig. 5 show that the relative angular velocity also converges.

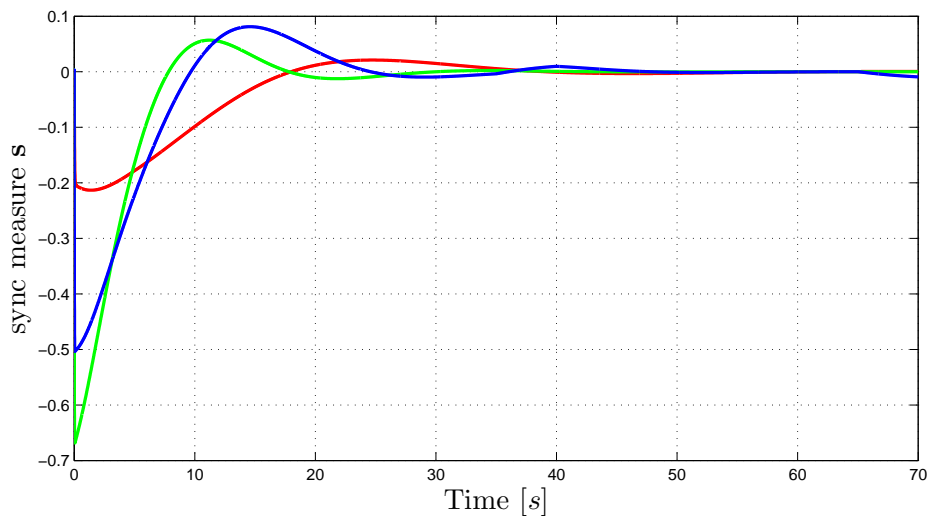


Figure 7.1: Synchronization measure s .

7.5 Conclusion

In this chapter we have considered the problem of controlling the relative attitude in a leader-follower spacecraft formation. A controller-observer output feedback approach has been proposed, which guarantees that the relative attitude converge to a ball about the origin, and that the closed-loop system is uniformly practically asymptotically stable. The performance of the proposed scheme has been investigated through numerical simulations in MATLAB SIMULINK, and the results supported our theoretical findings. In chapter 9 we will investigate the performance of this control scheme further as we implement it on our experimental platform AUVSAT.

7.6 Appendix

7.6.1 Bound on Δ_ω

In this appendix we give the calculation of the bound on Δ_ω

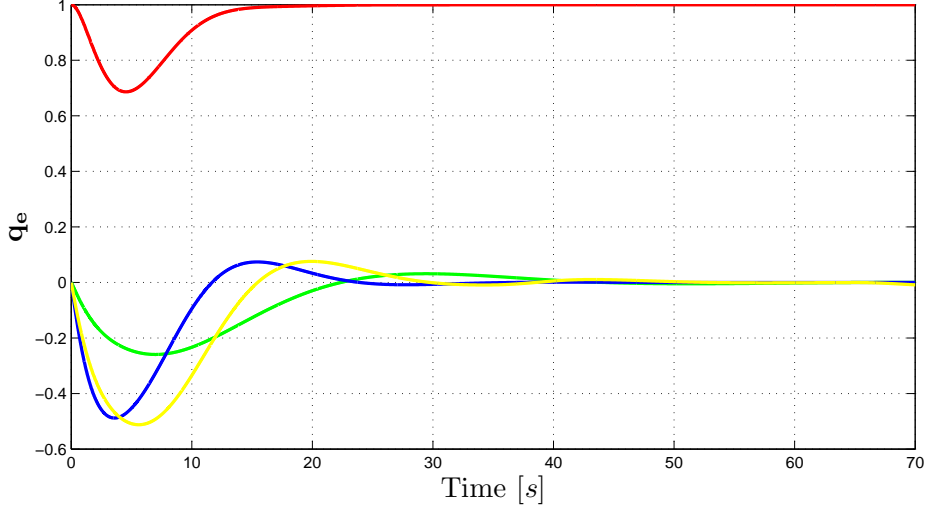


Figure 7.2: Attitude synchronization error q_e .

$$\Delta_\omega = \chi^T \begin{bmatrix} -\mathbf{J}\dot{\omega}_r \\ 0 \\ -\mathbf{J}\dot{\omega}_r \\ 0 \end{bmatrix} \quad (7.35)$$

and

$$\|\Delta_\omega\| \leq 2\|\chi\|\|\mathbf{J}\dot{\omega}_r\| \quad (7.36)$$

where

$$\mathbf{J}_f \dot{\omega}_r = \mathbf{J}_f (\dot{\mathbf{R}}_f^l)^T \omega_{il}^l + \mathbf{J}_f (\mathbf{R}_f^l)^T \dot{\omega}_{il}^l - \lambda \mathbf{J}_f \dot{\epsilon}_e \quad (7.37)$$

$$= -\mathbf{J}_f \mathbf{S} (s - \lambda \epsilon_e) (\mathbf{R}_f^l)^T \omega_{il}^l + \mathbf{J}_f (\mathbf{R}_f^l)^T \dot{\omega}_{il}^l \quad (7.38)$$

$$+ \lambda^2 \eta_e \mathbf{J}_f \epsilon_e - \lambda \mathbf{J}_f (\eta_e \mathbf{I} + \mathbf{S}(\epsilon_e)) s \quad (7.39)$$

Using the bounds on the leader angular velocities and angular acceleration, we obtain

$$\|\mathbf{J}_f \dot{\omega}_r\| \leq c_1 \|\chi\| + c_2 \quad (7.40)$$

where the constants c_1 and c_2 are given by

$$c_1 = 2j_m \beta_l + 4\lambda j_m + \lambda^2 j_m \quad (7.41)$$

$$c_2 = j_m \beta_{al} \quad (7.42)$$

and we have used $\|\omega_{il}^l\| \leq \beta_l$, $\|\dot{\omega}_{il}^l\| \leq \beta_{al}$, $\|\mathbf{J}_f\| \leq j_m$, $\|(\mathbf{R}_f^l)^T\| \leq 1$, $\|\eta_e \mathbf{I} + \mathbf{S}(\epsilon_e)\| \leq 2$.

OUTPUT FEEDBACK CONTROL OF RELATIVE SPACECRAFT ATTITUDE

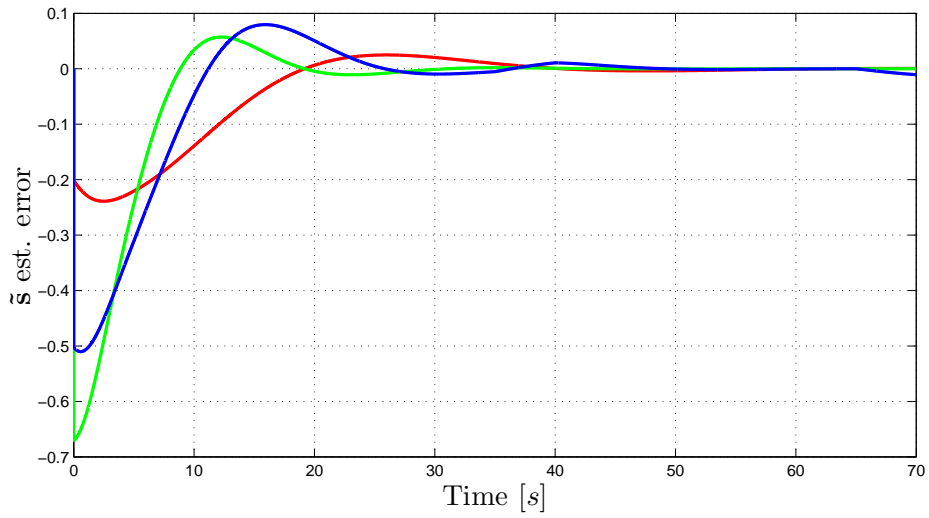


Figure 7.3: Synchronization measure s .

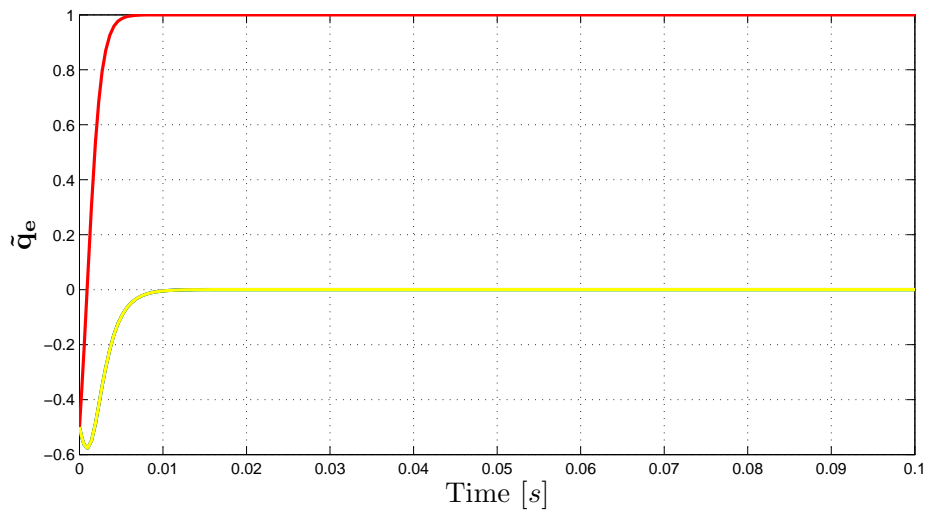


Figure 7.4: Attitude synchronization error q_e .

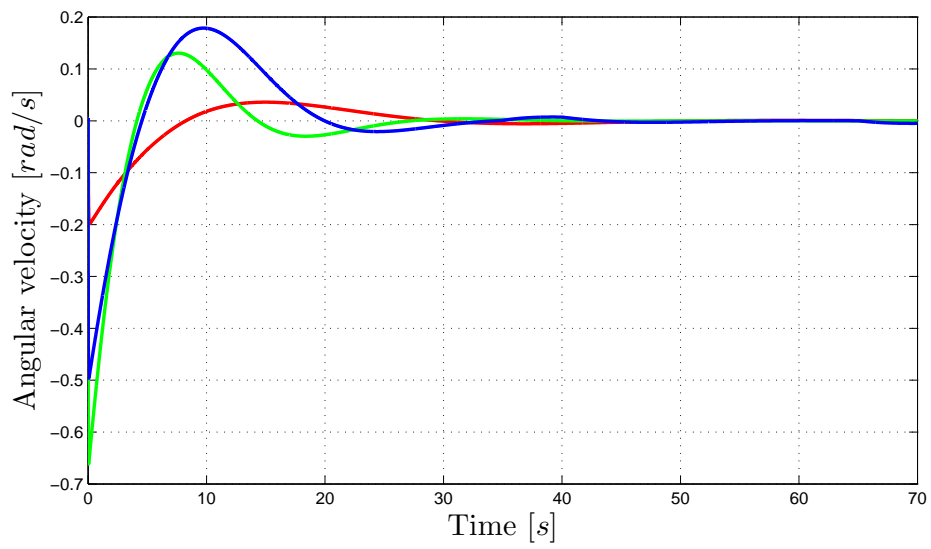


Figure 7.5: Synchronization angular velocity error ω_e .

OUTPUT FEEDBACK CONTROL OF RELATIVE SPACECRAFT ATTITUDE

Chapter 8

AUVSAT - an experimental platform for spacecraft formation flying

In this chapter we present the design of an underwater experimental platform for relative attitude control of spacecraft. The platform is part of the AUVSAT project at the Department of Engineering Cybernetics at the Norwegian University of Science and Technology, a project with the goal of creating an underwater experimental laboratory for formation control of underwater vehicles and spacecraft. In this work the laboratory was used to obtain experimental results for two of the main contributions. In the following we describe the design and the specifications leading to it. The content of this chapter is based on (Krogstad, Gravdahl, Pettersen & Børhaug 2008).

8.1 Introduction

The motivation for building an experimental platform is to provide a set-up for experimental verification of theoretical results on spacecraft formation flying demonstrating the strengths and shortcomings of the theory, and in this way contribute to bridge the gap between theory and practice. NTNU has several laboratories for experimental verification of marine control systems, and we wanted to utilize the existing infrastructure when developing the experimental platform for spacecraft formation flying. To this end, we initiated a project to develop an underwater test facility. The facility would consist of two or more autonomous underwater vehicles (AUVs) and three underwater satellites, using an underwater environment and neutrally buoyant vehicles to emulate space.

Examples of existing satellite simulators include the air-bearing platforms described in (Jung & Tsiotras 2003) and (Kowalchuk & Hall 2005*b*). These both use the principle

AUVSAT - AN EXPERIMENTAL PLATFORM FOR SPACECRAFT FORMATION FLYING

of a balanced platform on a sphere shaped air-bearing, controlled by reaction wheels. Since they balance on a bearing, they have limited travel in pitch and roll. An example of a spacecraft simulator which can rotate freely about all axes, is the IAMBUS (Schultz & Woolsey 2003). This is a sphere shaped underwater vehicle and was used as a basis for our single vehicle design.

Experimental platforms for spacecraft formation control can also be found in the literature, i.e. the SPHERES project at MIT and the Distributed Spacecraft Attitude Control System Simulator at Virginia Polytechnic Institute and State University (Kowalchuk & Hall 2005a).

This chapter contains two main parts. In section 8.2 we give an introduction to the autonomous underwater vehicles, the focus is however on the spacecraft simulator, and we describe the vehicles and laboratory setup in section 8.3.

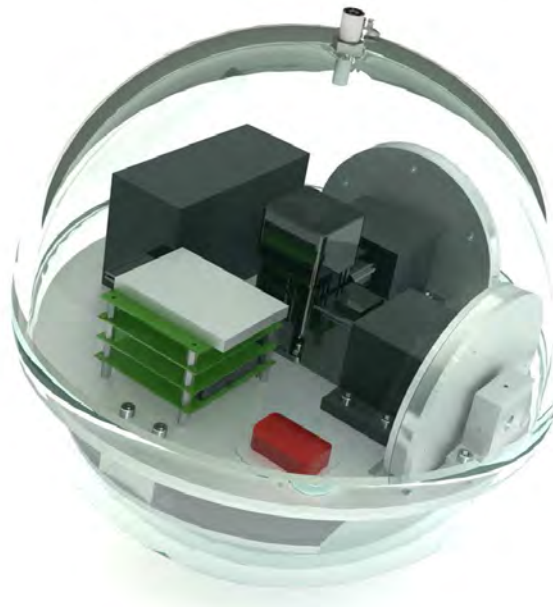


Figure 8.1: Computer design of the underwater satellite

8.2 Autonomous underwater vehicle design

The first stage of the project was the design of two autonomous underwater vehicles. This allowed us to take advantage of prior knowledge at the department. The AUV field is rapidly developing, and several commercial and military vehicles already exist and are applied in numerous tasks, most of which are in the surveillance and survey category. These types of operations require speed and agility, and most vehicles are therefore

8.2. AUTONOMOUS UNDERWATER VEHICLE DESIGN

shaped to minimize drag and are usually controlled by means of propeller and control surfaces at the rear of the vehicle. With this in mind the design and construction of the torpedo shaped Skarv AUV was initiated in 2004 (Børhaug 2005) and was finished early 2006.

However, future AUV operations include inspection and maintenance tasks, where the importance of position keeping will arise. This formed the specifications for the second vehicle of the underwater formation control platform. In the following we give a short summary of the design of this vehicle, the Munin AUV.

8.2.1 Specifications

When designing the second vehicle of the AUV experimental platform, the following set of specifications was chosen to guide the design. Firstly, to keep it small-sized, to be able to operate it in our indoor facilities and to field test it without the need for a lot of equipment and manpower to set it afloat. Secondly, to be maneuverable and able to dynamically position itself accurately in three dimensions. We now show how these guidelines influenced the design.



Figure 8.2: Illustration of the Munin AUV performing hovering inspection of an offshore oil and gas installation.

8.2.2 Hull and construction

The design of the hull of Munin had to take both guidelines of the previous section into consideration. The size and weight of the vehicle were the first factors considered. The length of the vehicle was chosen to be about 1.5 m and the dry-weight had to be no more than 80 kg. This allowed the vehicle to be handled by two persons in the field

AUVSAT - AN EXPERIMENTAL PLATFORM FOR SPACECRAFT FORMATION FLYING

and during testing. The small size of the vehicle meant that care would have to be taken when selecting and placing internal hardware. It would also complicate maintenance and assembly. To overcome this the hull was sectioned into three compartments; the nose, middle and aft section. In addition to simplifying maintenance and assembly, this also gives flexibility to extend the vehicle by additional sections which may include more sensors, battery power, actuators etc.

To add maneuverability the hull would include 4 tunnel thrusters, as well as feedthroughs for propeller and dive plane shafts.

To simplify construction, the basic structure of each section was first shaped in high density polyurethane foam. This material is typically used in architectural modeling and prototyping, and is easily shaped to the desired profiles. The basic structure was then hollowed out to shape the internal compartments, and holes for feedthroughs and thrusters were drilled and reinforced using acrylic piping. The foam shell was covered in glassfibre reinforced plastics to add strength and make the vehicle watertight.

8.2.3 Sensors

Due to the compartment design and simple assembly and disassembly procedure, the AUV has flexibility to include a large number of different sensors, both for navigation and for mission-dependent measurement purposes. Currently the AUV is equipped with sensors measuring attitude, depth and surface position. The attitude sensor is the low-cost MEMS inertial measurement unit (IMU) Xsens MTi, chosen for its ease of use, small-size and prior utilization in underwater vehicles. Depth is measured using a Tectis pressure sensor. Additionally a Garmin GPS antenna is included to provide position measurements while surfaced. Moreover, it can provide absolute position estimate updates while surfaced, when using navigation grade IMUs to integrate position while operating underwater. Navigation grade refers to the amount of drift in position and attitude estimates obtained from accelerometer and gyro measurements.

Planned enhancements of the design include an additional section, including a Teledyne Explorer doppler velocity log (DVL) and a Kongsberg Seatex MRU, to provide more accurate position and velocity estimates during diving. Furthermore, a sonar will be incorporated to provide more accurate depth and bottom profiling.

8.2.4 Actuators

To satisfy the hovering requirement, the AUV is actuated by means of tunnel thrusters, propellers and dive planes. For low-speed positioning and attitude control, two pairs of vertical and horizontal tunnel thrusters are used in conjunction with two rear propellers. At higher speeds tunnel thrusters are less efficient, and depth is instead controlled using dive planes while heading is controlled by running the rear propellers differentially.

8.3. UNDERWATER SATELLITE DESIGN

The tunnel thrusters are powered by Maxon RE35 DC motors, providing 130 Watts of power, while the dive planes are controlled by two HiTec metal gear mini servos.

8.3 Underwater satellite design

In this section we present the design of the spacecraft simulator part of the underwater experimental platform, and the specifications which lead up to the final design. The motivation for our design came from the need to experimentally verify theoretical results on spacecraft control, and in particular verify control schemes for relative attitude control in spacecraft formations.

Table 8.1: Hardware overview for the underwater satellites

Device	Name	Description
Actuators		
Motor	SmartMotor SM2330D	Compact servo motor with integrated motor control hardware. Used to power the reaction wheels
Ballast system	XP250-12 Piston Tank	This is a piston operated ballast system, capable of adjusting the mass of the vehicle by 250 g.
Main control computer		
PC/104 CPU card	Kontron MOP-SlcdLX	Main board with 500MHz Pentium processor and 1 GB RAM
PC/104 Serial communication extension card	Xtreme-4/104	4 extra 16C654 UARTS, RS232/RS485 connections
PC/104 IO card	Access 104-AIO12-8	Analog and digital inputs and outputs.
Power supply	HESC104 Vehicle power supply	Powers the PC/104 stack and also has additional power connections for sensors and piston tank control motor.
Solid state storage	FlashDrive/104	4GB of flash storage

Table 8.2: Sensor properties

Sensor	Property	Accuracy
XSens MTi	Angular resolution	0.05 deg
	Static accuracy (Roll/Pitch)	< 0.05 deg
	Static accuracy (Heading)	< 1 deg
	Dynamic accuracy	2 deg RMS
Pressure sensor	Range	0-1 bar
	Accuracy	0.01 m

8.3.1 Hull design

The design of the hull was based on a need to minimize drag and other hydrodynamic effects, and to have a hull which made it easier to achieve a center of mass coinciding with the center of buoyancy. The decision to make the hull spherical therefore seemed sensible. Several options were considered, aluminum and glass-fibre reinforced plastics were some which were later discarded. Due to space-requirements of actuators, sensors and control hardware, the internal space required for the system suggested an diameter of 30-40 cm. The side-effect of this design choice is that the sphere creates a lot of buoyancy, to help counter this the material of the pressure hull should be dense. In addition the material could not have properties which interfered with magnetometer measurements, i.e. it should not contain ferromagnetic materials which interfere with the measured magnetic field used by the IMU as an absolute attitude reference. The choice finally fell on an 17" spherical glass instrument housing. This instrument housing, manufactured by Nautilus Marine Service GmbH, is typically used in deep sea research, and has precision cut mating edges. This enables the sphere to be kept closed by evacuating air through a pressure vent, requiring no exterior mechanical device to close the spheres, keeping the surface streamlined.

8.3.2 Sensors

Due to space restrictions, the low-cost and small-size Xsens MTi IMU was also chosen for the spacecraft simulator. This sensor uses three-axis gyro and magnetometer data to obtain attitude and angular velocity. The accuracy and noise ratio is provided in table 8.2. The sensor and vehicle computer communicates through a serial connection. The sensor can be programmed to send data at different rates from on-demand to 100 Hz, which is sufficient for our use. The sensor can also send the attitude data as quaternions, Euler angles or as a direction cosine matrix, and can also provide the actual magnetometer

data which can be convenient to simulate typical student-made cubesats, where the only sensors typically are magnetometers (Krogstad, Gravdahl & Tøndel 2005).

In addition to the IMU, a pressure sensor is also included. This is used when controlling the vertical position of the vehicles, to keep them fully submerged during experiments. We do not control the horizontal position in this setup. But since we will do experiments in an indoor pool, the horizontal position should be relatively stable and collisions can be avoided provided the initial distances between vehicles are kept large enough.

8.3.3 Actuators

To minimize drag and get experience with spacecraft related actuators, it was decided to internally actuate the vehicle using reaction wheel assemblies. Each vehicle has three assemblies mounted orthogonally along the x , y and z body axes. The reaction wheel assembly consists of an aluminum and lead momentum wheel, mounted to a servo motor. The servo motor is controlled to store and deliver momentum to the wheel. Three factors were considered when selecting the motor: size, torque and speed. Size was limited by the internal volume of the sphere, consequently limiting the maximum possible speed and torque. Moreover, torque and speed are competing features, i.e. by demanding high torque, the maximum speed is reduced and vice versa. In our case two factors dictated the choice of parameters. The top speed of the motor and inertia of the momentum wheel determines the amount of momentum which can be stored and hence, how long we can operate the vehicle before dumping momentum. The maximum torque determines the restoring moment which can be suppressed. The latter factor was deemed most important, as the inability to suppress the restoring moments would render the vehicle inoperable. Using an mathematical model of the vehicle, we did calculations and simulations to conclude. The choice was the Animatics SM2330 servomotor.

The Animatics motors are communicated with using RS232, to send torque commands and to obtain encoder readings.

In addition to the motors the vehicles are also equipped with a ballast tank system. This is to enable the vehicle to be completely submerged at all times.

8.3.4 Communication

Communication with the vehicles are done using Ethernet LAN, both from the on-shore computer to the vehicles and in-between each vehicle. Inter-vehicle communication is done using the UDP protocol. Using this communication tunnel, each vehicle shares its attitude and angular velocity with the other vehicles in the formation.

This wired communication form is not ideal for our purposes, but time constraints did not allow for further advancements in this area. Further extensions of the experimental

AUVSAT - AN EXPERIMENTAL PLATFORM FOR SPACECRAFT FORMATION FLYING

platform should therefore include researching the use of radio frequency or acoustic communications, enabling the vehicles to talk both to the on-shore computer and the other vehicles wirelessly.

8.3.5 Main computer

The main computer comprises PC/104 embedded computer boards, containing CPU motherboard, IO communication card, power supply card, serial communication extension card and solid state storage. The PC/104 form factor is a compact implementation of the PC bus as found in a desktop computer, but implemented on modular and stackable circuit boards. The standard was developed to alleviate the need for specially developed PC boards in embedded applications requiring the abilities of the desktop PC bus. The CPU board has a 500 MHz low power Pentium processor and 1 GB of RAM, which is more than sufficient for this application. The system has 4 GB of solid state storage, sufficient for OS requirements, main programs and data storage. The IO communication card carries digital and analog input and output cards to communicate with sensors. In addition a board with auxiliary serial ports is included, used for motor communication.

8.3.6 Software design

The software was designed to be used in both the AUVs and the spacecraft simulators. Therefore it was imperative that the software was reusable, modular and easy to maintain, keeping most vehicle specific code in low-level drivers. Implementation and design of control schemes should also be straightforward and intuitive. In addition the system needed to communicate with low-level hardware (sensors, actuators, communication devices, etc.) in a reliable and timely manner, meaning that some form of real-time capabilities would need to be implemented. As the laboratory was intended to also be used by master students and visiting researchers, implementing and design control algorithms and observers should be intuitive and simple.

Overall structure

The overall structure of the software is shown in fig 8.3. From this illustration we clearly see the modular design of the software. Where the user only needs to interact with the Simulink diagram and can change controllers and estimators, and obtain and analyze sensor and actuation data in the same manner as in a regular Matlab Simulink simulation. Matlab real-time workshop is used to interface the QNX system and low-level drivers which enables Simulink to control the vehicles.

8.3. UNDERWATER SATELLITE DESIGN

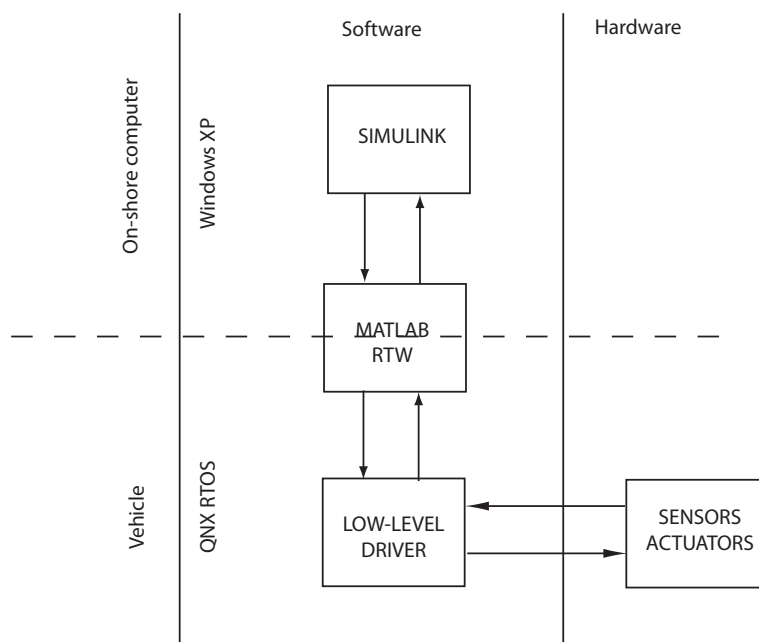


Figure 8.3: Overall structure

Operating system

The on-shore computer runs Windows XP, though any operating system (OS) capable of running Matlab and the real-time workshop toolbox could be used. There are no real-time requirements of the on-shore computer, as it is used only for off-line control system implementation and data gathering and analysis.

On the vehicle side, where the main components of the control system actually run, the ability to communicate with sensors and actuators in real-time is of the utmost importance. i.e. we need to handle incoming sensor data, make it available to the control algorithm and send the resulting command to the actuators with as little delay as possible. An operating system which satisfies these demands is therefore called a real-time operating system (RTOS). The QNX Neutrino is such a RTOS, in addition to being specifically designed for embedded systems. It is microkernel-based, i.e. the operating system is run as a number of small tasks or servers. The advantage is a very scalable OS, in that by shutting down features which are unnecessary it can be implemented in a very compact form advantageous for system with limited resources. It also includes real-time features such as task prioritizing and scheduling, and intertask communication and resource sharing.

Matlab Real-time workshop

The software connection between the on-shore computer and the vehicle is Matlab Real-time Workshop. This is toolbox for Matlab Simulink, which in combination with Simulink models facilitates rapid prototyping and implementation of control algorithms, in a way that feels seamless to a regular Simulink simulation. Real-time Workshop takes the Simulink model and all of its blocks, scripts and s-functions and generate C or C++ source code, which can be compiled and run on the target QNX computer. In addition to generating code, the toolbox also provides a communication interface between the program run on the target computer and the Simulink model on the on-shore computer. This makes it possible to graphically represent measurements and control signals in real-time in Simulink, and to log data for later analysis and presentation.

Simulink

Another advantage of using Matlab Real-time workshop, is the integration with the Simulink development environment. It has a graphical user interface, where dynamical models and algorithms are created by placing function blocks (i.e integrators, derivatives, gains, etc.) This also means that we can easily change between simulation and hardware implementation by just moving the block containing the control algorithm, provided we ensure that the two models contain equivalent inputs and outputs.

8.3. UNDERWATER SATELLITE DESIGN



Figure 8.4: Communication overview

Low level interfaces

As we are using devices which for the most part do not have readily available QNX drivers, these have been developed. The low-level drivers are implemented as shared libraries on the QNX target, and are loaded by the code generated by the RTW toolbox. These drivers are responsible for interfacing the vehicle’s hardware, i.e. sending control commands, requesting measurements, handling incoming data, initializing the hardware, etc. There are 5 such interfaces implemented on the vehicle

- Motor interface
- IMU interface
- ADC/DAC interface
- Servo motor interface
- UDP communication interface

The motor interface is responsible for initiating and maintaining communication with the motor driver cards on each motor. This includes sending torque commands, setting the correct communication protocols, receiving and parsing encoder data, and starting and braking the motors. The driver implements an interrupt driven serial protocol.

The IMU interface is similarly to the motor interface, based on interrupt driven serial communication. It is responsible for initializing the IMU, setting the correct output mode and output frequency, in addition to parsing the incoming messages. The parser extracts the orientation and angular velocity data from the received message, and makes it available for the control system.

The ADC/DAC interface handles communication with the AD/DA converter card and starts up sampling of the analogue inputs. It is also responsible for the timer circuits generating the servo signal used to control the ballast system.

8.3.7 Internal structure

The hardware components are mounted on a solid aluminum framework, to keep the system from vibrating, as shown in fig. 8.1. The Framework was designed using Autodesk Inventor to fit properly in the sphere shell hull, and mounting holes placed such as to provide a center of gravity as close to the center of buoyancy as possible. The framework was cut using CNC milling, and assembled at the mechanical workshop of the Department of Engineering Cybernetics. The reaction wheel assemblies are mounted orthogonal to each other along the body axes. In addition to the required hardware, lead weights were calculated and placed both to make the vehicle neutrally buoyant and to achieve a center of gravity coinciding with the center of buoyancy.

8.3. UNDERWATER SATELLITE DESIGN



(a) Animatics SmartMotor SM2330D



(b) Tecsis pressure sensor and XSens IMU. The battery is of size AAA



(c) Piston tank for the ballast system



(d) PC/104 embedded computer

Figure 8.5: Hardware parts for the AUVSAT

AUVSAT - AN EXPERIMENTAL PLATFORM FOR SPACECRAFT FORMATION FLYING

Chapter 9

Experimental results

In this section we present experimental results conducted to verify some of the theoretical contributions presented in earlier chapter of this thesis. The results which have been investigated are the PID+ backstepping controller and the output feedback controller presented in chapter 6 and 7, respectively. In addition we present some simpler controllers, similar to the ones given in chapter 4. These were implemented both to verify the functional design of the platform and to help remove errors in the software source code. This included a PD depth controller, a PID controller acting on the error in the yaw angle, and a full quaternion feedback PD controller with stabilized roll and pitch axes. The experiments were conducted on the AUVSAT experimental platform described in the previous chapter.



Figure 9.1: Outdoor facility

EXPERIMENTAL RESULTS

9.1 Mathematical model

As derived in section 3.5.2 the model of a gyrostat is given by

$$\mathbf{J}\dot{\boldsymbol{\omega}}_{ib}^b = \mathbf{S}(\mathbf{J}\boldsymbol{\omega}_{ib}^b)\boldsymbol{\omega}_{ib}^b + \mathbf{S}(\mathbf{A}\mathbf{I}_s\boldsymbol{\omega}_s)\boldsymbol{\omega}_{ib}^b - \mathbf{A}\boldsymbol{\tau}_a + \boldsymbol{\tau}_e \quad (9.1a)$$

$$\mathbf{I}_s\dot{\boldsymbol{\omega}}_s = \boldsymbol{\tau}_a - \mathbf{I}_s\mathbf{A}\dot{\boldsymbol{\omega}}_{ib}^b. \quad (9.1b)$$

9.1.1 Model parameters

The model parameters were derived from a CAD model of the vehicle, using Autodesk Inventors built-in tools for computing inertia of a multi-object mechanical model. This CAD model was also used to compute the center of gravity. A submerged vehicle is also subject to the effects of added mass, however in the case of a spherical vehicle there is no added mass effects in the rotational dynamics.

$$\mathbf{J} = \begin{bmatrix} 776184.075 & -4195.338 & 9168.238 \\ -4195.338 & 848286.933 & -27.891 \\ 9168.238 & -27.891 & 944457.837 \end{bmatrix} \cdot 10^{-6} \text{ kg s}^2 \quad (9.2)$$

$$\mathbf{I}_s = 0.14188 \cdot \mathbf{I}_{3 \times 3} \text{ kg s}^2 \quad (9.3)$$

$$\mathbf{A} = \mathbf{I}_{3 \times 3} \quad (9.4)$$

9.2 Measurements

The vehicles are equipped with pressure sensors and inertial measurement units, as described in chapter 8. In this section we comment on some challenges which surfaced during experiments, and which required some adaption.

It became evident that the pressure sensor, which was rated a 0-10 bar, was too insensitive. The measured pressure was below 1 bar in most experiments. This produced an analog output from the sensor of less than 1 V, which is less than 10% of the full range signal. Due to a noise component of almost 1% of full range the measurement was not accurate enough for precision depth control. However, after filtering the measurement could be used for approximate depth positioning.

The IMU also presented a challenge. Due to the small size of the vehicles the placement of the sensors were constrained, resulting in the magnetometer being affected by the magnetic field of the motor. The solution was to operate the sensors using only inertial measurements. Though this resulted in a drift in the absolute attitude, it was satisfactory for the short duration of our experiments.

9.3 Actuation

As previously described the vehicles are internally actuated by means of three reaction wheels in an orthogonal configuration, in addition to the piston tank which regulates the buoyancy of the vehicle. A drawback with reaction wheel actuation, is that as the vehicle is affected by external moments, momentum builds up in the wheels eventually saturating them. The most severe external moment acting in our setup is the restoring moment due to an offset between the center of buoyancy and center of gravity. This is the principle used by spacecraft stabilized by means of a gravity boom. However in this case this is an undesired effect since we would like to move the vehicle freely about all axes. In experiments it was observed that the restoring moment caused some difficulty for the vehicle to move accurately around the pitch and roll axes.

9.3.1 Moment mapping

The motors are commanded by sending a torque command to their respective motor controller. This torque command is given as an integer value in the range -1023 to 1023, ± 1023 corresponding to the minimum and maximum torque. Meaning that we cannot set the exact torque using this command, rather we have to create a mapping from the desired torque to the motor torque command. The max torque is dependent on several parameters

$$\tau_{\text{peak}} = K_t i_{\text{max}}, \quad (9.5)$$

where K_t is the motor torque constant and

$$i_{\text{max}} = \max(i_{\text{limit}}, i_{\text{max coil}}), \quad (9.6)$$

where i_{limit} is the current limit of the motor driver control electronics, 12.5 A and

$$i_{\text{max coil}} = \frac{u_{\text{bus}} - u_{\text{emf}}}{R_{\text{coil}}}, \quad (9.7)$$

where u_{bus} is the motor voltage, 37 V, R_{coil} is the coil resistance, and $u_{\text{back emf}}$ is the voltage generated by spinning the motor given by

$$u_{\text{emf}} = K_v \Omega_{\text{RPM}}, \quad (9.8)$$

where K_v is the motor voltage constant and Ω_{RPM} is the motor speed given in rotations per minute. The motor parameters are summarized in table 9.1.

EXPERIMENTAL RESULTS

Table 9.1: Motor parameters

Abbreviation	Name	Value
K_t	Torque constant	0.09 Nm/Amps
i_{limit}	Current limit	12.5 A
u_{bus}	Bus voltage	37 V
R_{coil}	Coil resistance	1.2 ohms
K_v	Voltage constant	9.32 V/kRPM

9.4 Experiment facilities

The experiments were conducted at two locations at the Department of Engineering Cybernetics. In our basement laboratory, seen in figure 9.2 and at the outdoor roof facility featured in figure 9.1. The basement laboratory had a small 1 m × 0.7 m. × 0.8 m tank, where we planned to do initial testing and control implementation. The roof laboratory had a larger pool 5 m in diameter and 70 cm deep. Here initial testing of leader-follower synchronization was conducted. However due to difficult access and weather conditions, most trials were conducted in the basement facilities.

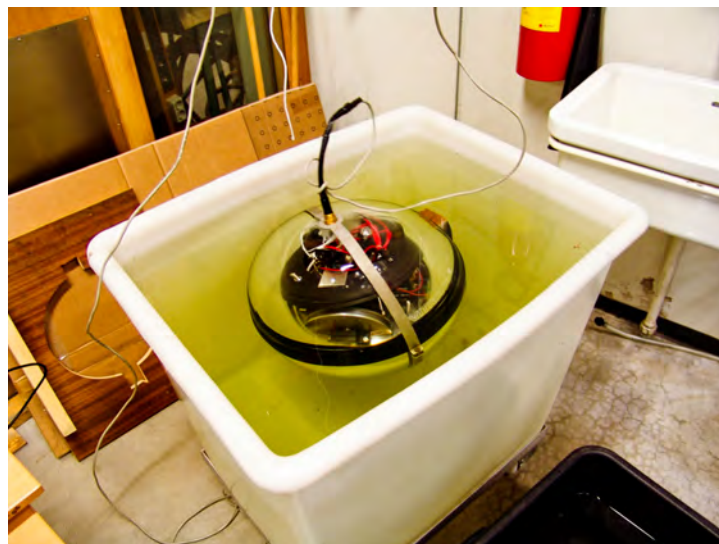


Figure 9.2: Basement facilities

9.5 Measurement filtering

When implementing control algorithms on a physical system rather than in a simulation environment, signal noise becomes a challenge which must be taken into account. The noise contribution is due both to sensor quality and noise in the signal transmission lines of analog sensor signals. The effect of using noise contaminated signals is high-frequency chattering in the actuator commands, which in general can excite unmodeled dynamics, lead to instability and destroy or severely reduce the life expectancy of actuators.

To avoid the mentioned problems we filtered the measured sensor signals. Figure 9.3 and 9.4 show the filtered pressure measurement and angular velocity respectively. The attitude measurement was however already filtered by a Kalman filter in the IMU’s on-board computer, and did not require further filtering. The filters implemented are simple first-order low-pass filters, but sufficient for our use since the noise component we want to attenuate is of high frequency.

The time constant of the filters depend on the dynamics they describe and the frequency of the noise component. Making the filters too fast will not reduce the noise enough, making them too slow will introduce too large phase shift around the bandwidth frequency of the system.

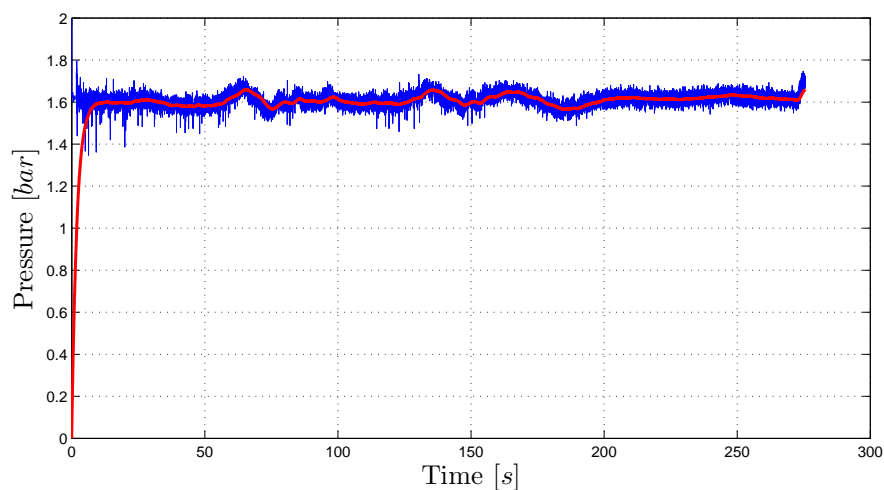


Figure 9.3: Measurement filtering. Pressure

9.6 Preliminary experiments

To verify the mechanical design, as well as control hardware and software design a series of preliminary experiments were conducted. Through the course of these trials we

EXPERIMENTAL RESULTS

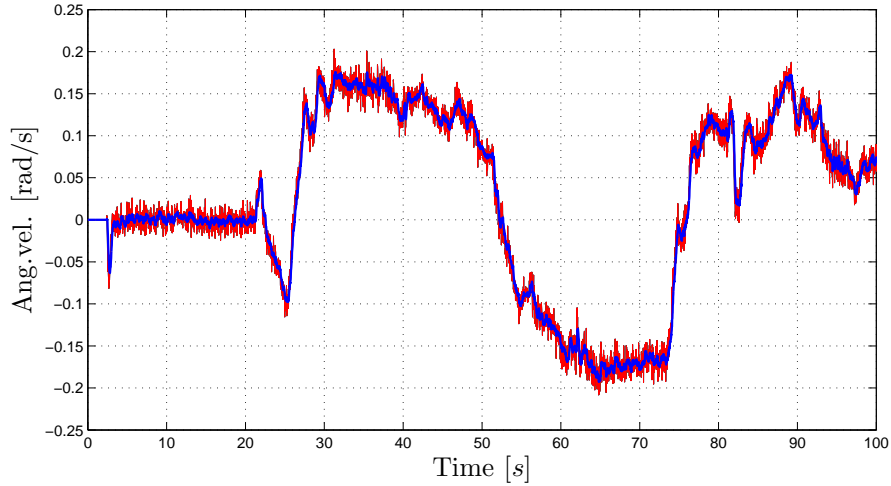


Figure 9.4: Measurement filtering. Angular velocity

uncovered and improved some mechanical problems and some issues in the control software. After these initial trials the feedback loops were closed in stages. This process is discussed in the remainder of this section.

9.6.1 Depth control

The depth control loop was the first feedback loop to be closed. As explained in chapter 8, depth control is accomplished using a piston tank actuated by a servo motor. The piston tank is first used to trim the vehicle to near neutral buoyancy. The output from the control algorithm is a deviation from this trim position, pumping water in to descend, pumping water out to ascend.

The controller is a PD-controller

$$u = k_p(\hat{p} - p_r) - k_d q \tag{9.9}$$

$$\dot{\hat{p}} = \frac{1}{T_p} (p - \hat{p}) \tag{9.10}$$

$$\dot{q} = \frac{1}{T_q} (\dot{\hat{p}} - q) \tag{9.11}$$

where p is the pressure measurement, \hat{p} the filtered pressure, p_r the desired pressure, q a filtered derivative signal, T_p and T_q the filter time constants, $\dot{\hat{p}}$ the derivative of the filtered pressure measurement, and k_p and k_d are positive constants. As can be seen from figure 9.3, due to large noise levels, the pressure measurement could not be used directly in the feedback loop, but was filtered to smooth the signal. From these initial tests it

became evident that the pressure sensor was not sensitive enough for our purpose, as the maximum pressure signal were below 1 V, which is less 10% of the sensor’s range.

9.6.2 Attitude control

A series of attitude control methods were also implemented, to verify the function of internal actuation, measurements and the controllability of the vehicle.

3-axes stabilized

The first attitude controller implemented was a purely stabilizing controller, using feedback from filtered angular velocity measurements,

$$\mathbf{u} = -\mathbf{K}_d \boldsymbol{\omega}_{ib}^b \quad (9.12)$$

where $\mathbf{K}_d = \mathbf{K}_d^T > 0$ and

$$\boldsymbol{\omega}_{ib}^b = \begin{bmatrix} \omega_x \\ \omega_y \\ \omega_z \end{bmatrix}, \quad (9.13)$$

is the angular velocity output from the IMU. This controller was used to check the sign of the torque command, and to verify the wheel axis matrix \mathbf{A} in (9.1).

2-axes stabilized, 1 axis tracking

The next attitude controller implemented was a PD-controller on the yaw-axis, while roll and pitch were stabilized using a proportional speed controller.

$$u_\phi = -k_{d_\phi} \omega_x \quad (9.14a)$$

$$u_\theta = -k_{d_\theta} \omega_y \quad (9.14b)$$

$$u_\psi = k_{p_\psi} (\psi_d(t) - \psi) - k_{d_\psi} \omega_z \quad (9.14c)$$

where k_{d_ϕ} , k_{d_θ} , k_{p_ψ} and k_{d_ψ} are positive constants, the reference signal $\psi_d(t)$ were chosen as

$$\psi_d(t) = \frac{\pi}{2} \sin\left(\frac{2\pi}{120}\right). \quad (9.15)$$

As can be seen from figure 9.5, we achieve satisfactory tracking of the desired yaw angle. Figure 9.7 displaying the actuator commands.

EXPERIMENTAL RESULTS

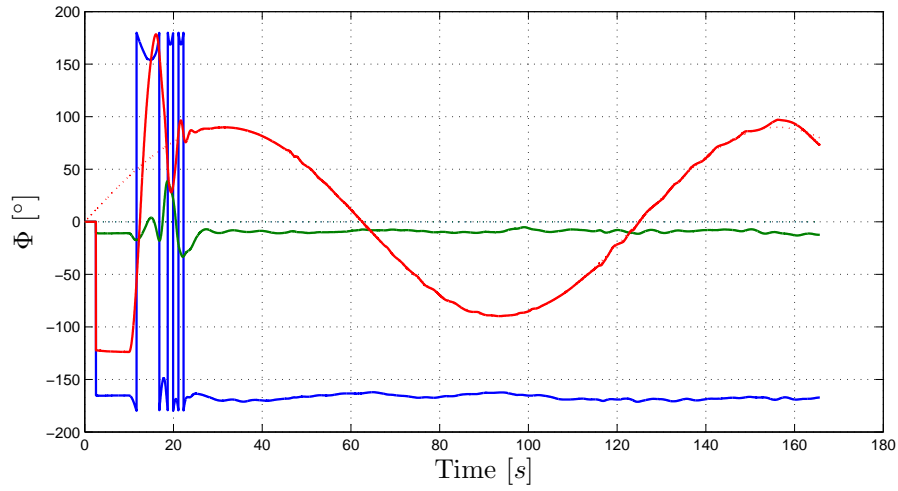


Figure 9.5: Results for (9.14). Measured euler angles vs. reference trajectory.

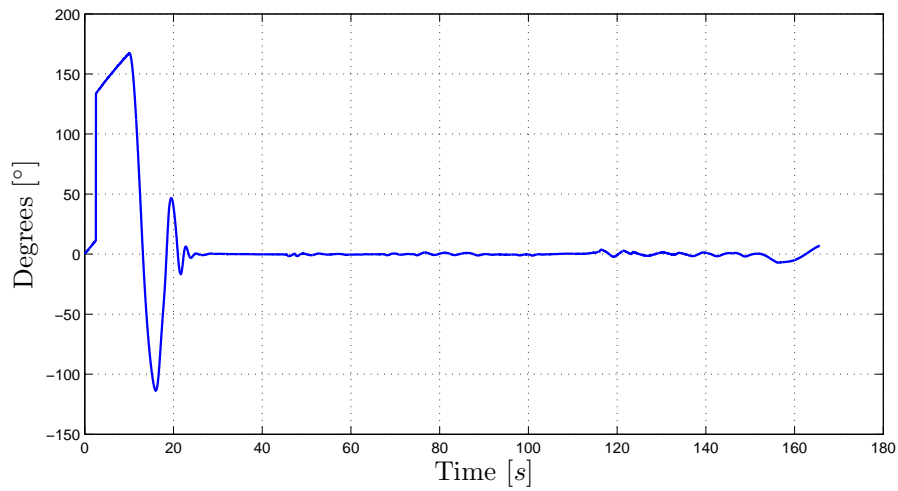


Figure 9.6: Results for (9.14). Tracking error, $\psi_d - \psi$.

9.7 Preliminary synchronization control

9.7.1 2 axes stabilized, 1 axis synchronizing

Here we present some experimental results using a preliminary synchronizing controller. The pitch and roll axis are stabilized, while a synchronization scheme is implemented on

9.7. PRELIMINARY SYNCHRONIZATION CONTROL

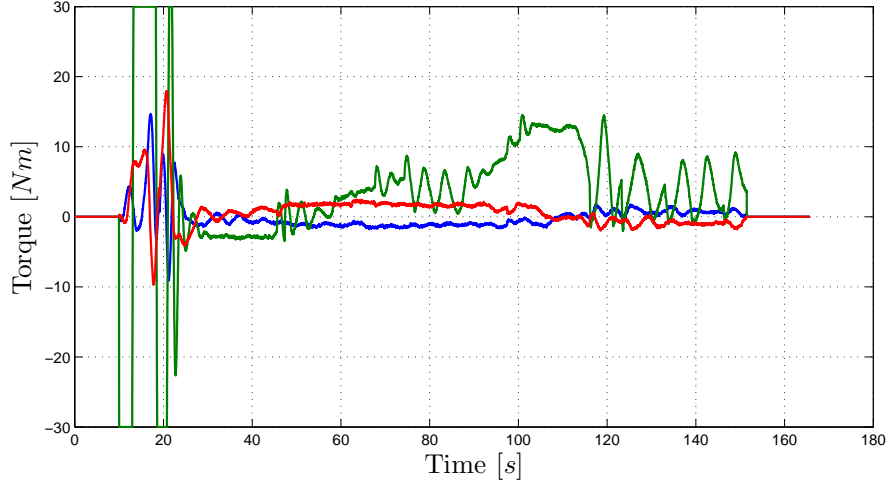


Figure 9.7: Results for (9.14). Torque input.

the yaw axis.

$$u_\phi = -k_{d_\phi} \omega_x \quad (9.16a)$$

$$u_\theta = -k_{d_\theta} \omega_y \quad (9.16b)$$

$$u_\psi = k_{p_\psi} (\psi_l - \psi_f) - k_{d_\psi} \omega_{z,f} \quad (9.16c)$$

where ψ_l and ψ_f are the leader and follower yaw angle respectively, and $\omega_{z,f}$

9.7.2 PD quaternion feedback synchronization scheme

Next we implemented the PD quaternion feedback control algorithm presented in Wen & Kreutz-Delgado (1991). The control algorithm is given by

$$\tau = -\mathbf{S} \left(\mathbf{J} \boldsymbol{\omega}_{ib}^b \right) \boldsymbol{\omega}_{ib}^b - \mathbf{K}_p \boldsymbol{\epsilon}_e - \mathbf{K}_d \boldsymbol{\omega}_e \quad (9.17)$$

where \mathbf{K}_p and \mathbf{K}_d are positive definite matrices and

$$\mathbf{q}_e \triangleq \begin{bmatrix} \eta_e \\ \boldsymbol{\epsilon}_e \end{bmatrix} = \mathbf{q}_l^{-1} \otimes \mathbf{q}_{\phi,\theta}^{-1} \otimes \mathbf{q}_f, \quad (9.18)$$

$$\boldsymbol{\omega}_e \triangleq \boldsymbol{\omega}_{il}^l - \boldsymbol{\omega}_{if}^f, \quad (9.19)$$

where \mathbf{q}_l is the leader attitude, $\mathbf{q}_{\phi,\theta}$ is a quaternion corresponding to the follower roll and pitch angles, \mathbf{q}_f the follower attitude. The reason for including the roll and pitch rotation, was that we were still only interested in synchronizing the yaw angle.

EXPERIMENTAL RESULTS

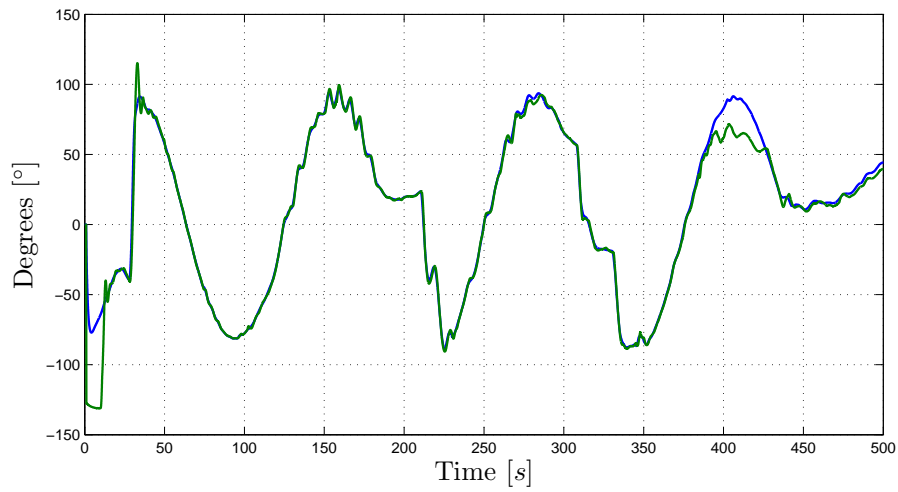


Figure 9.8: Results for (9.16). The red line shows the leader yaw angle, ψ_l , the blue line shows the follower yaw angle θ_f .

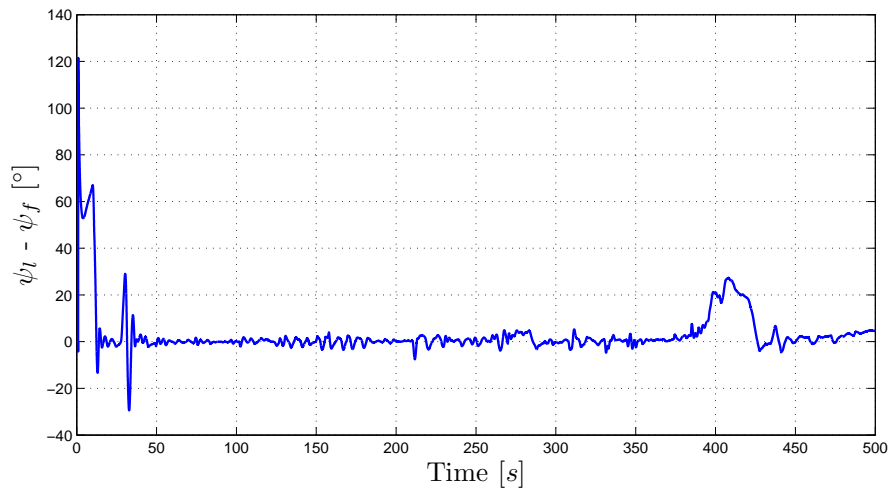


Figure 9.9: Results for (9.16). The synchronization error $\psi_l - \psi_f$.

9.7. PRELIMINARY SYNCHRONIZATION CONTROL

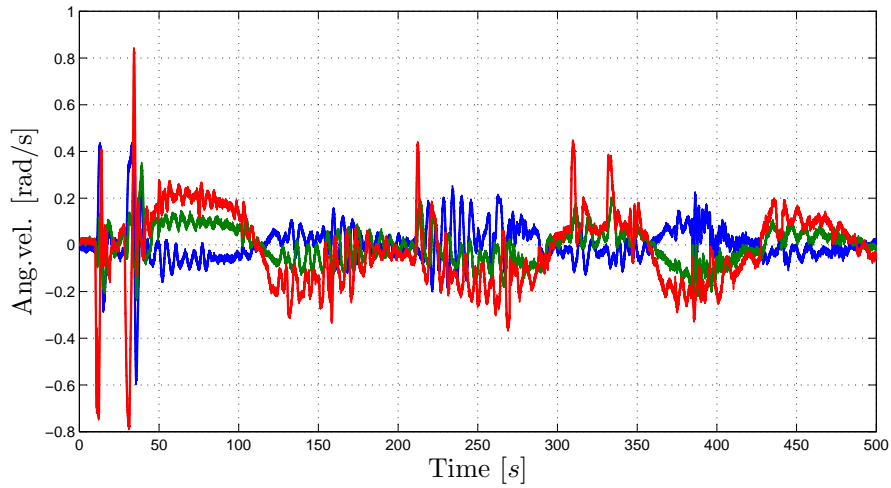


Figure 9.10: Results for (9.16). Angular velocity

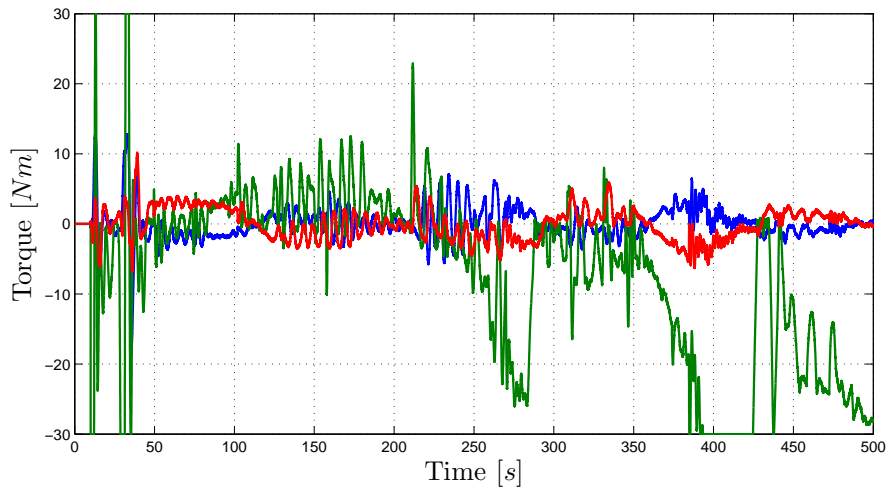


Figure 9.11: Results for (9.16). Torque command

EXPERIMENTAL RESULTS

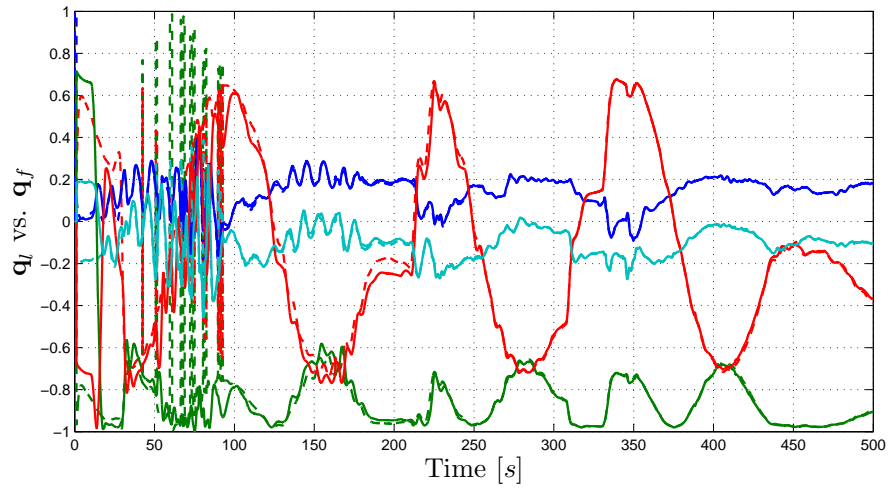


Figure 9.12: Results of (9.17). The plot shows q_l as the dotted lines and q_f as the solid lines.

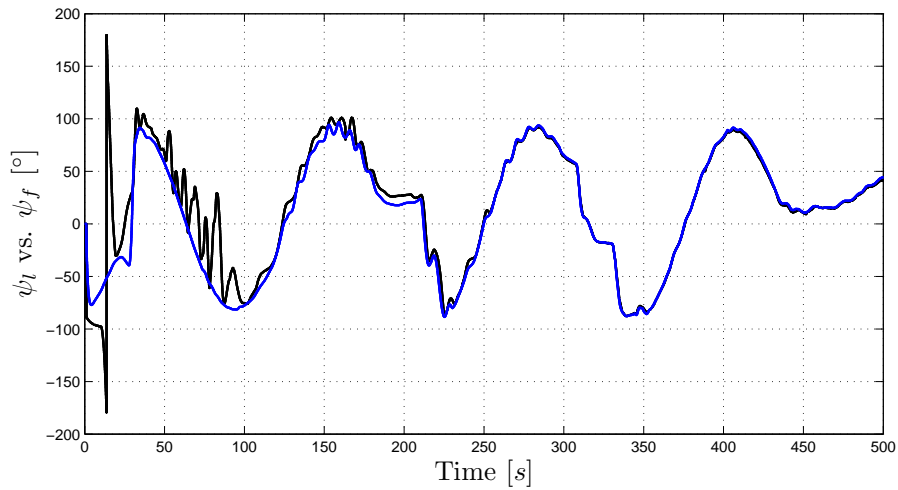


Figure 9.13: Results of (9.17). The plot shows ψ_l and ψ_f .

9.7. PRELIMINARY SYNCHRONIZATION CONTROL

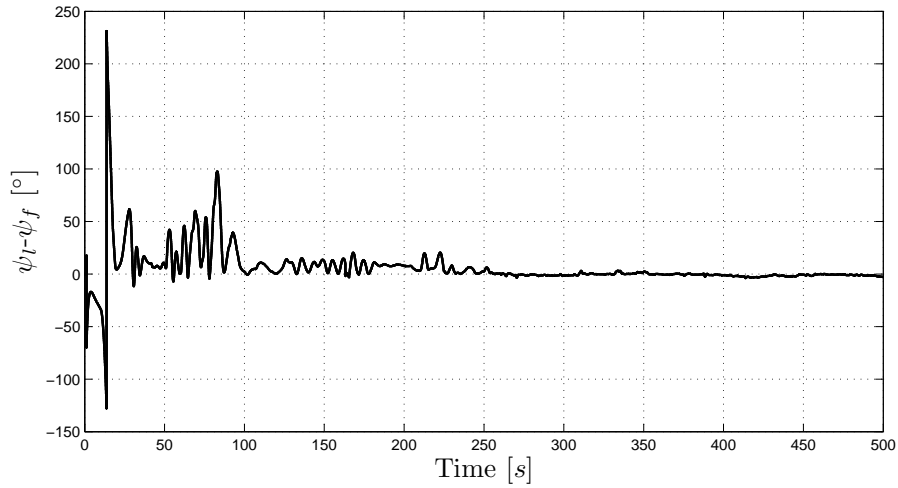


Figure 9.14: Results of (9.17). The plot shows $\psi_l - \psi_f$.

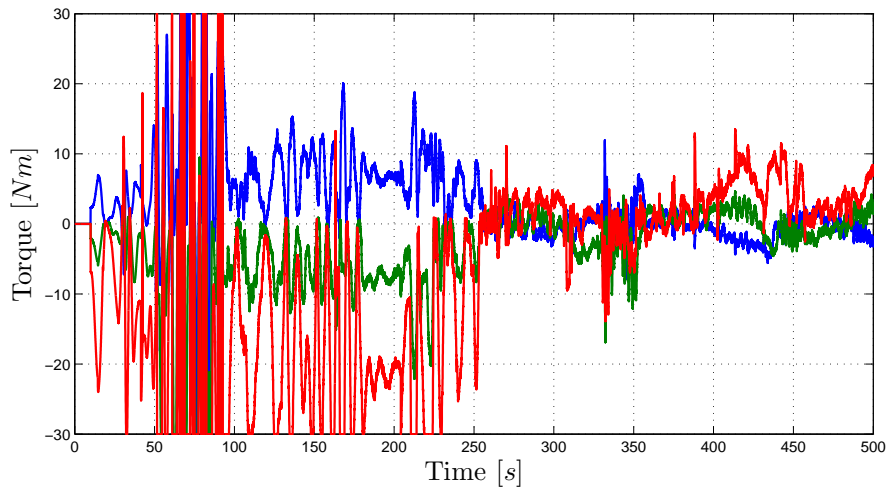


Figure 9.15: Results of (9.17). The plot shows the torque.

EXPERIMENTAL RESULTS

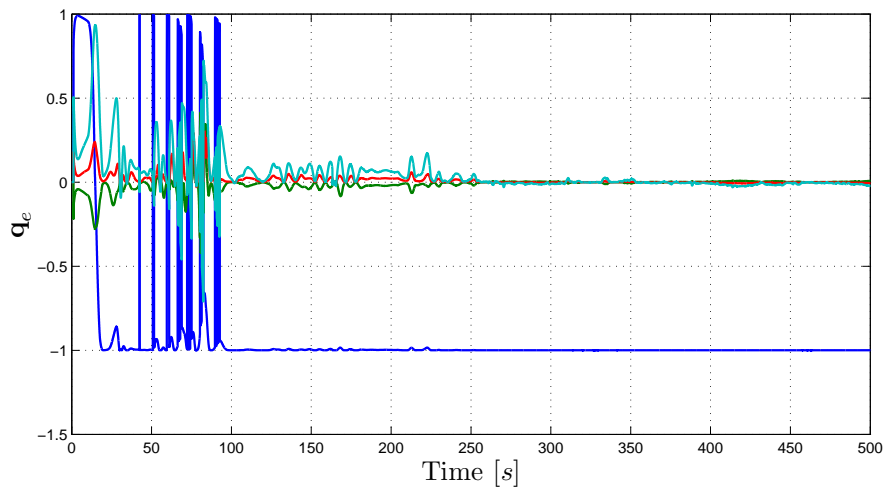


Figure 9.16: Results of (9.17). The plot shows the synchronization error q_e .

9.8 PID+ backstepping control of relative spacecraft attitude

In this section we present experimental results of the theoretical contribution presented in chapter 6. Some simplifications were made to the control algorithm, we removed the to terms in the controller which used high-order derivatives, of angular velocity signals. The noise content of these signals were too large to be useful for control purposes.

9.8.1 The implemented control algorithm

$$\tau = -\mathbf{K}_2 z_2 - \mathbf{S} \left(\mathbf{J} \omega_{ib}^b \right) \omega_{ib}^b - z_1 \quad (9.20)$$

where

$$z_0 = \int_{t_0}^t \sigma_e d\tau \quad (9.21)$$

$$\alpha_0 = -\mathbf{K}_0 z_0 \quad (9.22)$$

$$z_1 = \mathbf{K}_4 \sigma_e - \alpha_0 \quad (9.23)$$

$$\alpha_1 = \mathbf{G}^{-1} (-\mathbf{K}_1 z_1 + \dot{\alpha}_0 - \mathbf{K}_5 z_0) \quad (9.24)$$

$$z_2 = \omega_e - \alpha_1 \quad (9.25)$$

where $\mathbf{K}_0 = 0.5$, $\mathbf{K}_1 = 1$, $\mathbf{K}_2 = 1$, $\mathbf{K}_4 = 10$ and $\mathbf{K}_5 = 1$.

9.8.2 The results

The results are presented in figure 9.18 to 9.22.

EXPERIMENTAL RESULTS

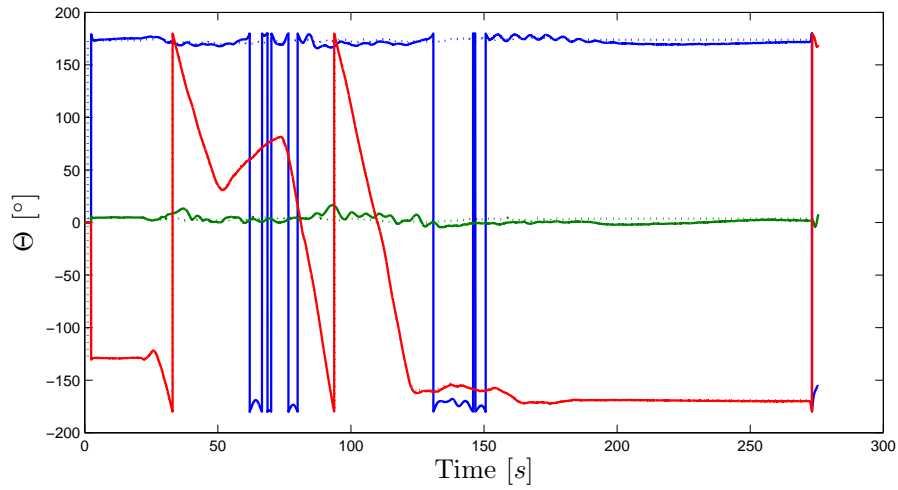


Figure 9.17: Results of (9.20). This figure shows the synchronization of the leader and follower yaw angle.

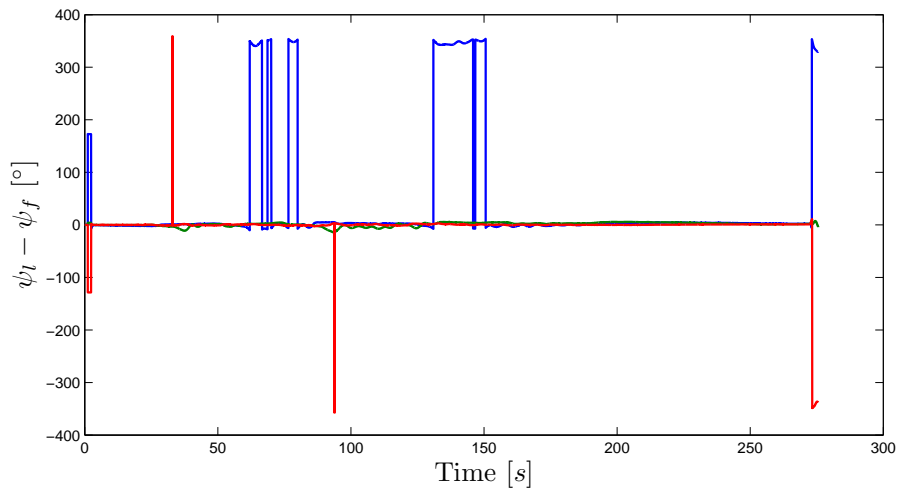


Figure 9.18: Results of (9.20). Synchronization error in Euler angles

9.8. PID+ BACKSTEPPING CONTROL OF RELATIVE SPACECRAFT ATTITUDE

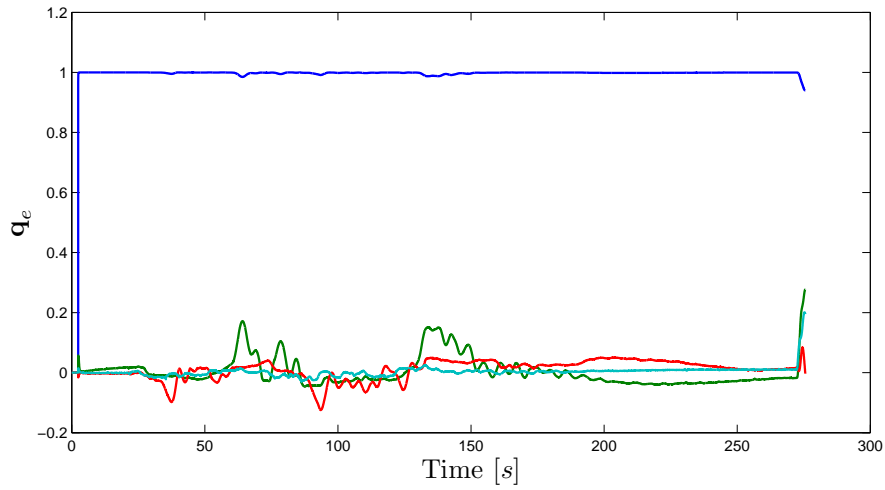


Figure 9.19: Results of (9.20). Synchronization error in quaternions

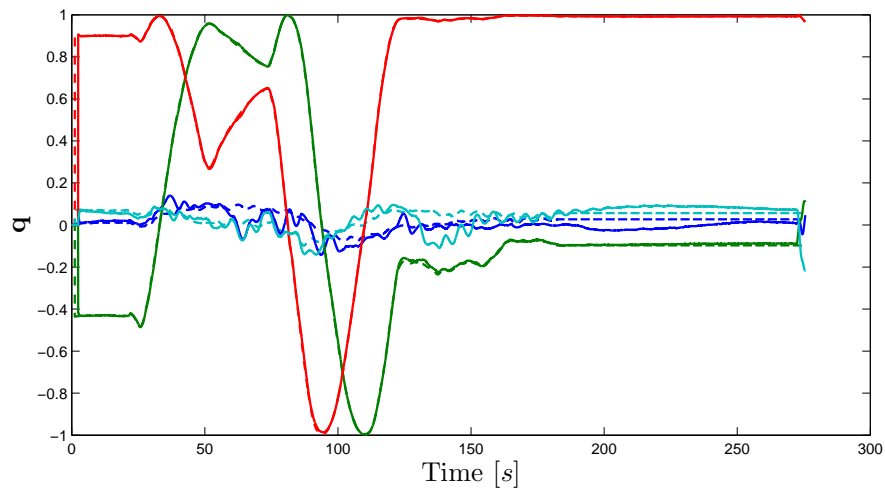


Figure 9.20: Results of (9.20). Lead vs. follower quaternion. The leader quaternion components are the dotted lines.

EXPERIMENTAL RESULTS

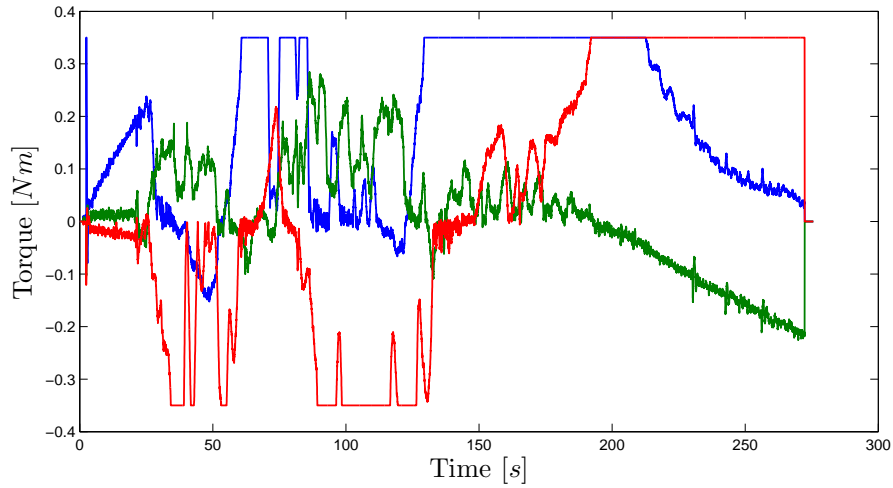


Figure 9.21: Results of (9.20). Torque

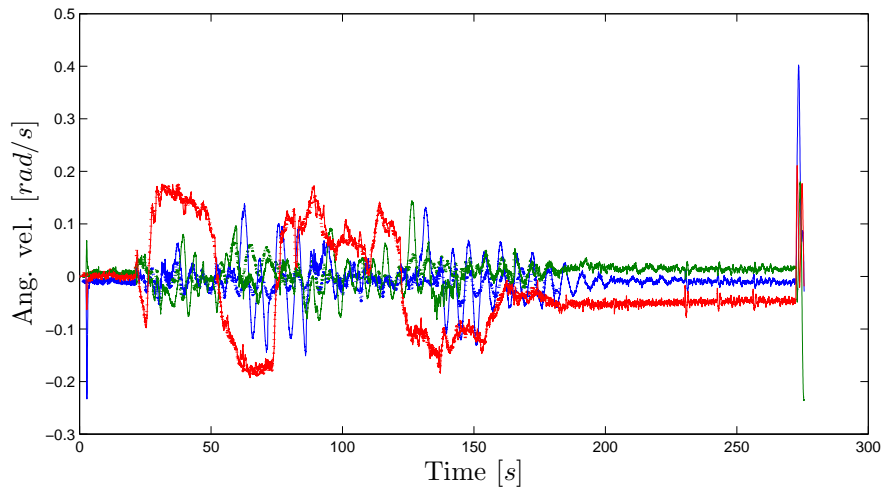


Figure 9.22: Results of (9.20). Leader vs. follower angular velocity. Leader velocities are dotted.

9.8.3 Discussion

The results in this section validated the theoretical contribution of chapter 6, although not to the full extent possible as some simplifications were necessary. This is a drawback often seen in backstepping controllers, where the final control algorithm contains high-order derivatives. These terms prove difficult to handle in practical implementations, where measurements often are noise contaminated. One way of circumventing the problem is to filter the measurements, however when the signals are to be differentiated one or two times, the phase shift introduced by the filters may cause instabilities in high-bandwidth systems.

Another challenge in implementing nonlinear control algorithms is the lack of any formal methods for tuning the controller gains. This becomes even more evident in backstepping based algorithms, where coordinate transformations can make the physical interpretation of variables difficult. Here, this problem was circumvented by implementing the controller in stages, starting with terms corresponding to proportional and derivative actions, and when stable adding integral and nonlinear terms to improve performance.

9.9 Output feedback control of relative spacecraft attitude

Here we present experimental results achieved for the output feedback controller presented in chapter 7. In this control scheme we assume that only relative attitude is measured, however in this experiment we actually know the absolute attitude of both vehicles from the IMUs and calculate the relative attitude.

9.9.1 The implemented control algorithm

The controller implemented is given by

$$\boldsymbol{\tau} = -\mathbf{S} \left(\mathbf{J} \boldsymbol{\omega}_{ib}^b \right) \boldsymbol{\omega}_{ib}^b - k_p \boldsymbol{\epsilon}_e - k_d \hat{\boldsymbol{s}}, \quad (9.26)$$

where $\hat{\boldsymbol{s}}$ is obtained from the observer

$$\mathbf{J}_f \dot{\hat{\boldsymbol{s}}} = \mathbf{S} \left(\mathbf{J}_f \boldsymbol{\omega}_{if}^f \right) \boldsymbol{\omega}_{if}^f + \boldsymbol{\tau}_f - l_2 \tilde{\boldsymbol{\epsilon}}_e \quad (9.27a)$$

$$\dot{\hat{\boldsymbol{q}}}_e = \frac{1}{2} \mathbf{Q}(\hat{\boldsymbol{q}}_e) (\tilde{\mathbf{R}}_e^T (\hat{\boldsymbol{s}} - \lambda \boldsymbol{\epsilon}) - l_1 \tilde{\boldsymbol{\epsilon}}_e). \quad (9.27b)$$

9.9.2 Results

In this section we present the results from (9.26) and (9.27), with the gains selected as

$$k_p = 10, \quad k_d = 0.5, \quad l_1 = 100, \quad l_2 = 50.$$

EXPERIMENTAL RESULTS

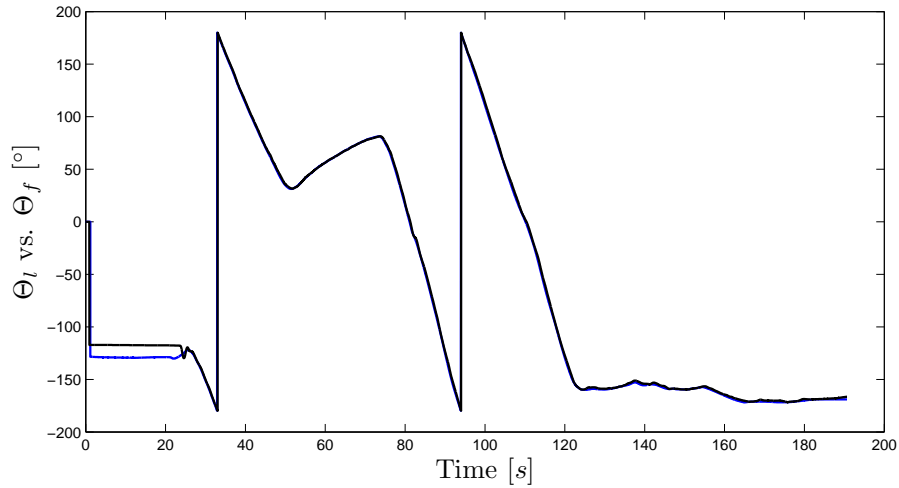


Figure 9.23: Results of (9.26). Leader vs. follower yaw angle. Leader is black.

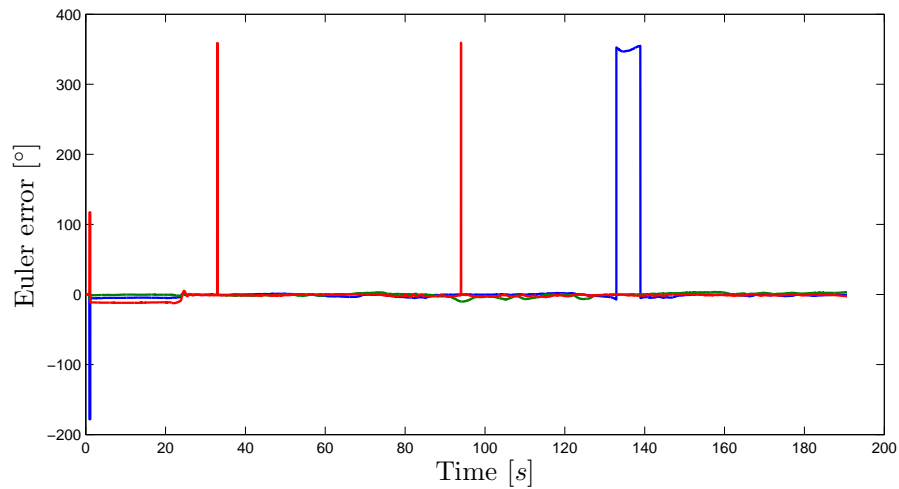


Figure 9.24: Results of (9.26). Synchronization error represented in Euler angles.

9.9.3 Discussion

From the results presented in figures 9.23- 9.28, we see that the proposed controller achieves the goals of synchronizing the attitude of the follower vehicle with that of the leader, as proved in the theoretical results in chapter 7. However we see that the synchronization measure estimation error s does not converge.

9.9. OUTPUT FEEDBACK CONTROL OF RELATIVE SPACECRAFT ATTITUDE

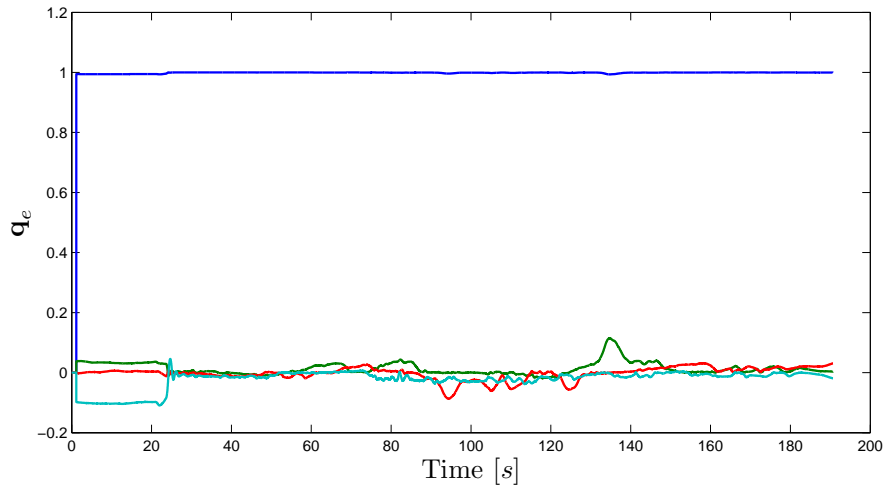


Figure 9.25: Results of (9.26). Synchronization error in quaternion representation.

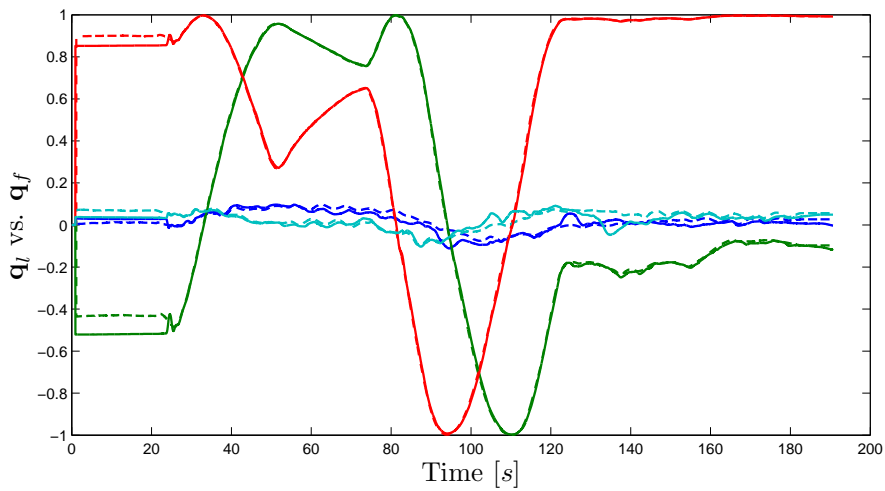


Figure 9.26: Results of (9.26). Leader vs. follower quaternion. Leader quaternion components are the dotted lines.

EXPERIMENTAL RESULTS

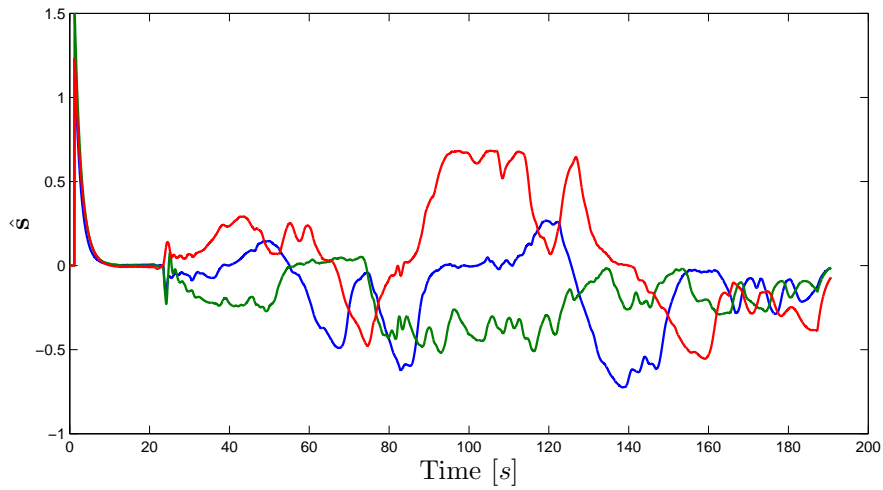


Figure 9.27: Results of (9.26). \hat{s}

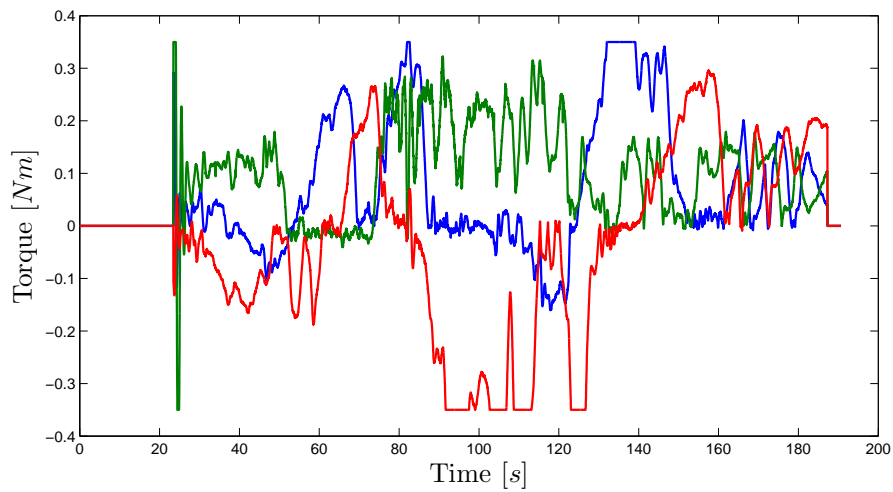


Figure 9.28: Results of (9.26). Torque.

9.10 Discussion

From the experimental results presented in this chapter we see that the controllers designed in previous chapters are suitable for practical implementation. We also see that we achieve better performance when using model based nonlinear controllers, than the out of the box PID controllers, though at the cost of more involved analysis, implementation and tuning.

There are obviously room for improvements in the way the experiments were conducted. The facilities where we performed most of our experiments were confined and created unnecessary disturbances to the vehicles.

The limitation in this setup with respect to emulating a space operating vehicle is unfortunately visible in the simulation results. It manifests itself in the *roll* and *pitch* motion of the vehicle, were we achieve bad tracking performance. The reason for this is the problem of properly placing the center of gravity at the center of buoyancy, resulting in restoring moments which rapidly saturate the wheels. Despite this shortcoming, we still consider the results of the experiments as valid performance indicators for control algorithms proposed.

EXPERIMENTAL RESULTS

Chapter 10

Concluding remarks

10.1 Concluding remarks

10.1.1 Theoretical work

In this thesis we have presented several control schemes for attitude synchronization in spacecraft formations. The focus have been on the relative attitude dynamics in leader-follower formations, and using nonlinear design techniques and analysis several schemes were developed.

In chapter 4 we presented an adaptive external synchronization scheme for a spacecraft actuated by means of reaction wheels. The controller used the quaternion parameterization of attitude, and was proved to be globally exponentially stable on $S(3) \times \mathbb{R}^3$ in the known parameter case and globally convergent when using adaptive feedback.

In chapter 5 we presented a control scheid referred to as mutual synchronization. In this scheme the goal was to derive an algorithm which could stabilize the relative position and attitude, and for the absolute attitude and position to track a trajectory. The controller was proved to be uniformly locally asymptotically stable, and the results where supported by numerical simulations in Matlab Simulink.

In chapter 6 we presented a PID+ controller for relative attitude synchronization. The controller was derived using the technique of integrator augmentation and backstepping, and was proved globally exponentially stable. Numerical simulations supported the theoretical proof, and suggested that the inclusion of integral action resulted in robustness against constant and slowly-varying disturbances.

In chapter 7 output feedback control of relative attitude was investigated. The goal was to synchronize the attitude in a leader-follower formation. The presented Lyapunov analysis proved that the combined observer-controller closed loop error dynamics, was uniformly practically asymptotically stable. This result was supported by numerical simulations of a leader-follower formation.

CONCLUDING REMARKS

10.1.2 Experimental work

In this thesis we have presented the design and implementation of an experimental platform for relative spacecraft attitude control, and we have presented results which support some of the theoretical findings.

The design of the AUVSAT vehicle, mechanical design and also hardware and software structure were presented in chapter 8. The vehicle is composed of a spherical glass shell, with an internal aluminum structure, which supports the internal hardware. The vehicles are actuated by means of reaction wheels, and the attitude is measured using a small-size inertial measurement unit.

In chapter 9 the functionality of the experimental platform was first validated through a series of preliminary control implementations, then it was used to experimentally verify the some of the theoretical contributions presented earlier in the thesis. The control schemes which was examined, included the PID+ backstepping controller of chapter 6 and the output feedback controller presented in chapter 7.

10.2 Future work

10.2.1 Theoretical

An interesting direction of research could be to design the synchronizing controllers in the $SO(3)$ framework instead of using attitude parameterizations. For purely kinematic models this was investigated in (Bullo 1999) and (Sarlette 2009). Extending these results to include vehicle dynamics, could be a viable direction of research.

The mutual synchronization controller was designed for a deep space formation, with simple position dynamics, a logical next step would be to include the relative position dynamics of (Kristiansen, Grøtli, Nicklasson & Gravdahl 2007). This would result in an attractive approach for Earth orbiting formations.

In this thesis we have not considered robustness issues. Though some controllers are locally exponentially stable, which yield some robustness properties. Analyzing the proposed scheme more rigorously with respect to noise, disturbances and actuator saturation should be considered.

10.2.2 Experimental

Further development of the experimental platform should be investigated. One drawback with the current platform is the umbilical network cable which limits the movement of the vehicles. To remedy this one should work on creating a wireless underwater link, either using an acoustic link or radio communication.

Another issue which has been commented on earlier in this thesis is the actuation limits imposed by using internal actuation. This requires the center of gravity to be placed

10.2. FUTURE WORK

close to the center of buoyancy to be able to control the roll and pitch axes properly. Although we were able to control roll and pitch to some degree in the experiments, the accuracy of the placement could be improved.

CONCLUDING REMARKS

Bibliography

- Akella, M. R. (2001), ‘Rigid body attitude tracking without angular velocity feedback’, *Systems & Control Letters* **42**(4), 321–326.
- Bai, H., Arcak, M. & Wen, J. (2008), ‘Rigid body attitude coordination without inertial frame information’, *Automatica* **44**(12), 3170–3175.
- Balch, T. & Arkin, R. C. (1998), ‘Behavior-based formation control for multirobot teams’, *IEEE Transactions on Robotics and Automation* **14**(6).
- Beard, R. (1998), Architecture and algorithms for constellation control, Technical report, Jet Propulsion Laboratory, California Institute of Technology, 4800 Oak Grove Dr., Pasadena, CA 91109. Available online [http://www.ee.byu.edu/grad1/users/beard/www_docs/research_formation.html].
- Beard, R. & Hadaegh, F. Y. (1998), Constellation templates: An approach to autonomous formation flight, in ‘World Automation Congress’, ISIAAC, Anchorage, Alaska, pp. pp. 177.1 – 177.6.
- Beard, R. W., Lawton, J. R. T. & Hadaegh, F. Y. (2001), ‘A coordination architecture for formation control’, *IEEE Transactions on Control Systems Technology* **9**, 777–790.
- Beichman, C., Woolf, N. & Lindensmith, C. (1998), *Terrestrial Planet Finder - Origins of Stars, Planets and Life*, National Aeronautics and Space Administration.
- Bhat, S. P. & Bernstein, D. S. (2000), ‘Topological obstruction to continuous global stabilization of rotational motion and the unwinding phenomenon’, *Systems & Control Letters* **39**(1), 63–70.
- Bondhus, A. K., Pettersen, K. & Gravdahl, J. (2005), Leader/follower synchronization of satellite attitude without angular velocity measurements, in ‘Proceedings of the 44th IEEE Conf. on Decision and Control’, Sevilla, Spain.
- Børhaug, E. (2005), Cross-track maneuvering and way-point tracking control of under-actuated auvs in particular and mechanical systems in general, Master’s thesis, Norwegian University of Science and Technology.

BIBLIOGRAPHY

- Bullo, F. (1999), *Nonlinear Control of Mechanical Systems: A Riemannian Geometry Approach*, PhD thesis, California Institute of Technology, Pasadena, California.
- Chaillet, A. (2006), *On Stability and Robustness of Nonlinear Systems: Application to Cascaded Systems*, PhD thesis, UFR Scientifique D’Orsay, Paris, France.
- Costic, B., Dawson, D., De Queiroz, M. & Kapila, V. (2000), A quaternion-based adaptive attitude tracking controller without velocity measurements, *in* ‘Proceedings of the 39th IEEE Conference on Decision and Control’, Vol. 3, Sydney, Australia, pp. 2424–2429.
- D’Amico, S., Ardaens, J.-S., De Florio, S. & Montenbruck, O. (2008), Autonomous formation flying - tandem-x, prisma and beyond, *in* ‘Proceedings of the 5th International Workshop on Satellite Constellation & Formation Flying’.
- Egeland, O. & Godhavn, J.-M. (1994), ‘Passivity-based adaptive attitude control of a rigid spacecraft’, *IEEE Transactions of Automatic Control* **39**(4), pp. 842 – 846.
- Egeland, O. & Gravdahl, J. T. (2002), *Modeling and Simulation for Automatic Control*, Marine Cybernetics, Trondheim.
- Fjellstad, O.-E. (1994), *Control of unmanned underwater vehicles in six degrees of freedom*, PhD thesis, Norwegian University of Science and Technology.
- Fjellstad, O.-E. & Fossen, T. I. (1994), ‘Position and attitude tracking of auv’s: a quaternion feedback approach’, *Oceanic Engineering, IEEE Journal of* **19**(4), 512–518.
- Fossen, T. (2002), *Marine Control Systems: Guidance, Navigation, and Control of Ships, Rigs and Underwater Vehicles*, Marine Cybernetics, Trondheim, Norway.
- Fragopoulos, D. & Innocenti, M. (2004), ‘Stability considerations in quaternion attitude control using discontinuous lyapunov functions’, *IEE Proceedings Control Theory and Applications* **151**(3), 253–258.
- Freedman, R. & Kaufmann III, W. (2002), *Universe*, sixth edition edn, Freeman.
- Fridlund, C. (2004), ‘The darwin mission’, *Advances in Space Research* **34**, 613–617.
- Godhavn, J.-M. & Egeland, O. (1995), Attitude control of an underactuated satellite, *in* ‘Proceedings of the 34th IEEE Conference on Decision and Control’, Vol. 4, New Orleans, USA, pp. 3986–3987.
- Hahn, W. (1967), *Stability of Motion*, Springer-Verlag.
- Hainsworth, F. R. (1987), ‘Precision and dynamics of positioning by canada geese flying in formation’, *The Journal of Experimental Biology* **128**, 445–462.

BIBLIOGRAPHY

- Horri, N. & Hodgart, S. (2003), Attitude stabilization of an underactuated satellite using two wheels, in ‘Aerospace Conference, 2003. Proceedings. 2003 IEEE’, Vol. 6, pp. 2629–2635.
- Hughes, P. C. (1986), *Spacecraft attitude dynamics*, John Wiley & Sons, New York.
- International Association of Geomagnetism and Aeronomy (2005), ‘International geomagnetic reference field, 10th generation’, ONLINE [<http://www.ngdc.noaa.gov/IAGA/vmod/igrf.html>]. [last accessed 02.05.2005].
- Jung, D. & Tsiotras, P. (2003), A 3-dof experimental test-bed for integrated attitude dynamics and control research, in ‘AIAA Guidance, Navigation and Control Conference’.
- Kang, W. & Yeh, H. (2002), ‘Co-ordinated attitude control of multi-satellite systems’, *International Journal of Robust and Nonlinear Control* **12**, 185–205.
- Khalil, H. (2000), *Nonlinear Systems*, 3 edn, Prentice Hall, Upper Saddle River, New Jersey.
- Kowalchuk, S. A. & Hall, C. D. (2005a), Distributed spacecraft attitude control simulator: Feedback control capabilities and visualization techniques, in ‘7th International Symposium on Quantitative Feedback Theory (QFT) and Robust Frequency Domain Design Methods’.
- Kowalchuk, S. A. & Hall, C. D. (2005b), Hardware-in-the-loop simulation of classical element feedback controller, in ‘Flight Mechanics Symposium’, NASA Goddard Space Flight Center, Greenbelt, Maryland.
- Kristiansen, R. (2008), Dynamic Synchronization of Spacecraft: Modeling and Coordinated Control of Leader-Follower Spacecraft Formations, PhD thesis, Norwegian University of Science and Technology and Narvik University College, Narvik, Norway.
- Kristiansen, R., Grøtli, E. I., Nicklasson, P. J. & Gravdahl, J. T. (2007), ‘A model of relative translation and rotation in leader-follower spacecraft formations’, *Modeling, Identification and Control* **28**(1).
- Kristiansen, R., Krogstad, T. R., Nicklasson, P. J. & Gravdahl, J. T. (2007), Spacecraft coordination control using pid backstepping, in ‘Proceedings of the 17th IFAC Symposium on Automatic Control in Aerospace (ACA)’, Toulouse, France.
- Kristiansen, R., Krogstad, T. R., Nicklasson, P. J. & Gravdahl, J. T. (2008), Pid+ tracking in a leader-follower spacecraft formation, in ‘Proceedings of the 3rd International

BIBLIOGRAPHY

- Symposium on Formation Flying, Missions and Technologies (ISFF)', Estec, Holland.
- Kristiansen, R., Loría, A., Chaillet, A. & Nicklasson, P. J. (2009), 'Spacecraft relative rotation tracking without angular velocity measurements', *Automatica* **45**(3), 750–756.
- Kristic, M., Kanellakopoulos, I. & Kokotovic, P. (1995), *Nonlinear and Adaptive Control Design*, Wiley Interscience.
- Krogstad, T. R. & Gravdahl, J. T. (2006a), 6-dof mutual synchronization of formation flying spacecraft, in 'Proceedings of the 45th IEEE Conference on Decision and Control', San Diego, USA.
- Krogstad, T. R. & Gravdahl, J. T. (2006b), *External synchronization of relative spacecraft attitude*, number LNCIS 336 in 'Lecture notes in control and information science', Springer-Verlag, Berlin, Heidelberg.
- Krogstad, T. R. & Gravdahl, J. T. (2009a), 'Output feedback control of relative spacecraft attitude', *Automatica* . Submitted.
- Krogstad, T. R. & Gravdahl, J. T. (2009b), Output feedback control of relative spacecraft attitude, in 'Proceedings of the 2009 European Control Conference', Budapest, Ungarn.
- Krogstad, T. R., Gravdahl, J. T., Pettersen, K. Y. & Børhaug, E. (2008), Auvsat - an experimental platform for spacecraft formation flying, in 'proceedings of the 59th International Astronautical Congress', Glasgow, Scotland.
- Krogstad, T. R., Gravdahl, J. T. & Tøndel, P. (2005), Explicit model predictive control of a satellite with magnetic torquers, in '2005 IEEE International Symposium on Intelligent Control and 13th Mediterranean Conference on Control and Automation, Jun 27-29 2005', Limassol, Cyprus, pp. 491–496.
- Krogstad, T. R., Kristiansen, R., Gravdahl, J. T. & Nicklasson, P. J. (2007), Pid+ backstepping control of relative spacecraft attitude, in 'Proceedings of the 7th IFAC Symposium on Nonlinear Control Systems', Pretoria, South Africa.
- Kyrkjebø, E. (2007a), Leader-follower synchronization control of euler-lagrange systems with leader position measurements only, in 'Proc. Mediteranean Conf. on Control and Automation', Athens, Greece.
- Kyrkjebø, E. (2007b), Motion Coordination of Mechanical Systems: Leader-Follower Synchronization of Euler-Lagrange Systems using Output Feedback Control, PhD thesis, Norwegian University of Science and Technology, Trondheim, Norway.

BIBLIOGRAPHY

- Lawton, J. R. T. (2000), A Behavior-Based Approach to Multiple Spacecraft Formation Flying, PhD thesis, Brigham Young University, Dept. of El. and Comp. Engineering.
- Lewis, M. A. & Tan, K. (1997), ‘High precision formation control of mobile robots using virtual structures’, *Autonomous Robots* **4**, 387–403.
- Lizarralde, F. & Wen, J. (1996), ‘Attitude control without angular velocity measurements: A passivity approach’, *IEEE Transactions on Automatic Control* **41**(3), pp. 468–472.
- Loria, A., Panteley, E., Popovic, D. & Teel, A. (2002), An extension of matrosov’s theorem with application to stabilization of nonholonomic control systems, in ‘Proceedings of the 41st IEEE Conference on Decision and Control’, Vol. 2, pp. 1528–1533.
- Lyapunov, A. M. (1992), *Stability of Motion*, Taylor & Francis. English translation.
- Mali, A. D. (2002), ‘On the behavior-based architectures of autonomous agency’, *IEEE Transactions on Systems, Man and Cybernetics, Part C: Applications and Reviews* **32**(3).
- Mataric, M. J. (1992), Minimizing complexity in controlling a mobile robot population, in ‘1992 IEEE Int. Conf. on Robotics and Automation Proceedings’, Vol. 1, pp. 830–835.
- Matrosov, V. M. (1962), ‘On the stability of motion’, *Journal of Appl. Math. Mech.* **26**, 1337–1353.
- Nijmeijer, H. & Rodriguez-Angeles, A. (2003), *Synchronization of Mechanical Systems*, World Scientific, Singapore.
- Okubo, A. (1986), ‘Dynamical aspects of animal grouping: Swarms, schools, flocks, and herds’, *Advances in Biophysics* **22**, 1–94.
- Paden, B. & Panja, R. (1988), ‘Globally asymptotically stable ‘pd+’ controller for robot manipulators’, *International Journal of Control* pp. 1697–1712.
- Pan, H. & Kapila, V. (2001), Adaptive nonlinear control for spacecraft formation flying with coupled translational and attitude dynamics, in ‘Proceedings of the 40th IEEE Conference on Decision and Control’.
- Ren, W. & Beard, R. W. (2004), Formation feedback control for multiple spacecraft via virtual structures, in ‘2004 IEEE Proceedings of Control Theory Application’.

BIBLIOGRAPHY

- Rodriguez-Angeles, A. (2002), Synchronization of Mechanical Systems, PhD thesis, Technische Universiteit Eindhoven.
- Sarlette, A. (2009), Geometry and Symmetries in Coordination Control, PhD thesis, Université de Liège, Liège, Belgium.
- Schultz, C. & Woolsey, C. A. (2003), An experimental platform for validating internal actuator control strategies, in ‘Proc. 1st IFAC Workshop on Guidance & Control of Underwater Vehicles’.
- Shuster, M. D. (1993), ‘A survey of attitude representations’, *The Journal of the Astronautical Sciences* **41**(4), 439–517.
- Singh, S. & Yim, W. (1995), Dynamic feedback linearization and large pitch attitude control of satellite using solar radiation pressure, in ‘Proceedings of the 1995 American Control Conference’, Vol. 5, American Control Conference 1995, pp. 3131–3135.
- Singh, S. & Yim, W. (1996), ‘Feedback linearization and solar pressure satellite attitude control’, *IEEE Transactions on Aerospace and Electronic Systems* **32**(2), 732–742.
- Singh, S. & Yim, W. (2002), Nonlinear adaptive backstepping design for spacecraft attitude control using solar radiation pressure, in ‘Proceedings of the 41st IEEE Conference on Decision and Control’, Vol. 2, Las Vegas, USA, pp. 1239–1244.
- Singla, P., Mortari, D. & Junkins, J. L. (2005), How to avoid singularity when using euler angles?, in ‘Advances in the Astronautical Sciences’, Vol. 119, Univelt Inc., San Diego, CA 92198, United States, Maui, HI, United States, pp. 1409–1426.
- Singla, P., Subbarao, K. & Junkins, J. L. (2006), ‘Adaptive output feedback control for spacecraft rendezvous and docking under measurement uncertainty’, *Journal of Guidance, Control, and Dynamics* **29**(4), 892–902.
- Tipler, P. (1999), *Physics for Scientists and Engineers*, W.H. Freeman and company and Worth Publishers.
- Tsiotras, P. (1996), ‘Stabilization and optimality results for the attitude control problem’, *Journal of Guidance, Control, and Dynamics* **19**(4), 772–779.
- Vallado, D. A. (2001), *Fundamentals of Astrodynamics and Applications*, Kluwer Academic Publishers.
- Venkatachalam, R. (1993), ‘Large angle pitch attitude maneuver of a satellite using solar radiation power’, *IEEE Transactions on Aerospace and Electronic Systems* (4), 1164–1169.

BIBLIOGRAPHY

- Vidyasagar, M. (1993), *Nonlinear Systems Analysis*, Prentice Hall.
- Wallace, R., Ayon, J. & Sprague, G. (2000), Interstellar probe mission/system concept, in ‘2000 IEEE Aerospace Conference Proceedings’, Vol. 7.
- Wang, P. K. C., Hadaegh, F. Y. & Lau, K. (1999), ‘Synchronized formation rotation and attitude control of multiple free-flying spacecraft’, *Journal of Guidance, Control and Dynamics* pp. 28–35.
- Wang, P. K. C., Hadaegh, F. Y. & Mokuno, M. (2003), Formation flying of multiple spacecraft with automatic rendezvous and docking capability, in ‘2003 AIAA Guidance, Navigation and Control Conference and Exhibit Proceedings’.
- Wen, T.-Y. J. & Kreutz-Delgado, K. (1991), ‘The attitude control problem’, *IEEE Transactions on Automatic Control* **36**(10), pp. 1148–1162.
- Wertz, J. R. (1978), *Spacecraft Attitude Determination and Control*, Kluwer Academic Publishers.

BIBLIOGRAPHY

Appendix A

Mathematical tools and definitions

This chapter summarizes some of the mathematical tools and definitions, which are relevant for understanding the analysis in the previous chapters of this thesis. The contents of this section are available in textbooks or articles publicly available, but have been made available here for ease of reference and completeness of the thesis. Where relevant specific references are given.

A.1 Mathematical preliminaries

A.1.1 Vectors

To represent forces, velocities, torques, positions and so on, vector notation will be applied. Vectors \vec{v} are described by their length or magnitude $|\vec{v}|$ and their direction. We will in the following only consider vectors in 3-dimensional space.

A vector may be expressed in a reference frame \mathcal{F}_a , by a 3×1 array consisting of its components along the reference frame’s basis vectors. Such a vector is referred to as a *column vector*, and is denoted v^a to distinguish it from the *Gibbsian* or *coordinate free* vector \vec{v} .

Definition A.1. *The column vector written with respect to the reference frame \mathcal{F}_a may be defined as follows*

$$v^a = \begin{bmatrix} v_1 \\ v_2 \\ v_3 \end{bmatrix} \quad (\text{A.1})$$

Here the components are defined as the scalar product between \vec{v} and the basic vectors of the reference frame \mathcal{F}_a

$$v_i = \vec{v} \cdot \vec{a}_i \quad (\text{A.2})$$

MATHEMATICAL TOOLS AND DEFINITIONS

A.1.2 Vector cross product

The vector cross product between two coordinate free vectors \vec{v} and \vec{u} , is given by

$$\vec{v} \times \vec{u} = \vec{n} |\vec{v}| |\vec{u}| \sin \theta. \quad (\text{A.3})$$

To be able to evaluate the cross product between two column vectors, we define the skew-symmetric matrix operator $\mathbf{S}(\cdot)$.

Definition A.2. *Skew-symmetric cross product matrix*

$$\mathbf{S}(\mathbf{v}) = \mathbf{v}^\times \triangleq \begin{bmatrix} 0 & -v_3 & v_2 \\ v_3 & 0 & -v_1 \\ -v_2 & v_1 & 0 \end{bmatrix} \quad (\text{A.4})$$

Where v_i is given by (A.2).

Property 1. *Properties of the skew-symmetric operator*

- $\mathbf{S}(\beta \mathbf{a} + \gamma \mathbf{b}) = \beta \mathbf{S}(\mathbf{a}) + \gamma \mathbf{S}(\mathbf{b})$
- $\mathbf{S}(\mathbf{a})\mathbf{b} = \mathbf{a}^\times \mathbf{b}$
- $\mathbf{S}(\mathbf{a})\mathbf{S}(\mathbf{b}) = \mathbf{b}\mathbf{a}^T - \mathbf{a}^T\mathbf{b}\mathbf{I}_{3 \times 3}$
- $\mathbf{S}[\mathbf{S}(\mathbf{a})\mathbf{b}] = \mathbf{b}\mathbf{a}^T - \mathbf{a}\mathbf{b}^T$
- $\mathbf{a}^T \mathbf{S}(\mathbf{b})\mathbf{a} = 0$
- $\mathbf{S}(\mathbf{a})\mathbf{a} = 0$

A.1.3 Time derivative of vectors

The time derivative of a vector \vec{v} with reference to the frame \mathcal{F}_a may be written

$$\frac{{}^a d}{dt} \vec{v} \triangleq \dot{v}_1^a \vec{a}_1 + \dot{v}_2^a \vec{a}_2 + \dot{v}_3^a \vec{a}_3. \quad (\text{A.5})$$

Which can be given as the time derivative of the vector in another frame and the cross product of the angular velocity between the coordinate systems and the vector.

$$\frac{{}^a d}{dt} \vec{v} = \frac{{}^b d}{dt} \vec{v} + \vec{\omega}_{ab} \times \vec{v} \quad (\text{A.6})$$

For a column vector this may be written:

$$\dot{\mathbf{v}}^a = \begin{bmatrix} \dot{v}_1^a \\ \dot{v}_2^a \\ \dot{v}_3^a \end{bmatrix} \quad (\text{A.7})$$

A.2 Quaternion operations

A.2.1 Quaternion multiplication

The quaternion multiplication is denoted \otimes and for two unit quaternions $\mathbf{q}_i = [\eta_i, \boldsymbol{\epsilon}_i^T]^T$ it is defined as:

$$\mathbf{q}_1 \otimes \mathbf{q}_2 = \begin{bmatrix} \eta_1 \\ \boldsymbol{\epsilon}_1 \end{bmatrix} \otimes \begin{bmatrix} \eta_2 \\ \boldsymbol{\epsilon}_2 \end{bmatrix} = \begin{bmatrix} \eta_1 \eta_2 - \boldsymbol{\epsilon}_1^T \boldsymbol{\epsilon}_2 \\ \eta_1 \boldsymbol{\epsilon}_2 + \eta_2 \boldsymbol{\epsilon}_1 + \mathbf{S}(\boldsymbol{\epsilon}_1) \boldsymbol{\epsilon}_2 \end{bmatrix} \quad (\text{A.8})$$

where $\mathbf{S}(\cdot)$ is the cross-product operator on a row-vector defined as

$$\mathbf{S}(\mathbf{x}) \triangleq \begin{bmatrix} 0 & -x_3 & x_2 \\ x_3 & 0 & -x_1 \\ -x_2 & x_1 & 0 \end{bmatrix}. \quad (\text{A.9})$$

A.3 Derivation of the differential kinematics

Given a quaternion

$$\mathbf{q} = \begin{bmatrix} \eta \\ \boldsymbol{\epsilon} \end{bmatrix} \quad (\text{A.10})$$

corresponding to the rotation matrix $\mathbf{R}_b^i = \mathbf{R}_e(\eta, \boldsymbol{\epsilon})$, where $\mathbf{R}_e(\eta, \boldsymbol{\epsilon})$ is given by

$$\mathbf{R}_e(\eta, \boldsymbol{\epsilon}) = \mathbf{I}_{3 \times 3} + 2\eta \mathbf{S}(\boldsymbol{\epsilon}) + 2\mathbf{S}^2(\boldsymbol{\epsilon}). \quad (\text{A.11})$$

A transformation or a rotation of a vector \mathbf{v} may be described using unit quaternions as

$$\begin{bmatrix} 0 \\ \mathbf{R}_b^i \mathbf{v}^b \end{bmatrix} = \mathbf{q} \otimes \begin{bmatrix} 0 \\ \mathbf{v}^b \end{bmatrix} \otimes \mathbf{q}^{-1}, \quad (\text{A.12})$$

where \otimes is the quaternion product, which for the unit quaternion is defined as

$$\mathbf{p}_1 \otimes \mathbf{p}_2 \triangleq \begin{bmatrix} \eta_1 \eta_2 - \boldsymbol{\epsilon}_1^T \boldsymbol{\epsilon}_2 \\ \eta_1 \boldsymbol{\epsilon}_2 + \eta_2 \boldsymbol{\epsilon}_1 + \mathbf{S}(\boldsymbol{\epsilon}_1) \boldsymbol{\epsilon}_2 \end{bmatrix}. \quad (\text{A.13})$$

This is derived in (Egeland & Gravdahl 2002, pp. 235, eq. 6.199). Where it is also shown how to do composite rotations.

It can be shown that the time derivative of a rotation matrix is given by

$$\dot{\mathbf{R}}_b^i = \mathbf{S}(\boldsymbol{\omega}_{ib}^i) \mathbf{R}_b^i = \mathbf{R}_b^i \mathbf{S}(\boldsymbol{\omega}_{ib}^b). \quad (\text{A.14})$$

Taking the time derivative of (A.12), we get

$$\begin{bmatrix} 0 \\ \dot{\mathbf{R}}_b^i \mathbf{v}^b \end{bmatrix} + \begin{bmatrix} 0 \\ \mathbf{R}_b^i \dot{\mathbf{v}}^b \end{bmatrix} = \dot{\mathbf{q}} \otimes \begin{bmatrix} 0 \\ \mathbf{v}^b \end{bmatrix} \otimes \mathbf{q}^{-1} + \mathbf{q} \otimes \begin{bmatrix} 0 \\ \dot{\mathbf{v}}^b \end{bmatrix} \otimes \mathbf{q}^{-1} + \mathbf{q} \otimes \begin{bmatrix} 0 \\ \mathbf{v}^b \end{bmatrix} \otimes \dot{\mathbf{q}}^{-1} \quad (\text{A.15})$$

MATHEMATICAL TOOLS AND DEFINITIONS

Some manipulation results in

$$\begin{bmatrix} 0 \\ \dot{\mathbf{R}}_b^i \mathbf{v}^b \end{bmatrix} = 2 \begin{bmatrix} 0 \\ \mathbf{S}(\eta \dot{\epsilon} - \dot{\eta} \epsilon + \mathbf{S}(\epsilon) \dot{\epsilon}) \mathbf{R}_b^i \mathbf{v}^b \end{bmatrix}, \quad (\text{A.16})$$

which shows that the angular velocity may be given by

$$\boldsymbol{\omega}_{ib}^i = 2(\eta \dot{\epsilon} - \dot{\eta} \epsilon + \mathbf{S}(\epsilon) \dot{\epsilon}) \quad (\text{A.17})$$

Using

$$\dot{\mathbf{q}} \otimes \mathbf{q}^{-1} = \begin{bmatrix} 0 \\ \eta \dot{\epsilon} - \dot{\eta} \epsilon + \mathbf{S}(\epsilon) \dot{\epsilon} \end{bmatrix}, \quad (\text{A.18})$$

leads to the result

$$\begin{bmatrix} 0 \\ \boldsymbol{\omega}_{ib}^i \end{bmatrix} = 2\dot{\mathbf{q}} \otimes \mathbf{q}^{-1} \quad \text{and} \quad \begin{bmatrix} 0 \\ \boldsymbol{\omega}_{ib}^b \end{bmatrix} = 2\mathbf{q}^{-1} \otimes \dot{\mathbf{q}}, \quad (\text{A.19})$$

and finally the kinematical differential equation in terms of the unit quaternion

$$\dot{\mathbf{q}} = \frac{1}{2} \begin{bmatrix} 0 \\ \boldsymbol{\omega}_{ib}^i \end{bmatrix} \otimes \mathbf{q} \quad \text{and} \quad \dot{\mathbf{q}} = \frac{1}{2} \mathbf{q} \otimes \begin{bmatrix} 0 \\ \boldsymbol{\omega}_{ib}^b \end{bmatrix} \quad (\text{A.20})$$

Appendix B

Mechanical and electrical design

In this chapter we give an outline to the main components of the mechanical and electrical design of the AUVSAT vehicles.

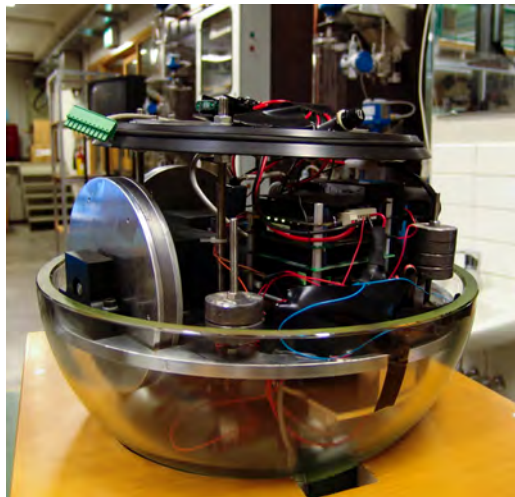


Figure B.1: The vehicle with the top sphere detached to reveal the inner structure and hardware layout.

B.1 Electrical design

The electrical circuit design consists of the main power network distributing power from the main battery to the motors and vehicle power card, low voltage auxiliary power circuits, supplying power to the servos, PC/104 stack, pressure sensor and IMU, in addition to the serial communication network and analog signal lines.

MECHANICAL AND ELECTRICAL DESIGN

B.1.1 Main power network

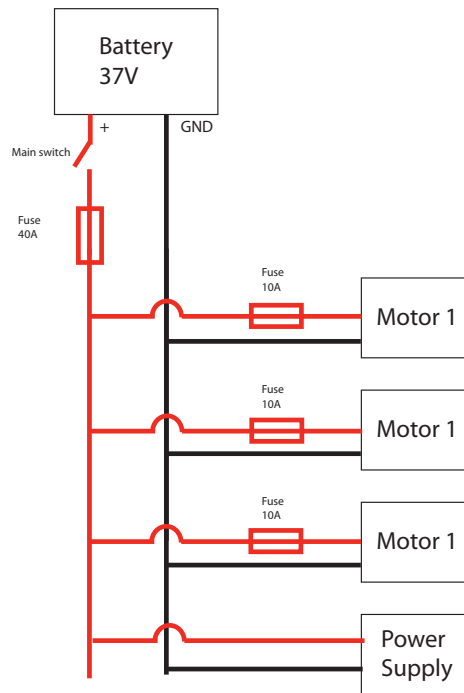


Figure B.2: Main power network - This network connects the battery to the three motors and the PC/104 power supply card. The circuit is protected by a 30A main fuse, in addition to 10A fuses on each motor connector, protecting the motors from overloading. A main switch is connected to the battery to enable power during assembly and disassembly.

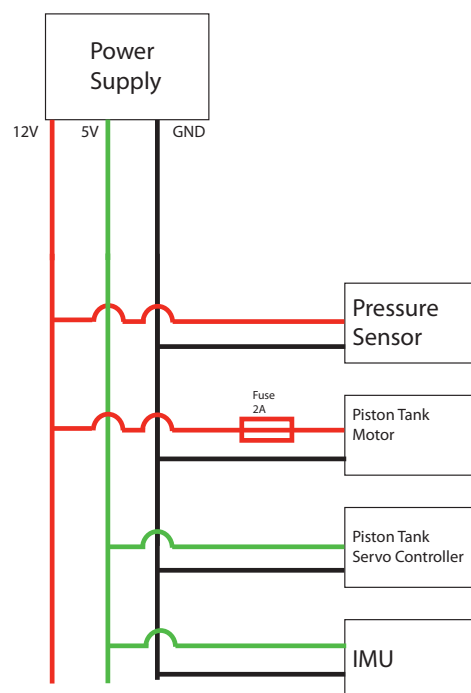


Figure B.3: Auxiliary power network - The auxiliary power network distributes power from the power supply card to hardware without internal voltage regulators. There are two power rails, a +5V and a +12V rail.

MECHANICAL AND ELECTRICAL DESIGN

B.1.2 Actuator and sensor signal transmission lines

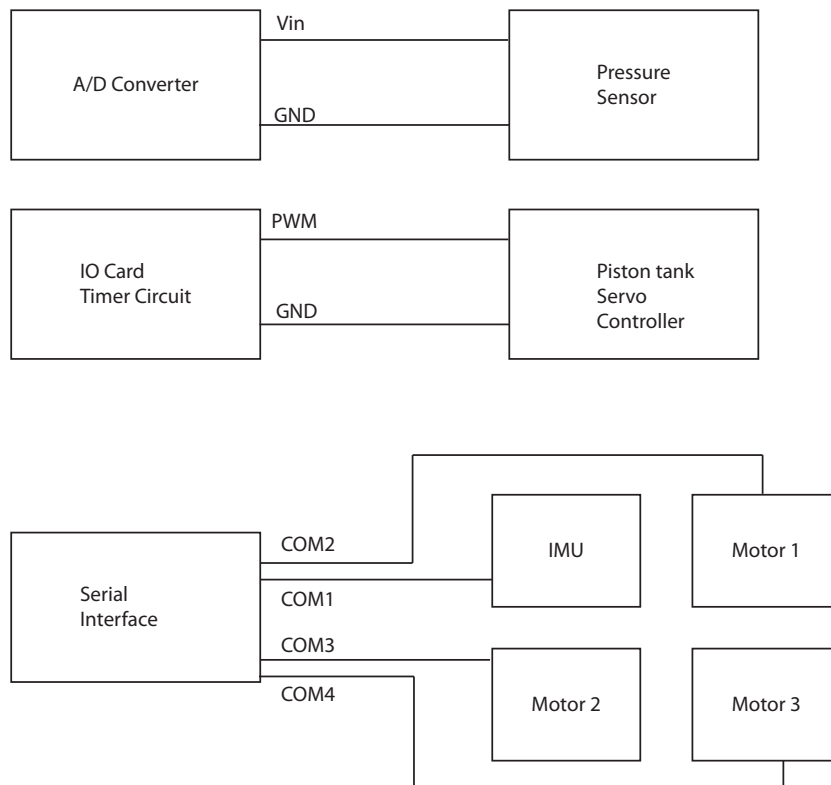


Figure B.4: This figure gives an overview of the actuator and sensor signal transmission lines. These transmission lines carry analog voltage readings from the pressure senso, a PWM signal controlling the piston tank servo controller and serial communication to and from the IMU and motor controllers.

B.2 Mechanical design

The AUVSAT vehicles were designed using the Autodesk Inventor Professional software package. Using this software we were able to accurately position actuators and other hardware, to achieve the requirements of the design.

B.2.1 Main assembly

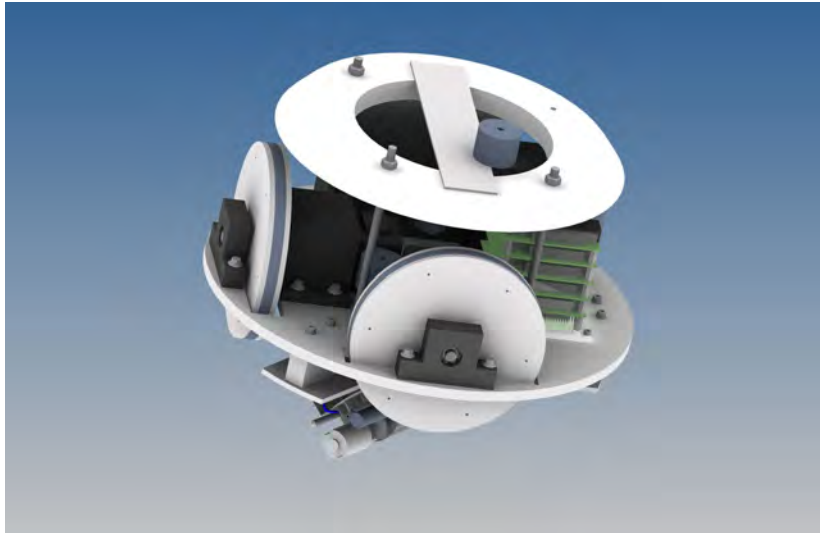


Figure B.5: This figure shows how the different hardware components are attached to the framework.



Figure B.6: This figure shows how the different hardware components are attached to the framework. Viewed from below.

MECHANICAL AND ELECTRICAL DESIGN

B.2.2 Mechanical drawings

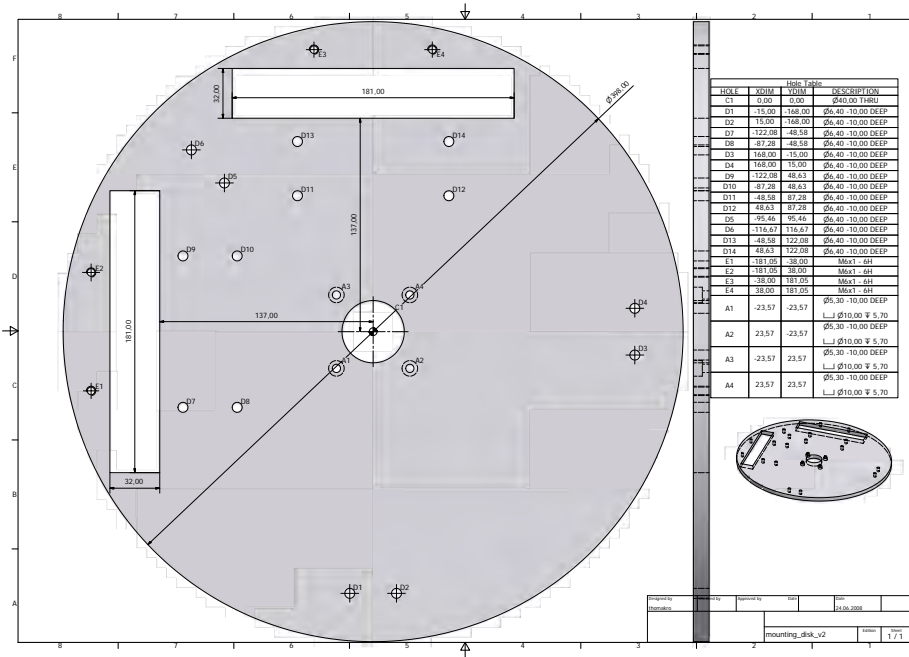


Figure B.7: Upper mounting disc

B.2. MECHANICAL DESIGN

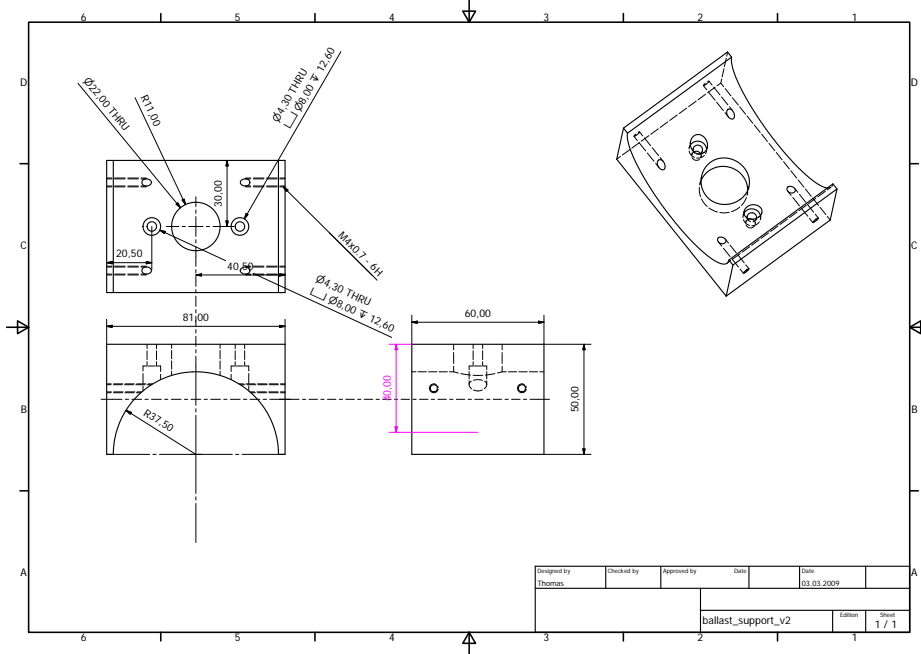


Figure B.8: Piston tank mounting bracket

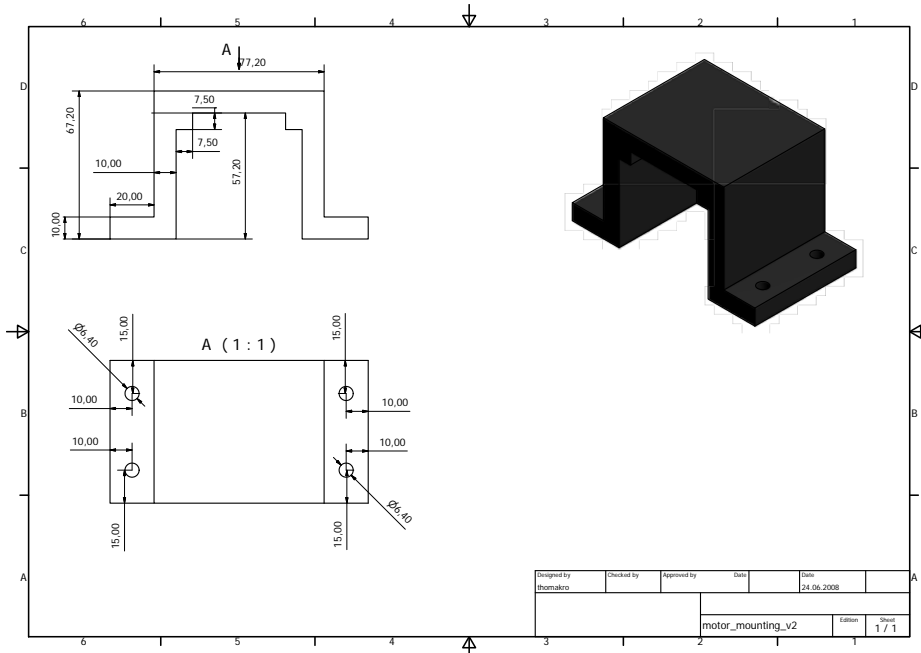


Figure B.9: Motor mounting bracket

MECHANICAL AND ELECTRICAL DESIGN

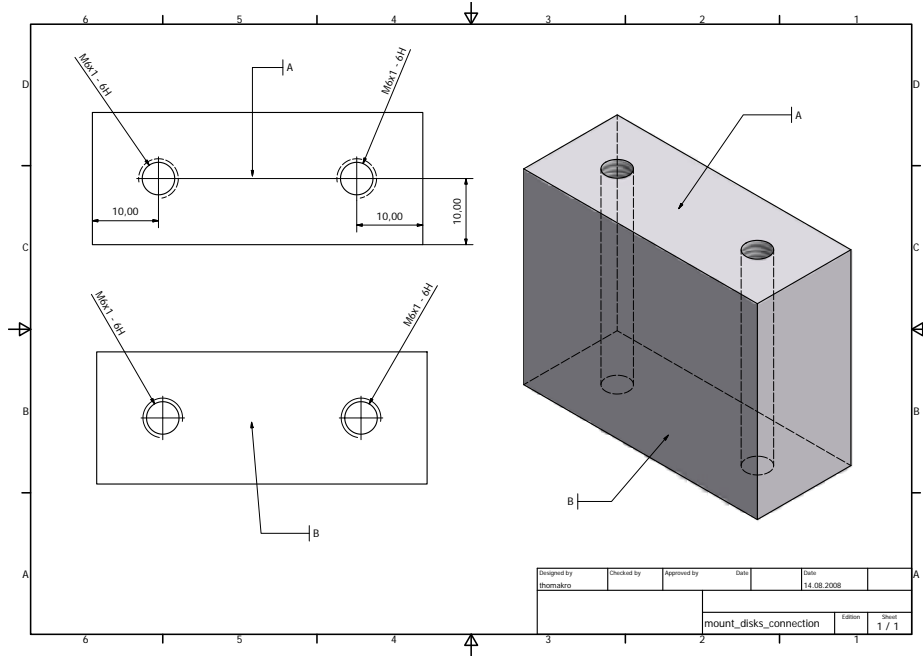


Figure B.10: Mounting disc connector

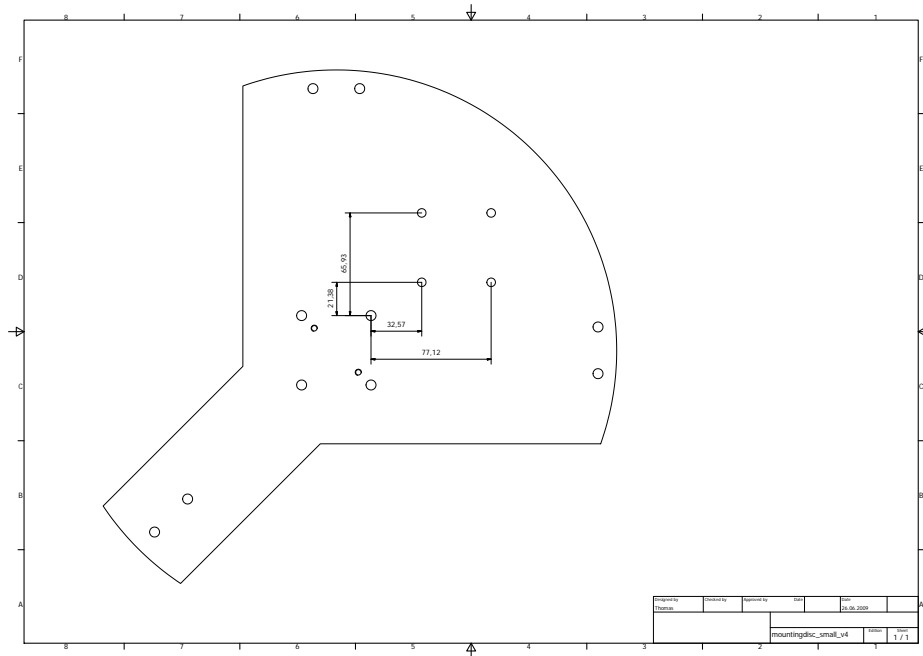


Figure B.11: Lower mounting disc

B.2. MECHANICAL DESIGN

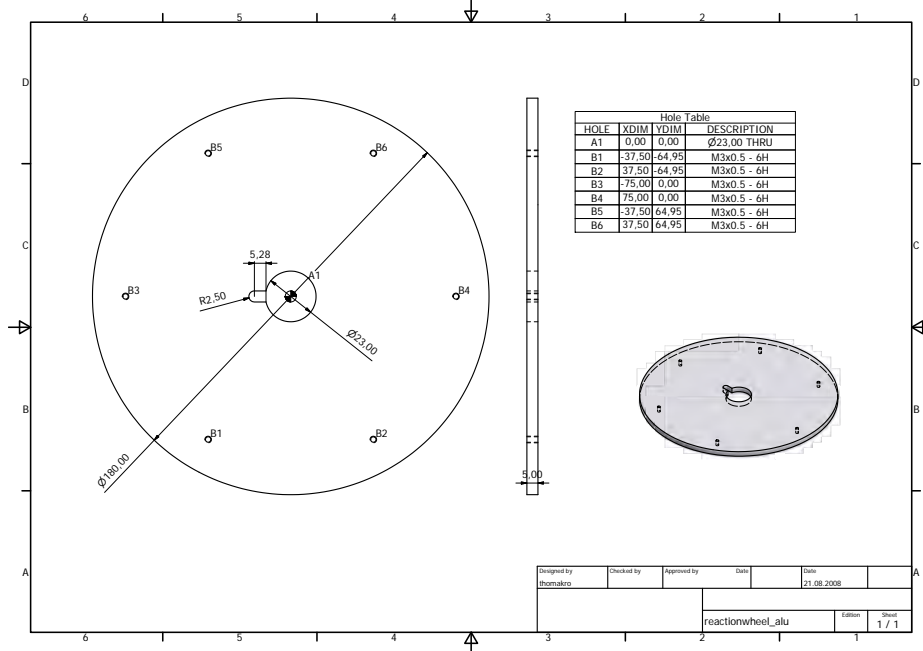


Figure B.12: Aluminum part a of reaction wheel

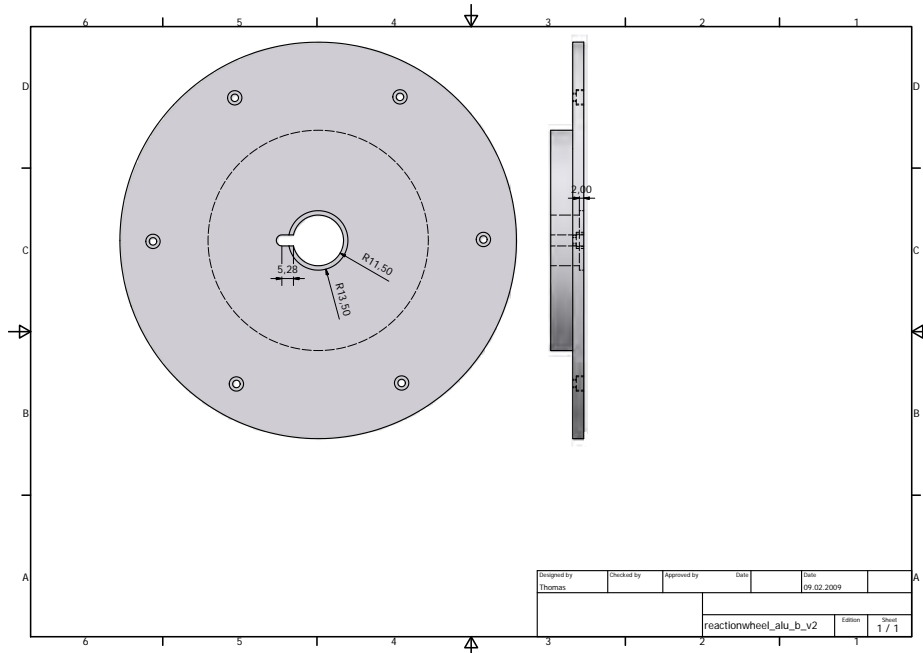


Figure B.13: Aluminium part b of reaction wheel

MECHANICAL AND ELECTRICAL DESIGN

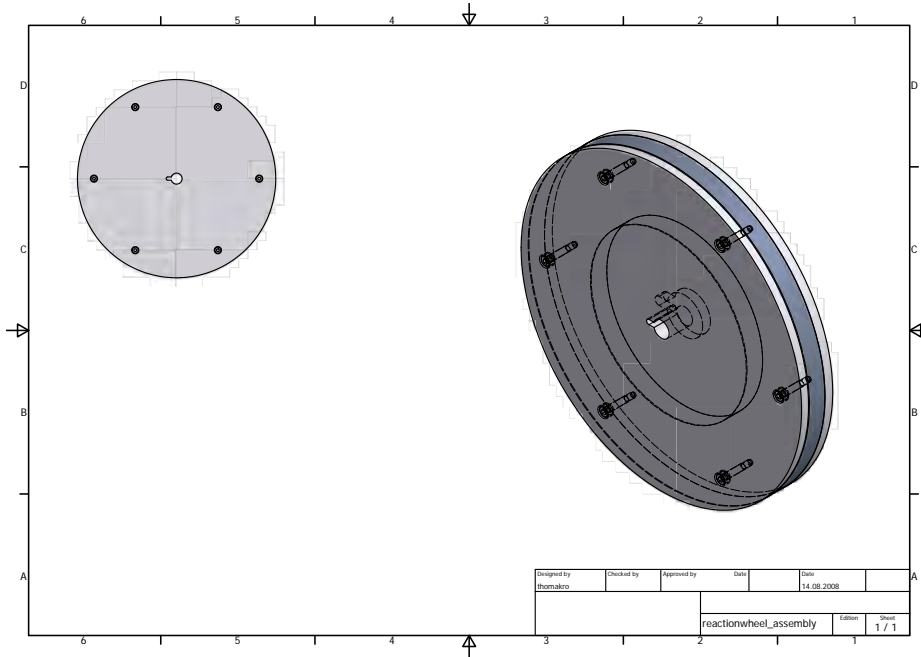


Figure B.14: Assembled reaction wheel

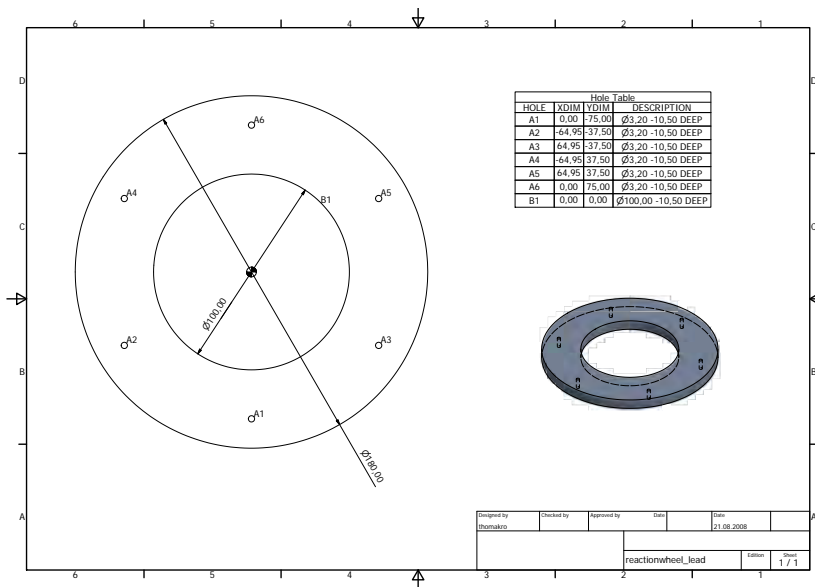


Figure B.15: Reaction wheel lead core

MECHANICAL AND ELECTRICAL DESIGN

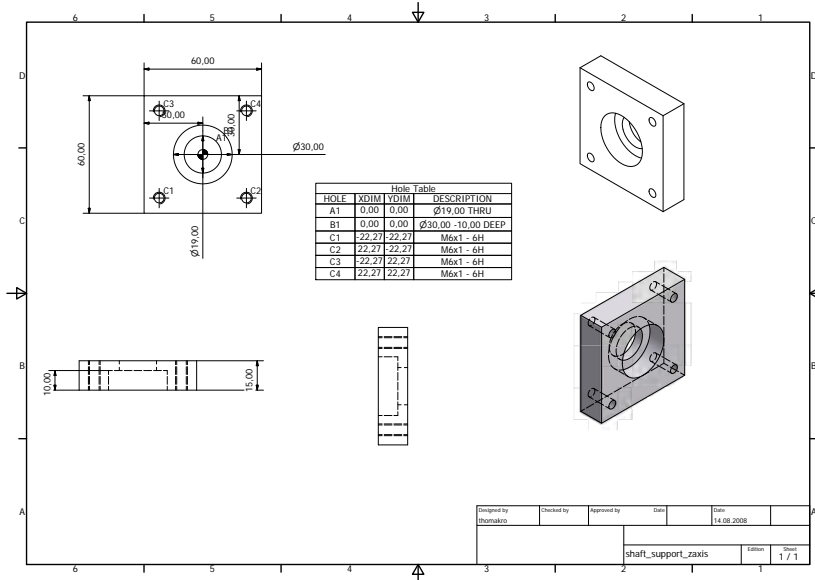


Figure B.18: Reaction wheel shaft for the yaw axis motor. Connecting the reaction wheels to the motor shaft.

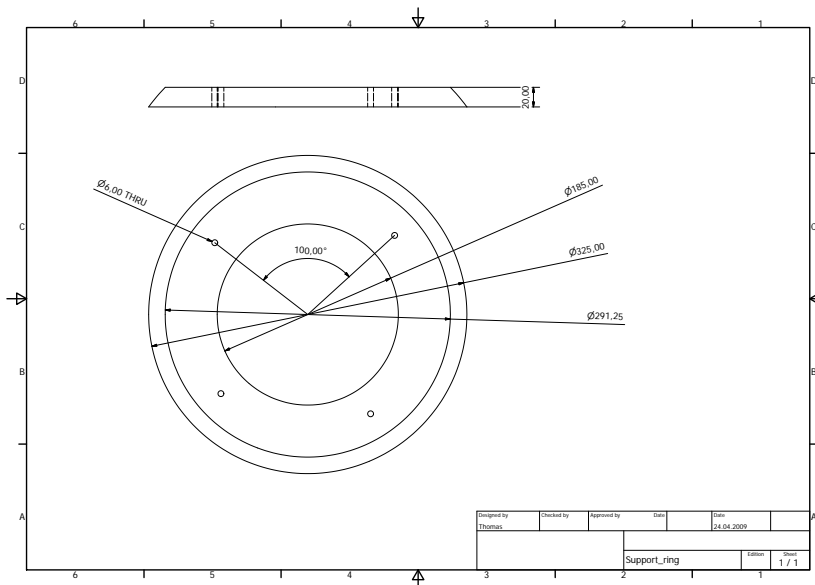


Figure B.19: Support framework. Supports the inner assembly inside the glass sphere when the vehicle is rotating.